RESIDUAL STRESSES AND WEB FRACTURE

IN ROLLER-STRAIGHTENED RAIL

by

SARAH J. WINEMAN

S.M. Mechanical Engineering, M.I.T. (1987)

S.B. Mechanical Engineering, M.I.T. (1985)

Submitted to the Department of
Mechanical Engineering
in Partial Fulfillment ot the Requirements
for the Degree of

DOCTOR OF PHILOSOPHY
in Mechanical Engineering

at the

Massachusetts Institute of Technology

June, 1991

Signature of Author ....
U
Department of Mechanical Engineering
June, 1991

Certified by ....
Prof. Frank A. McClintock
Professor, Department of Mechanical Engineering
Thesis Supervisor

Accepted by ....
Prof. Ain A. Sonin
Chairman, Departmental Graduate Committee

RESIDUAL STRESSES AND WEB FRACTURE IN ROLLER-STRAIGHTENED RAIL

by

SARAH J. WINEMAN

Submitted to the Department of Mechanical Engineering
on March 15, 1991, in partial fulfillment of the
requirements for the Degree of Doctor of Philosophy in
Mechanical Engineering

Abstract

Roller-straightening of railroad rails is a final or near-final step in manufacture which introduces longitudinal residual stresses throughout the rail section. These stresses can be severe enough to drive a crack in the rail web, causing derailments. Residual stress creation in the roller-straightener is a three-dimensional problem which can, however, be idealized as plane stress. Two-dimensional, plane stress, models of the straightener agree with experimental data and show that the unfavorable residual stress arises in the lightly loaded final straightener rolls, where the low bending moment but high contact stress causes the rail to yield only in the flange near the roll. Maintaining high bending moments through the straightener may avoid the formation of the unfavorable U-shaped residual stress distribution.

At a rail end, the longitudinal residual stress distribution of the mid-rail region must drop to zero and other components of residual stress may develop. Finite element and analytical models show that the distance from a cut rail end to develop the mid-rail stress is approximately one rail height for both a free end and an end with fixed base. At the end near mid-web, a vertical tensile residual stress develops of 1.35 and 1.10 times the maximum longitudinal stress for a free and fixed end, respectively. An estimate of the Mode I stress intensity on a short crack in this vertical stress field gives a K_I increasing with crack length and reaching approximately 2/3 of the typical carbon rail steel fracture toughness for cracks 13 mm (0.07 rail height) long. Therefore, although K_I on a short crack may not be sufficient in itself to drive fracture, in the presence of service loads the risk of fracture is greatly increased. The risk is still greater in alloy rails with low fracture toughness.

A saw-cutting test can give an estimate of the stress intensity K_I acting on a web crack at the saw-cut location. The test is simple, requiring a longitudinal saw cut of the web, measurement of the curvature changes of the split ends, and an algebraic calculation.

Thesis Committee: Prof. Frank A. McClintock, thesis supervisor
Prof. David E. Hardt
Prof. David M. Parks
Dr. Oscar Orringer, US DOT/TSC

2

Acknowledgments

Contents

Chapter 1

Introduction

After railroad rail is hot-rolled to shape, it is cooled to near room temperature. During cooling the rail warps due to its non-uniform section and the resulting non-uniform rate of cooling. There may also be initial curvature from the hot mill. Therefore current railroad-rail manufacture in the U.S., Europe, the Soviet Union, and Japan usually includes roller-straightening of each rail after it has cooled from the hot working temperature. In roller-straightening, the rail is passed through staggered rolls (Fig. 1), which plastically deform and straighten the rail. However, roller-straightening leaves longitudinal tensile residual stress in the rail head and base, and compression in the web (Fig. 2), according to European, Soviet, and Japanese experimental stress measurements. With high-strength rails, this residual stress field can be severe enough to drive web fracture, as evidenced by a derailment in 1983 with four fatalities (John et al. 1984), and as demonstrated by a fracture stability analysis (Wineman and McClintock 1987). Ways of eliminating or reducing the residual stresses in rail are therefore of great concern. Roller-straightening is also done on certain wide-flange beams (Samways 1986, Tselikov and Smirnov 1965). An understanding of residual stress formation and modification in rails could lead to reducing the residual stresses created in other sections, such as I-beams and T-beams.

In Chapter 2 of this work, models for the creation of residual stresses during roller-straightening are developed. The effects of straightener parameters on the severity of the residual stresses formed are investigated, and modification of these

parameters to minimize unfavorable residual stresses is suggested.

At a rail end, the mid-rail longitudinal residual stress must drop to zero, and other components of residual stress may develop, such as a vertical tensile stress in mid-web. In Chapter 3, these stress transients are estimated from finite element and analytical models, and their resulting stress intensity K_I on a short web crack at the rail end is estimated.

The severity of longitudinal residual stress in a given rail can be quantified with a saw-cutting test, described in Chapter 4. Such a test requires a longitudinal saw cut in the web, measurement of the curvature change of the cut ends, and an algebraic calculation, and gives an estimate of the stress intensity K_I acting on a web crack at the saw cut location. The saw-cutting procedure is applied to experimental data for split rails.

1.1   References

1. R.R. John et al. (1984) "Task force report-rail failure evaluation", DOT Transportation Systems Center, Cambridge, MA.

2. S.J. Wineman, F.A. McClintock (1987) "Rail web fracture in the presence of residual stresses", *Theoret. Appl. Fracture Mech.*, 8, 87-99.

3. Samways, N.L. (1986) "Wheeling-Pittsburgh's modern continuous casting/rail mill complex", *Iron and Steel Engineer*, June, 25-31.

4. Tselikov, A.I., Smirnov, V.V. (1965) *Rolling Mills*, Pergamon, p. 254-278.

driving rolls

idler rolls

roll spacing 1500 mm

roll diameter 950 mm

rail height 185 mm
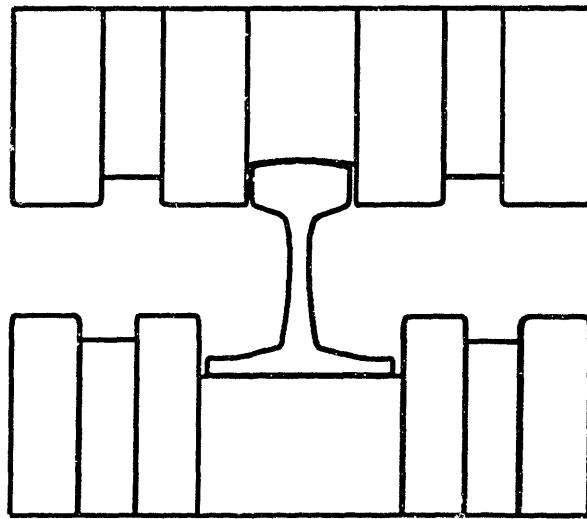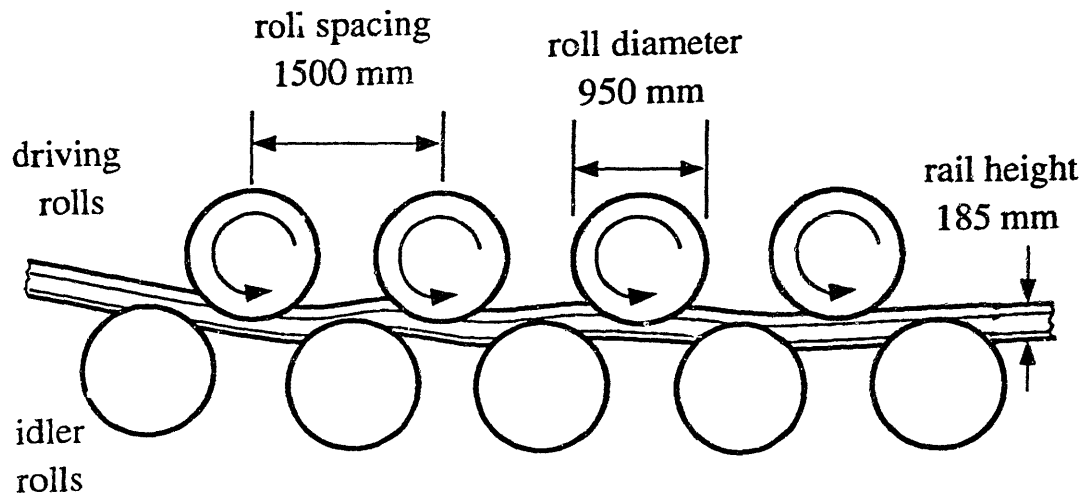
Fig. 1. Schematic of the roller-straightener (exaggerated amplitude of rail deflection).
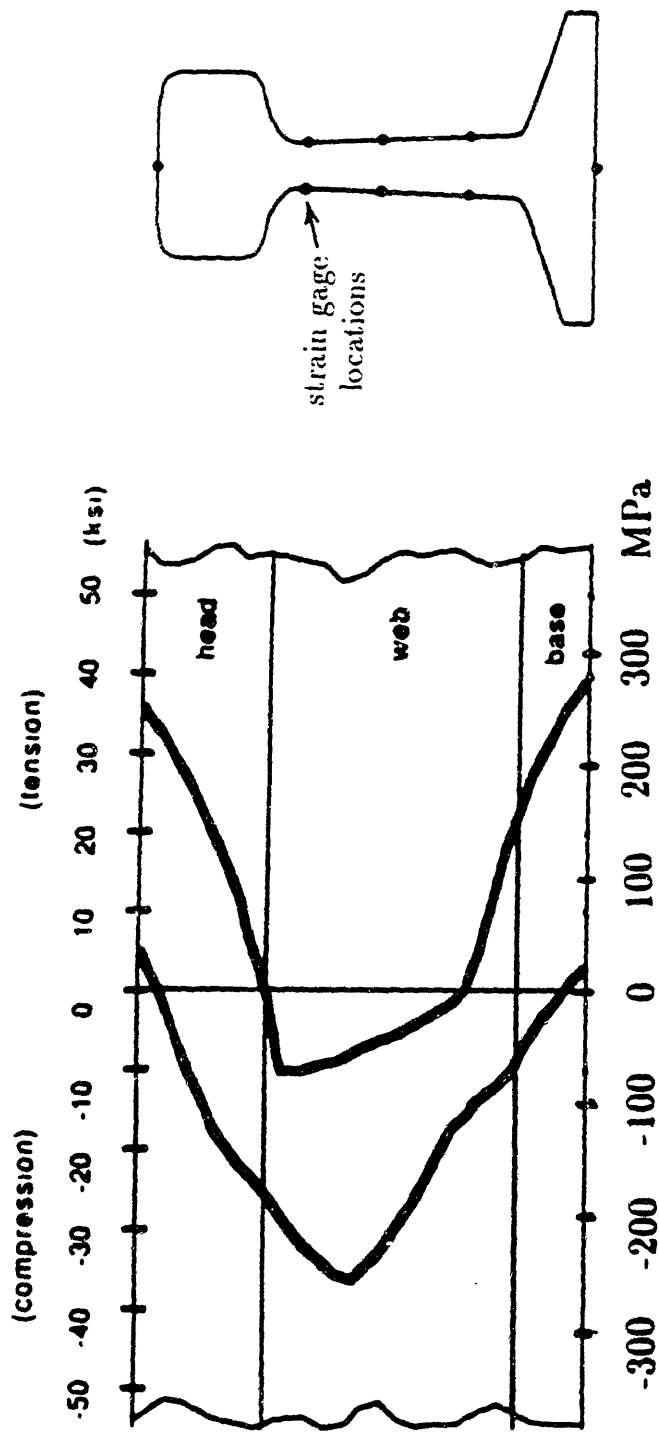
Fig. 2. Scatterband of longitudinal residual stress due to roller-straightening (sources: ORE 1984, Deroche 1982, Konyukhov, Reikhart, and Kaportsev 1973, Masumoto et al. 1982).

Chapter 2

The creation and modification of residual stresses during roller-straightening

2.1 Introduction

Several aspects of the roller-straightening process make it unusual and challenging to analyze. First, the stress states in the rail as it passes through the straightener are complex. The rail is subjected to bending, shear, and roll contact stresses, with lateral spreading in the flanges nearest the rolls. Since this preferential flange deformation is the key mechanism creating the observed longitudinal residual stresses, straightener models must be detailed enough to capture this local deformation. Second, the straightener cannot be idealized as a periodic problem, since the magnitudes of the alternating applied loads or deflections decrease through the straightener. Third, the effects of the rolls are coupled: the stresses under each roll are affected by the other roll settings, and the residual stresses from one roll are modified by subsequent rolls. Fourth, as material passes under a roll it is subjected to rapidly varying ratios of stress components, including rotation of principal stress axes. Simple kinematic hardening material behavior may not give an accurate response to this loading history.

A simultaneous, as yet unpublished, study of roller-straightening (Wunderlich Brünig and Obrecht 1988) has succeeded in obtaining reasonable agreement with

experimentally measured residual stresses. Published analyses of straightening processes and on rolling either are not applicable to the complex roller-straightening process, or fall short of accurate residual stress prediction. In analyzing the roller-straightener, Tselikov and Smirnov (1965) treat the process as pure bending. In one study (ORE 1987) the straightener is modelled using beam finite elements near the rolls that can carry bending, shear, and an assumed distribution of vertical stress. Neither model gives the U-shaped longitudinal residual stresses observed in roller-straightened rails. Studies of other straightening processes, such as cross-roll straightening (Tokunaga 1961, Das Talukder and Johnson 1981, Tselikov and Smirnov 1965), and tension-levelling (Roberts and Sheppard 1971, Hibino and Kunii 1971, Sheppard and Roberts 1972, Noé, Fischer and Schwenzfeier 1986), treat the processes as pure bending. Rolling analyses (for example Numiform 86, 89) are often for large strains (roller-straightening is a small-strain problem), and for plane strain or uniform-width slabs, unlike the varying-width rail. In addition, rolling analyses treat the effects of one roll stand at a time, unlike the many, coupled rolls in the roller-straightener. Dawson's streamline technique (Lee, Dawson and Dewhurst 1989) is capable of modelling three-dimensional problems (such as a study of plate bulging, in Numiform 89), but it has not yet been adapted to multiple roll stands or the kinematic hardening material behavior appropriate for rail steel. Shakedown analyses are not useful: the roller-straightener loads are expected to be too large and too few for the shakedown techniques of Orkisz (1988) to apply.

The goals of this work are first, to develop models for residual stress formation during roller-straightening of rails. Then, the effects of process parameters (such as roll offset or load, roll horizontal spacing and roll diameter) on the severity of residual stresses formed are investigated, and modification of these parameters to minimize unfavorable residual stresses is discussed.

2.2   The roller-straightening process

Modelling roller-straightening first requires knowledge of the rails used and the straightening process. Information from North America, Europe, the Soviet Union,

and Japan on rails, their conditions before and after straightening, and roller-straighteners is summarized below.

2.2.1 Rail sections and material properties

Rail sections. There are many different types of rail cross section in service today (see, for example, the AREA manual (1978) for sections in use in the U.S.). In the U.S., the 136RE (136 lb/yd, or 68 kg/m) (Fig. 1) is commonly used for freight. In Europe, UIC60 (60 kg/m) and S49 (49 kg/m) rails are commonly used (Figs. 2 and 3). Much of the experimental data on residual stresses and dimensional changes are for these sections, although data on other European and Soviet rail sections also exist. In this work, a 136RE section was used for most models. A UIC60 section was used when needed for comparison with existing experimental data.

Material properties. Rail steels can be characterized by their alloy composition, which affects their mechanical properties. Heat treatment and cooling schedules further determine the properties of the rail. Table 1 shows values of composition, yield strength, tensile strength, and hardness for carbon and several alloy rail steels. Heat treatments are chosen by the rail producers to meet the required mechanical properties. Variation of mechanical properties other than hardness over the rail cross section is not well documented, but hardness may vary as much as ±10% over the rail cross section (McEvily and Ochi 1985, Frommann 1965). In head-hardened rails, the head can have a hardness 30% higher than that of the web and base (McEvily and Ochi 1985).

In modelling the roller-straightener, it is desirable to have material data for the multiaxial, non-proportional, transient cyclic loading that takes place in the straightener. However, most existing stress-strain data are restricted to monotonic data from tensile tests, cyclic stress-strain curves obtained from the locus of tips of steady-state hysteresis loops (for example Sunwoo, Fine, Meshii, and Stone 1982, Park and Fletcher 1982, Rice and Broek 1982, Scutti 1982, Dabell et al. 1978, and Leis 1978), and some transient cyclic data (ORE 1987, Journet 1983, Rice and

Broek 1982). All of the above data are for uniaxial loading. Hahn et al. (1988) has shown that for the small strain amplitudes present under wheel loading, kinematic hardening gives better correlation with experimental data than isotropic hardening. Bower (1989) has compared a non-linear kinematic hardening model with cyclic data for both proportional and non-proportional loading of rail steel. Bower was able to predict the amount of ratchetting but not the shape of the individual hysteresis loops. Although the effects of non-proportional loading under the straightener rolls should be investigated, this is beyond the scope of this work.

The modelling described below uses a bilinear stress-strain curve approximating that of the cyclic curve for carbon rail steel, and kinematic hardening (Fig. 4). There is considerable variation in yield strength and hardening over different rail steels. For most finite element models, a yield strength Y of 480 MPa and hardening modulus h of 0.09 times the elastic modulus E, representative of carbon rail for the U.S., was used. When comparing finite element results with experimental data, the yield strength was increased to 500 MPa to more closely approximate the rail steel (alloy 90A) used. Throughout this work it has been assumed that rails are straightened at room temperature. This is sometimes not true, although rails are not straightened red-hot or glowing. Also, rolling speeds are assumed to be slow enough that strain-rate effects are negligible.

2.2.2 Condition of rail before straightening

After the rails are hot-rolled, they are cooled to room temperature, or heat treated and then cooled. After such heating and cooling, the rails are usually curved due to the uneven cooling rates of the thick head and the thinner web and base and also due to pre-curvature in the hot mill. The rails also contain low values of residual stress from cooling. Table 2 summarizes the curvatures and residual stresses in rails before and after straightening.

Initial curvatures. Curvatures of rails entering the straightener vary widely from mill to mill, both in their magnitude and sense. These variations occur partly

from attempts to pre-curve the rails in the hot mill to compensate for the curvature acquired during cooling. Therefore, there are instances of rails bowed away from the rail head (Marcelin Abouaf and Chenot 1986), bowed towards the rail head (ORE 1987), and even rails with reversing curvatures (ORE 1987). Values of deflection quoted in the literature differ in whether the rail shape is corrected for gravity. Measurements that do not correct for gravity cite "small" deflections of from 10-40 mm on a 25-m rail fc · oil quenching after high-frequency induction heating (Babich et al. 1982), and "large" deflections of 500-800 mm on a 25-m rail (Vorozhishchev et al. 1983). An ORE study (1987) which corrected for the effects of gravity obtained deflections ranging from almost zero to a maximum of approximately 120 mm over a 20-m rail. Marcelin, Abouaf. and Chenot (1986) calculated the final deflection of a rail due to air cooling to be about 400 mm on a 36-m rail (no gravity present).

The above are vertical curvatures; the rails can also acquire lateral curvatures. However, since lateral symmetry should greatly reduce warpage due to uneven cooling, and since roller-straightening to remove *vertical* curvatures introduces the observed residual stresses, lateral curvatures have been neglected in this work.

Initial residual stresses. Fig. 5 shows scatterbands of measured longitudinal residual stresses in unstraightened rail (ORE 1984). Marcelin, Abouaf and Chenot (1986) have calculated longitudinal residual stresses from cooling of a straight rail using a thermo-mechanical finite element model with both elastoplastic and elasto-viscoplastic material behavior (Fig. 6). Their calculated values fall within the scatterband of measured stresses for unstraightened rail at the locations of residual stress measurement (Fig. 5), except for the stress at the top of the head in the elasto-viscoplastic case. The maximum initial stress inside the head and base reaches at worst about half the maximum residual stress after straightening.

Typical values. Because of the wide variation in rail curvatures, it is impossible to choose a typical curvature. Because of this, and because straightening above a certain level of roll loads or deflections produces straight rails independently of the

initial curvatures, initially straight rails were modelled. Since the initial longitudinal residual stresses are small compared to those produced by the straightener, zero initial residual stresses were assumed before straightening.

2.2.3   The roller-straightener

The rail is passed through rolls with horizontal axes, to straighten the rail in the stiffest, vertical, direction by alternately pressing on the top of the head and bottom of the base. In many mills, the rail leaving this "horizontal" straightener immediately enters the "vertical" straightener: rolls with vertical axes to straighten the rail in the horizontal direction by pressing on the side of the web or the side of the head. This work investigates the "horizontal" straightener, where the rolls press vertically on the rail head and base, since this is the chief straightening operation and is the cause of the longitudinal residual stress that can cause web fracture.

Fig. 7 shows various roller-straightener configurations used in North America, Europe, and the Soviet Union. North American and European (German-made) roller straighteners usually have 9 rolls: 4 fixed driven rolls on top, and 5 vertically-adjustable idler rolls on the bottom. In some European mills, the outer two lower rolls are not used. Soviet-made roller-straighteners can have 6 or 8 rolls. Either vertical force or displacement control can be used. In the straighteners observed in North America, there is force control on the three central idler (lower) rolls and displacement control on the outer two idler rolls. In Europe and in the Soviet Union displacement control is preferred for all the idler rolls. No lubrication is used between rolls and rail.

The parameters of these roller-straighteners are summarized in Table 3.

Typical straightener.   The straightener used in modelling is shown in Fig 8. The upper rolls are fixed, and the lower rolls have applied vertical displacements.

2.2.4   Condition of rail after straightening

After roller-straightening at room temperature, the rails are nominally straight and contain significant longitudinal residual stresses. These have been summarized in

15

Table 2.

Final curvatures. In the United States, the recommended overall vertical deflection of rails after straightening is less than 19 mm (0.75 in) over a 11.9-m (39-ft) rail (AREA 1975). An ORE study (1987) gives final deflections for European roller-straightened rails of less than 20 mm over a 20-m rail. Babich et al. (1982) give final deflections of less than 12 mm over a 25-m rail length for rails in the Azovstal' steel-works in the Soviet Union. In the ORE study, correction is made for the weight of the rail. The measurement of Babich et al. was done with the rail standing vertically on its base, with no weight correction.

Final residual stresses. The longitudinal residual stresses for carbon and alloy rails fall in the scatterband shown in Fig. 2 of Chapter 1, based on residual stress data from Europe, the Soviet Union, and Japan. This U-shaped stress distribution of tension-compression-tension in the head, web, and base has maximum magnitudes of 100-300 MPa (14.5-43.5 ksi). The data are for plain carbon and alloy rails, and for both heat-treated and non-heat-treated rails. An exception is head-hardened rail, which has compression in the head after head-hardening and roller-straightening (Fig. 9) (Masumoto et al. 1982). Vertical residual stresses in the head and web have also been measured but have relatively low magnitudes and less effect on web fracture, as shown in Wineman and McClintock (1987).

Dimensional changes. Roller straightening produces a decrease in rail height and length, and an increase in head and base width (Frommann 1965, Didyk 1988, Christiansen 1988). The overall strains corresponding to these dimensional changes are from 0.3 to 1.8 times the yield strain. In one study (ORE 1987), the rail head showed a slight decrease in width instead of an increase. Frommann (1965) studied dimensional changes for a 7-roll straightener and found that almost all of the dimensional change occurred under the second and third rolls.

End effects. The length from an untrimmed rail end needed to achieve the mid-rail residual stress and dimensional change can be estimated easily if there is significant mill scale on the rails during straightening. This oxide layer falls off in the fillet regions over the entire rail length except for a half-roll-spacing length (about 750 mm, or 30 in) at each end. Dimensional changes measured at the ends by Deroche et al (1982), and residual stresses ultrasonically measured by Utrata (1989) agree with this half-roll-spacing end effects region. Frommann (1965) found that the mid-rail dimensions were attained an entire roll spacing (1500 mm) from the ends. Note that this is much longer than the one rail height from a cut rail end needed to attain the mid-rail stress distribution, discussed in Chapter 3.

These mill ends are often not straight, and in addition each end is often deformed from hitting the rolls. Many mills trim some distance from the ends and often manually press-straighten the ends.

2.3   Model selection

It is desirable to select models of the roller-straightener that are as simple as possible but which capture the essentials of the residual stresses. A key to understanding residual stress creation is the dimensional changes induced in the rail by straightening: an overall shortening in the rail height and length and a lateral spreading of the head and base. Under a straightener roll, the flange (head or base) is in longitudinal compression due to bending, and in vertical compression due to the roll (Fig. 10). These dimensional changes suggest, then, that under these applied stresses the flange yields, shortens in length and height, and spreads laterally. The shortening near the roll is greater than any lengthening of the flange away from the roll, and the final product is a rail with head and base preferentially shortened with respect to the web. This gives the U-shaped residual stress distribution of longitudinal tension-compression-tension through the head, web, and base. This physical insight was made by Meier as early as 1936 (Meier 1936, in Frommann 1965). In fact, the above is an oversimplification; the actual stress states are three-dimensional. As shown in the three-dimensional studies described below, the loaded

17

rail is closer to a plane strain state near the center under the roll, and is closer to plane stress away from the roll and near the tips of the flange under the roll. The tips of the base and the bottom of the head remain elastic and constrain the flow of the yielding material. However, it turns out that 2-D plane stress models provide an adequate representation of the 3-D centerline residual stresses. This is probably because the elastic material surrounding the yielding regions provides only partial constraint from lateral spreading, and the resulting deformation is closer to plane stress than to plane strain.

An additional point to be kept in mind when selecting models is that the rolls are not at the maximum points of deflection of the rail as it passes through the straightener. Since each roll is at the point of maximum bending moment, producing a *change* in curvature of the rail, the rolls should be at the *points of inflection* of the sinusoidal rail trajectory. Although in practice this is difficult to verify since the rail deflections are very small, this was the case for the finite element results. It is interesting to note that this could account for the discrepancy between the rolling and stopped roll loads measured by the ORE (1987). When the machine is stopped, the rail may be rolled backwards or forwards a small amount toward the maxima of its trajectory, accompanied by unloading.

The work described below compares three- and two-dimensional finite element models and a simple analytical model, for selection of the optimum model to use in parametric studies.

An assumption common to all the models is the idealization of roll-rail contact. The rail head and base are assumed flat, with flat rolls which are as wide as the head or base. In the real straightener, the head roll is originally contoured to fit the head radius of approximately 300-355 mm, but the trough flattens with use. The rail base roll is flat but only contacts the central two-thirds of the rail base. In the two-dimensional and analytical models discussed below, the base rolls are assumed to contact the entire base. In the three-dimensional models of base rolling, anticlastic curvature of the base causes the base tips to lift off the roll, resulting in an effective contact width approximately equal to that in the real straightener.

18

Friction was neglected in the 3-D and 2-D finite element models having just one loaded roll contacting the rail and in the 2-D, 9-roll models for static loading. In models having multiple rolls and rail travel through the straightener, friction was used on one of the upper rolls to drive the rail through the straightener, since pulling the rail through the rolls could lead to spurious bending moments and plastic deformation.

2.3.1 Three-dimensional studies

A comparison of three- and two-dimensional finite element models was done to assess the accuracy of two-dimensional models of the straightener. Two cases of static loading were studied: loading and unloading of the roll on the rail head and on the rail base. In addition, a case of base loading with 19 mm (0.75 in) roll travel before unloading was studied. All finite element analysis was done using the program ABAQUS (1987, 1989).

Initial residual stress. Before loading, the rail was given initial longitudinal residual stresses. These initial stress distributions were brought to equilibrium with a preliminary loading step; the equilibrated initial stresses are shown in the figures below. The initial stresses were taken from two-dimensional plane stress models in which loaded head and base rolls were displaced along an entire 762-mm (30-in) length of rail, with end moments mimicking the rest of the rail in the straightener (the "single-roll" model, described below). The residual stresses from these models are necessarily uniform across the flanges (head or base). However, experimental data show that the centerline tensile stress decreases towards the flange tips (Konyukhov, Reikhart, and Kaportsev 1973, Lempitskiy and Kazarnovskiy 1973, Konyukhov Rabinovich et al. 1969, McEvily and Ochi 1985). Therefore the 3-D models used the 2-D result as the centerline stress, decreasing to 1/3 the centerline value at the tips of the head and to zero 2/3 of the way out along the base. Across the web the stress was assumed to be uniform. In addition, the maximum centerline residual stress in the 3-D head static loading model was increased so that the average residual stress was closer to the 2-D value. This was thought to be

19

especially important in the region of high residual stress in the head. In the head loading (Fig. 11) there was initial residual stress only after the roll, corresponding to the first upper roll in the straightener. In the base loading and travel, there were different stress distributions before and after the roll (Fig. 12). In all cases, stresses were smoothed over a transition region under the roll by a cubic weighting function. This transition region was assumed to be approximately one roll contact length under the roll (0.027 times the rail height) and one rail height long on the opposite side of the rail. These approximations to the actual residual stresses were considered better than having no initial residual stresses, since the magnitudes of residual stress are significant, with maxima approaching yield. Such approximations remain useful for comparison of corresponding two- and three-dimensional models.

Displacement histories. During loading and roll travel, longitudinal and vertical displacement histories were applied at the ends of the mesh to mimic the rest of the rail in the straightener. Again, these were taken from 2-D modelling, and for the 3-D models the displacements were assumed constant across the web and flanges.

Static loading on rail head and base Three models were compared: 3-D, 2-D plane stress, and 2-D plane strain. An initial loading step was used to introduce and equilibrate the initial longitudinal stresses. Longitudinal end displacements were held at zero during this step. Then, a roll load was applied to the rail head or base and removed. The head roll load of 874.8 kN (89.2 tonnes) and the base roll load of 1083.7 kN (110.5 tonnes) are similar to the loads on the first head roll and the second base roll of a North American 9-roll straightener. At the same time, nonzero longitudinal and vertical end displacements were applied during the loading steps to mimic the rest of the rail. Note that since the displacements on "unloading" were approximations taken from a previous 2-D model, they do not necessarily correspond to a state of zero end-tractions and equilibrated stresses.

Fig. 13 shows the 3-D finite element mesh for head static loading, and Fig. 14 shows the 2-D mesh for head loading. Figs. 15 and 16 show the 3-D and 2-D meshes

for base static loading. The 2-D models used 8-node (quadratic displacement) elements and the 3-D models used 8-node brick (linear displacement) elements. In the refined central region of the 3-D meshes, therefore, 4 elements were substituted for each 1 element in the plane of the 2-D meshes.

When a roll load is applied, the stresses under the applied roll load are highest in the center over the web and decrease towards the flange tips. This effect is most pronounced in the base loading. Figs. 17-19 are contour plots of the normal components of stress (σ_{xx}, σ_{yy}, σ_{zz}) for the 3-D head loading. Figs. 20-22 are similar plots for the base loading. Shear stresses were small compared to the high normal stresses under the roll, although they were not negligible compared to the normal components of deviatoric stress. Figs. 23-30 compare the applied stresses of the 3-D centerline, plane stress, and plane strain models for the rail head and base loadings. Under the roll, the 3-D centerline stress is closest to plane strain, but near the flange tips and in the rest of the rail the 3-D stresses are closest to plane stress.

As the rail bends over the roll, there is anticlastic curvature in the flanges. In Figs. 31 and 32 the regions of non-zero vertical applied stress correspond roughly to the roll "footprint" on the head and base. There is no liftoff in the head loading, but in the base loading the outermost third of the base lifts off the roll. It is interesting that in the real straightener the base rolls extend only under the center of the base, ending at roughly this liftoff point.

When the roll load is removed, residual stresses remain. Figs. 33 and 34 compare the longitudinal residual stresses for the head and base loading models. The other components of residual stress are negligibly small, except for a centerline transverse residual stress in the region of roll loading in the 3-D models. This stems from constraint of the yielded material in the center by the surrounding elastic flanges.

Roll travel on rail base Figs. 35 and 36 show the 3-D and 2-D meshes for roll travel along the rail base. Fig. 37 compares the roll "footprints" (regions of non-zero vertical stress) for the static and travelling base rolls. Fig. 38 shows the

longitudinal residual stresses left in the roll wake for the 3-D, plane stress, and plane strain models: note that near the base they are different from the static residual stresses of Fig. 34.

Conclusions on 3-D versus 2-D models   In order to model even 3 or 4 rolls, it was necessary to choose the best two-dimensional model, since three-dimensional studies are prohibitively large and time consuming. For example, the largest three-dimensional model above, that allowing 75 mm (3 in) maximum roll travel along the base, was approximately 12,000 degrees of freedom and required approximately 40 hours CPU time for 19 mm roll travel, using an Alliant FX/8 with vectorized code (approximately 2 mflops listed for a simple test case). Since the goals of this work are to model the creation of residual stresses, particularly the longitudinal residual stress of concern for web fracture, attention is focussed on the ability of the models to reproduce longitudinal residual stresses. In the comparisons of longitudinal residual stresses (Figs. 33, 34, and 38), the residual stresses for the 3-D, plane stress, and plane strain models are very close to one another except in the region near the roll. Especially in the roll wake (Fig. 38), the 3-D model gives stresses which are different from both the plane stress and the plane strain model. However, since plane stress allows lateral spreading of the flanges, which is necessary to reproduce the dimensional changes measured in roller-straightened rails, plane stress was judged to be the best two-dimensional model and is used in subsequent studies.

2.3.2   Choice of two-dimensional plane stress model

After the choice of element type for the 2-D model, the choice of physical configuration remains. There are several possibilities for modelling the roller-straightener using 2-dimensional, plane stress finite elements. Modelling the entire 9-roll straightener with a lagrangian mesh requires too large a model to even crudely reproduce residual stresses. Therefore, it is necessary to explore possibilities of local refinement or modelling parts of the straightener. The two approaches that seemed most promising were therefore compared.

22

The first, called the "single-roll" model, uses a mesh 1/2 roll spacing long and an upper and lower roll consecutively. The straightener is simulated by moving the loaded rolls along the mesh, with end tractions simulating the moment history seen by the length of rail moving through the straightener (Fig. 39). The roll forces and corresponding moment distribution are found from static loading on a coarse mesh of the entire straighter. This approach has the advantage of small mesh size, but cannot model the actual trajectory of the rail in the straightener. Also, the rolls are loaded with force boundary conditions, not the mixed force and displacement conditions actually present in the straightener.

The second approach, called the "quasi-Eulerian" model, uses a mesh as long as the straightener being considered, with refined regions under and some distance ahead of each roll (Fig. 40). Initial guesses for the wakes of residual stresses after the rolls are used as initial stress conditions, then the rolls are loaded or displaced onto the rail and the rail is moved a short distance with respect to the rolls. The new wake of residual stresses is compared with the initial guess, and this new wake is used in a second iteration of the problem if they are very different. This approach has the advantage of allowing the real, mixed boundary conditions to be applied to the rolls.

To compare the two approaches, a three-roll "straightener" was modelled. For the "single-roll" model, the corresponding moment history was used to apply time-varying end pressures as the rolls moved along the mesh. For the "quasi-Eulerian" model, the mesh was refined under and 200 mm ahead of the rolls. An initial longitudinal stress distribution, taken from the results of the "single-roll" model, was introduced before displacing the mesh 200 mm through the rolls. The stresses left by the center roll were then used as an initial guess in a second iteration. As the second iteration of the "quasi-Eulerian" model gave stresses after the roll that were at worst 25% low under the roll, with agreement within 10% elsewhere, the model was deemed to have sufficiently converged on the final residual stress distribution. Fig. 41 shows the resulting residual stresses for the "single-roll" and for the two iterations of the "quasi-Eulerian" model.

It was concluded that the quasi-Eulerian approach is the best, since it allows specification of the mixed force and displacement boundary conditions present in the real straightener and converges to an acceptable result after several iterations. However, the "single-roll" models give reasonable estimates of residual stress and are in fact used for initial stress to use in the "quasi-Eulerian" model. In the 2-D runs discussed below, the "single-roll" model only was used, since time constraints did not permit setting up and running "quasi-Eulerian" models.

2.3.3 Analytical model

A rail, or beam, subjected to bending develops a distribution of longitudinal residual stress that is Z-shaped, not the U-shaped distribution observed in roller-straightened rail. A simple analytical model was developed which serves to illustrate the development of residual tension in the flange near a roll.

The model considers a symmetrical I-section as a beam in bending, with applied end moments M, leading to a longitudinal stress distribution σ_{zz}. However, it is assumed that the vertical roll stress σ_{yy} combines with the longitudinal stress and serves to reduce the amount of longitudinal stress needed to produce yielding. Fig. 42 shows this idealization of the loaded rail and the assumed region on the yield locus of the yielding part of the flange. Unloading superposes a linear longitudinal stress with resultant $-M$ on the applied stress, with the resulting residual stress distribution also shown in Fig. 42.

The applied and residual longitudinal stress distributions can be determined for a given bending moment M and vertical stress σ_{yy} as follows. The applied stress distribution must give zero net longitudinal force:

$$\Sigma F_z = 0 = \int \sigma_{zz} dA_{rail} \ . \tag{2.1}$$

The resultant bending moment must be equal to the applied bending moment M:

$$\Sigma M_b = M = \int \sigma_{zz} y dA \ . \tag{2.2}$$

Also, the longitudinal stress σ_f in the yielding region near the roll and the vertical stress σ_{yy} combine in the Mises yield criterion, where Y is the yield stress:

24

$$\left[\sigma_{yy}^2 - \sigma_{yy}\sigma_f + \sigma_f^2\right]^{1/2} = Y^2 .$$ (2.3)

These three equations allow solution for the parameters σ_f, σ_b, and c, of the applied stress distribution, in terms of the roll stress σ_{yy} and bending moment M and chosen height of yielding material a. The residual stress distribution is then obtained by superposing a linear distribution with resultant moment $-M$.

A numerical example of this is given in Fig. 43, for a bending moment M of 0.95 the yield moment, σ_{yy} of -1.1 Y, and an assumed height a of the yielding region of 0.05 times the total height. This choice of a is similar to the height observed in some of the 2-D finite element models over which the longitudinal stress deviates from a roughly linear distribution. The resulting residual stress has maxima of 0.1, -0.01, and 0.005 times yield.

This model illustrates the development of tension in the flange after a roll pass. The model is limited as a predictive tool, since there is actually pre-existing residual stress in the rail and since in the real case, there may be yield due to longitudinal stress alone. The shortcomings of the model are further highlighted by its relatively low values of residual stress, compared to observed values, and by the fact that the envelope of parameters σ_{yy} and M needed to produce a tension-compression-tension distribution through the section is very small—in practice, many different roller-straightened rails have been found to have a U-shaped stress distribution. However, the model demonstrates the importance of the combined effect of vertical and longitudinal stress in producing the observed residual stress.

2.4   Comparison with experimental data

The finite element models were compared with experimental data where possible. First, static loading of a 9-roll straightener was done with applied roll displacements, and the finite element roll loads were compared with measured loads. Then, results of the "single-roll" model for this straightener were compared with residual stress data for a partially-straightened rail. Since time did not permit simulating the entire straightener, development of the U-shaped stress distribution in the last rolls was

25

demonstrated by subjecting rail with residual stress from the first two straightener rolls to the last two rolls.

2.4.1 Static 9-roll model for roll loads

Existing data on roll loads (ORE 1987), for a UIC60 rail section and Grade 90A carbon rail, were compared with calculated loads from a coarse finite element mesh of a 9-roll straightener. This mesh is shown in Fig. 44 for plane stress elements. Unsymmetrical I-beam elements were also used. Table 4 shows the experimental straightener settings, the actual displacements when loaded, and the measured loads when rolling and after stopping the straightener. The measured loads in the stopped straightener are lower than the measured operating loads, probably due to the rail moving backwards or forwards in the stopped rolls and partially unloading. These loads are therefore not analogous to static loading of the rail. The finite element loads, of static loading on virgin material, should be closer to the operating loads than to the stopped loads, with differences due to the presence of residual stresses, curvatures, and hardening in the operating straightener. Table 4 also shows the finite element roll loads for plane stress and for beam elements, with a comparison of finite element and experimental loads in Fig. 45. The finite element roll loads are lower than, but within 12% of, the operating loads. This agreement with experimental data suggests that the 9-roll static loading models can be used to obtain corresponding roll loads for displacement-controlled straighteners, which can then be used as boundary conditions for the "single-roll" model.

It is interesting to note the difference in load sequencing between the above European straightener and the straighteners common in North America. The straighteners in European studies have decreasing displacements applied through the straightener; North American straighteners use decreasing applied forces. This experimental study suggests that the maximum loads in both types of straighteners are similar, but that the maximum load occurs in the middle of the straightener in European straighteners, instead of at the beginning as in North American straighteners.

2.4.2 "Single-roll" model for residual stresses

The "single-roll" model provides initial guesses for residual stress, to be used in "quasi-Eulerian" models, and also provides estimates of residual stress in its own right. The "single-roll" model was used to model the 9-roll straightener shown in Fig. 46 (Schweitzer, Flügge, Heller 1985). This straightener was stopped and the rolls disengaged during straightening so that the intermediate curvatures, height decrease, and residual stresses could be measured. The 9-roll plane stress model for static loading was used to determine the roll loads for these straightener settings, with the nominal settings of rolls 2, 4, and 6 decreased by the 3 mm of settling under load (ORE 1987). The roll loads and accompanying moment history for the first two loaded rolls (rolls 1 and 2 in Fig. 46) were used in the "single-roll" model. The mesh used is shown in Fig. 47, and the resulting longitudinal residual stress is shown in Fig. 48, along with the experimentally measured values. Considering the many idealizations involved in the finite element model, and the possible inaccuracy in strain gage data, this agreement is excellent. However, one thing is surprising– the stress distribution is a Z-shape characteristic of bending, and not the U-shape observed in roller-straightened rail.

Fig. 49 shows the measured longitudinal stresses after each roll, along with our postulated stress distributions between the three strain-gage locations. The figure also shows the bending moment distribution through the straightener, normalized by the moment to cause initial yield in an unstraightened rail. The residual stress distribution takes a Z-shape throughout most of the straightener. The U-shape appears after roll 6, when the bending moment first decreases below the yield moment. Time constraints did not permit running the "single-roll" model for this whole straightener. However, the resulting deformed mesh from the first two straightener rolls was subjected to rolls 6 and 7 of the experimental straightener. The resulting longitudinal residual stress, as well as the measured residual stresses after roll 7, are shown in Fig. 50. Passage of roll 7 over the rail head has caused the compressive residual stress in the head from roll 6 to become tensile, with little change in the rest of the residual stress distribution. This effect was also seen in another case when a

mesh of 136RE section with a Z-shaped stress distribution was passed through rolls 6 and 7, with moments and roll loads scaled up according to the heavier section.

It seems, then, that the unfavorable U-shaped distribution of longitudinal residual stress occurs not from the heavily loaded rolls at the start of the straightener, which cause mostly bending deformation, but from the lighter roll passes at the end. Here, bending stresses may be insufficient to cause yield, and yield occurs near the roll due to contact stresses.

2.5 Effects of straightener parameters on residual stresses

It is desirable to quantify the variation of residual stress with straightener parameters such as roll load, diameter, and spacing. This is useful both to obtain less unfavorable residual stress with existing straighteners and to design the optimum straightener. Frommann (1965) performed parametric studies on a 7-roll straightener but focussed on the dimensional changes of the straightened rail, giving only limited, unexpected data for the resulting residual stresses.

The sections below discuss the determination of the important parameters for residual stress formation and some limited studies on a 4-roll straightener to investigate the effects of roll load and diameter. Four rolls are the minimum needed to obtain a straight rail. First, a beam model of an entire 4-roll straightener was used to determine roll deflections and corresponding forces to obtain a straight rail. Then, the "single-roll" model was used for two different straight-rail settings to investigate the effects of roll force/deflection on residual stress. Lastly, a larger roll was used for another case to investigate the effects of roll diameter.

2.5.1 Determination of most important parameters for study

Table 5 lists the many parameters that may affect residual stresses and straightness of the rail. The rail material and geometry, the straightener geometry and settings, and the guide rolls and lateral straightening may all influence the final state of the rail. However, the parameters most important for rail deformation and residual

28

stress are three of those inside the straightener: roll loads or displacements, roll spacing, and roll diameter. Appendix 1 discusses in detail the rationale for the choice of important parameters.

2.5.2 4-roll beam model for curvatures and roll forces

A 4-roll straightener was modelled to find settings for a "straight" rail (curvatures within AREA guidelines (1975) of less than 19 mm (0.75 in) deflection over a 11.9-m (39-ft) rail). Although the I-beam elements used only capture the bending of the rail, not local deformation, and thus are incapable of correctly modelling residual stress formation, they are quick to run and give insights on final curvatures of the rail and roll forces.

The beam element model (Fig. 51) consisted of four rigid rolls and 50 beam elements (a 5000 mm long rail). The upper rolls, 2 and 4, were fixed in the vertical and horizontal directions. The lower rolls, 1 and 3, were restrained horizontally and were given prescribed vertical displacements. Friction on roll 2 and a prescribed rotation were used to drive the rail through the straightener. Rolls 1, 3, and 4 were frictionless.

Instead of considering the vertical displacements of rolls 1 and 3 as independent variables, they can be combined in two pairs: the average upward roll displacement (bending at the first roll) and the slope of the line joining their centers. The amount of deformation occuring under roll 2 is affected only by the average displacement:

$$ave.\ upward\ displacement \equiv (u_1 + u_3)/2 . \tag{2.4}$$

The deformation under roll 3 is affected by this displacement and also by the slope of the line joining the centers of rolls 1 and 3, proportional to the difference in their respective displacements:

$$slope\ of\ roll\ 1 - 3\ axis \propto u_3 - u_1 . \tag{2.5}$$

The above expression has dimensions of length. Normalization by the roll spacing would give a slope.

Fig. 52 shows the variation of final curvature $1/R$ (normalized by the yield curvature $1/R_y$) with the slope of the roll 1-3 axis, for three different values of average upward displacement. The straightener settings for a "straight" rail are also indicated, and these settings are listed in Table 6 along with the roll loads.

The curvature study also gives an insight on straightener design. The average vertical deflections studied in the 4-roll beam model, and their accompanying roll loads, are typical of the first few (3-5) rolls of current roller-straighteners. The curvatures produced under such heavy settings are greater (at least 10 times) than incoming rail curvatures. This suggests that in multi-roll straighteners, the first few rolls serve to *produce* a large, reproducible curvature. Subsequent rolls, with gentler deformations, are set to remove this curvature, and the resulting machine does not have to adjust to fluctuations in initial curvature. In practice, some mills use lighter roll settings and have to do more "tuning" of the straightener to obtain a straight rail (Sydney Steel, private communication, 1989).

2.5.3 Effects of roll loads and diameter: studies with "single-roll" model

Effect of roll displacements/loads. Two straightener settings were used, corresponding to those in Table 6 with average displacement of 20 and 30 mm. The same, coarse, mesh was used as that for the 3-roll straightener studies (Fig. 39). The final longitudinal residual stress distributions for both cases (Fig. 53) have the Z-shaped distribution typical of bending. The values of stress are similar in the head and base, with discrepancies in the web that are probably due to the coarse mesh (2 8-node elements high) there. This study, giving Z-shaped residual stress distributions, does not shed light on the effects of roll loads and moment distributions on the magnitude of the U-shaped distribution arising from the last few straightener rolls.

Effects of roll diameter. Roller-straighteners have horizontal roll spacings of 1140-1800 mm, with a typical spacing chosen to be 1500 mm. Changing this spacing would require redesign and rebuilding of the straightening machine. Therefore,

variations in roll diameter are practically limited by the roll spacing. It was felt that an increase in roll diameter should be studied, since this should decrease the local deformation and resulting residual stresses. With a spacing of 1500 mm, the largest possible roll diameter was estimated to be 1150 mm, a 20% increase from the typical diameter of 950 mm. The "single-roll" model was used to compare the final residual stresses for these two roll diameters, using settings for the 9-roll straightener of Fig. 46. Fig. 54 shows the residual stress after roll 2, for the standard and larger roll diameter. The stress distributions are almost identical. This is also the case for the stress after roll 7 (skipping rolls 3-5), shown in Fig. 55. It can therefore be concluded that both for the bending regime where the rolls produce a Z-shaped stress distribution, and for the end of the straightener where a U-shape appears, there is no noticeable effect of increasing the roll diameter by 20%. This may not be surprising, since even under the last rolls a significant portion of the head or base is yielding under the roll and plastic strains are as much as 5 times the yield strain. This is far too much for application of the elastic (Hertz) theory of contact, which predicts decreasing stress with increasing roll diameter.

2.6   Recommendations for straightening

It has been demonstrated that the unfavorable U-shaped residual stress arises in the last straightener rolls, where the bending moment is less than that to produce yielding but where there is still significant deformation under the roll. The question of development of unfavorable residual stresses, then, reduces to that of the tendency of the last rolls to change a Z- to a U-shape. Increasing the roll diameter by 20% seems to have no effect on the residual stresses. A straightener having high loads and high bending moments under all but the last roll may leave only a Z-shape in the rail if the last roll is lightly loaded enough so as not to cause significant deformation. This could be assured by increasing the horizontal spacing to the last roll, so that a light load on this roll creates a significant bending moment at the previous roll. However, further investigation should be done to find combinations

of roll loads and moments needed to avoid a U-shaped stress distribution.

2.7 Alternative processes

The work described above has focussed on analyzing the roller-straightening process in order to suggest improvements which reduce the unfavorable residual stresses produced. However, roller-straightening is only a small part of the process of rail manufacture. Avoiding unfavorable residual stresses requires consideration of the entire process, giving several possible approaches: avoid the need to straighten, improve the roller-straightener, or use an alternate method of straightening.

Rail manufacturers often attempt to compensate for curvature due to cooling by pre-curving the rails in the hot mill. This does not seem to be done with enough accuracy to achieve the desired straightness. Some mills keep the rail base hot while the head cools, reducing warpage. Unfortunately, some of these mills still need to roller-straighten the rail. A third way to obtain straight rail is by using an induction heat-treating process (Sommer et al. 1988) which holds the rail straight as it cools, giving straight, heat-treated rail without unfavorable residual stress. However, unlike roller-straightening, this process operates at less than the usual production speed, requiring several such heat-treaters to be installed.

Improving the roller-straightener may be possible by proper adjustment of imposed roll displacements or loads. In addition, heating the rail web after straightening to relieve residual stresses, and straightening with a hot web, have been considered (Heller et al. 1987), but it is not clear whether such steps are taken in actual rail production.

An alternate method of straightening is stretch-straightening (Deroche et al. 1982), in which a rail is pulled between grips so that it straightens. This method gives straight rails with essentially no residual stress (Deroche et al. 1982, ORE 1987), but is slow and wastes material at either end of the rail. However, with the current trend toward longer rails, this technique may become more economical.

There are, then, several ways to minimize the problem of unfavorable residual

stress in rails, such as those from the roller-straightener. Decisions on what method to use will probably need to be made individually by each mill, taking into account the specific process, plant layout, and customer requirements, and the associated economics.

2.8 Conclusions

In this work, models for residual stress formation during roller-straightening were developed. Then, the effects of process parameters (applied roll load or displacement, roll diameter and spacing) were investigated in order to suggest ways to minimize unfavorable residual stresses.

1. The deformation of the rail in the straightener is really a three-dimensional problem. However, plane stress models of the straightener are adequate to model the resulting residual stresses.

2. A plane stress, "single-roll" model for the first two loaded rolls in the straightener gives qualitative agreement with strain gage data taken at three locations on the rail. Disparities between experimental and calculated residual stresses appear to result from idealization of boundary conditions and material behavior in the finite element model, and from the coarse mesh used.

3. The unfavorable, U-shaped longitudinal residual stress distribution found in roller-straightened rail arises from the last straightener rolls, where the bending moment is relatively low and most of the plastic deformation occurs under the roll, due to the high contact stresses there.

4. Increasing the roll diameter by 20% has no effect on residual stresses, both in the initial, heavier loaded rolls, and in the final rolls producing the U-shaped stress distribution. This is not surprising since the amount of plastic deformation is too great for the elastic (Hertz) theory of contact to apply.

5. A straightener that maintained high bending moments throughout would avoid the U-shaped residual stress distribution, giving instead a Z-shape from bending deformation. This may mean that the spacing to the last roll must be very large, so that there can be a small force on the last roll and still a large moment at the next-to-last roll. Further investigation is needed to determine the combinations of roll force and bending moment to avoid the U-shaped residual stress distribution.

6. The best solution to the problem of unfavorable residual stresses from straightening must be based on the overall process of rail manufacture. It may be more economical to avoid the need to straighten by reducing or avoiding initial curvatures or to use an alternate method of straightening than to redesign the roller-straightener.

2.9 References

1. ABAQUS (1987, 1989) A general-purpose finite element code with emphasis on nonlinear applications, versions 4.6, 4.7, and 4.8, *Hibbitt, Karlsson, and Sorensen Inc.*, Providence, RI.

2. AREA (1975) *Manual for Railway Engineering (Fixed Properties)*, American Railway Engineering Association, Washington, D.C., Chapter 4, Sec. 4-2-4.2.

3. AREA (1978) *Manual for Railway Engineering (Fixed Properties)*, American Railway Engineering Association, Washington, D.C., Chapter 4, Sec. 4-1-6.

4. Babich, A.P., Bikhunov, L.Ya., Chernov, E.I., Vereshchaga, E.A. (1982) "Influence of cold straightening on quality of rails quenched after high frequency current heating", *Steel in the USSR*, **12**(7), 318-320.

5. Botschen, K.F., Steck, R. (1982) "Bearing rigidity, a precondition for straightening section material", *Ball and Roller Bearing Engineering*, **21**(2), 23-25.

6. Bower, A.F. (1989) "Cyclic hardening properties of hard-drawn copper and rail steel", *J. Mech. Phys. Solids*, **37**, 455-470.

7. Christiansen, H.P. (1988) Colorado Fuel and Iron, Pueblo, CO, private communication and tour of facility.

8. Dabell, B.J., Hill, S.J., Watson, P. (1978) "An Evaluation of the fatigue performance of conventional British rail steels", *Rail Steels–Developments, Processing, and Use, ASTM STP 644*, D.H. Stone and G.G. Knupp, eds., American Society for Testing and Materials, 430-448.

9. Das Talukder, N.K., Johnson, W. (1981) "On the arrangement of rolls in cross-roll straighteners", *Int J. Mech. Sci.*, **23**, 213-220.

10. Deroche, R.Y., et al. (1982) "Stress releasing and straightening of rails by stretching", Paper no. 82-HH-17, *Proc. Second International Heavy Haul Railway Conference*, Colorado Springs, CO.

11. Didyk, S.H. (1988) Sydney Steel, Sydney, Nova Scotia, private communication.

12. Frommann, K. (1965) "Über die Formänderungen beim Richten von Schienen auf einer Rollenrichtmaschine", Doktor-Ingenieurs Dissertation, Fakultät für Bergbau und Hüttenwesen der Rheinisch-Westfälischen Technischen Hochschule Aachen.

13. Hahn, G.T., Bhargava, V., Chen, Q. (1988) "The cyclic stress-strain properties, hysteresis loop shapes and kinematic hardening of a rail steel", unpublished, Vanderbilt University, Nashville, TN   37235.

14. Heller, W., Weber, L., Schweitzer, R., Flügge, J. (1987) *Method for Reducing Internal Stresses of Roller Straightened Rails*, U.S. Patent No. 4,659,398, Apr. 21, 1987.

15. Hibino, F., Kunii, A. (1971) "Residual stress after roller levelling", *Annals of the C.I.R.P.*, **XVIV**, 347-360.

16. Journet, B. (1983) "Fatigue properties of rail steels", S.M. thesis, Department of Materials Science, M.I.T.

17. Konyukhov, A.D., Rabinovich, D.M., Vinokurov, I.Ya., Serebryakov, V.S. (1969) "Effects of production methods on the residual stresses in completely quenched rails", *Stal* (English), **6**, 591-3.

18. Konyukhov, A.D., Reikhart, V.A., Kaportsev, V.N. (1973) "Comparison of two methods for assessing residual stresses in rails", *Industrial Laboratory (USSR)*, **39**, 117-119.

19. Lee, Y.-S., Dawson, P.R., Dewhurst, T.B. (1989) "Bulge predictions in steady state bar rolling processes", *Numiform 89*, Thompson et al. eds., Balkema, Rotterdam, 323-330.

20. Leis, B.N. (1978) "Cyclic inelastic deformation and fatigue resistance characteristics of a rail steel", *Rail Steels–Developments, Processing, and Use, ASTM STP 644*, D.H. Stone and G.G. Knupp, eds., American Society for Testing and Materials, 449-468.

21. Lempitskiy, V.V., Kazarnovskiy, D.S. (1973) "Improving the service life and reliability of railroad rails", *Russian Metallurgy*, **1**, 111-117.

22. Marcelin, J.L., Abouaf, M., Chenot, J.L. (1986) "Analysis of residual stresses in hot-rolled complex beams", *Computer Methods in Applied Mechanics and Engineering*, **56**, 1-16.

23. Masumoto, H., et al. (1982) "Production and properties of a rail of high serviceability", 61st Transportation Research Board Annual Meeting, Washington, D.C.

24. McEvily, A.J., Ochi, Y. (1985) "A comparison of six rail steels", final report to Conrail, Institute of Materials Science, University of Connecticut, Storrs, CT.

25. Meier, H. (1936) "Eigenspannungen in Eisenbahnschienen", *Organ Fortschr. Eisenbahnwesen*, **91**, 321-329.

26. Noé, A., Fischer, F.D., Schwenzfeier, W. (1986) "Theoretische und praktische Untersuchungen zum Streckbiegerichten", *Stahl und Eisen*, **106**(21), 1131-1137.

27. *Numiform 86: Numerical Methods in Industrial Forming Processes: Proceedings* (1986) Mattiasson, K., Samuelsson, A., Wood, R.D., Zienkiewicz, O.C., eds., A.A. Balkema, Rotterdam.

28. *Numiform 89: Numerical Methods in Industrial Forming Processes: Proceedings* (1989) Thompson et al. eds., A.A. Balkema, Rotterdam.

29. ORE (1984) "Factors influencing the fracture resistance of rails in the unused condition", in: *Possibilities of Improving the Service Characteristics of Rails by Metallurgical Means, Report No. 1*, Office for Research and Experiments of the International Union of Railways (ORE/IUR), Utrecht.

30. ORE (1987) "Studies concerning the measurement and improvement of the level of residual stresses", in: *Possibilities of Improving the Service Characteristics of Rails by Metallurgical Means, Report No. 4*, Office for Research and Experiments of the International Union of Railways (ORE/IUR), Utrecht.

31. Orkisz, J., Harris, A. (1988) "Analysis of residual stresses at shakedown: a hybrid approach", *Theor. Appl. Frac. Mech.*, 9, 109-121.

32. Orringer, O., Morris, J.M., Steele, R.K. (1984) "Applied research on rail fatigue and fracture in the United States", *Theor. Appl. Fracture Mech.*, 1, 23-49.

33. Roberts, J.M., Sheppard, T. (1971) "On the mechanics of the tension-levelling process", *J. Inst. Metals*, 99, 293-301.

34. Samways, N.L. (1986) "Wheeling-Pittsburgh's modern continuous casting/rail mill complex", *Iron and Steel Engineer*, 25-31.

35. Schmedders. H. (1979) "A chromium-vanadium alloyed rail steel for heavy duty requirements", in: *Vanadium in Rail Steels*, Proc. Seminar in Chicago, Nov. 1979, VANITEC, London, 3-11.

36. Schweitzer, R., Flügge, J., Heller, W. (1985) "Einflüsse auf das Bruchverhalten von Schienen", *Stahl und Eisen*, 105, 1451-1456.

37. Scutti, J.J. (1982) "Fatigue properties of rail steel", S.M. thesis, Department of Materials Science, M.I.T.

38. Sheppard, T., Roberts, J.M. (1972) "On the strip-to-roll conformity in the tension-levelling process", *J. Inst. Metals*, 100, 130-135.

39. Sommer, R.A., Faber, M.R., Jennings, R.E. (1988) *Method for Heat Treating Rail*, U.S. Patent No. 4,749,419, June 7, 1988.

40. Sunwoo, H., Fine, M.E., Meshii, M., Stone, D.H. (1982) "Cyclic Deformation of pearlitic eutectoid rail steel", *Met. Trans. A*, 13A, 2035-2047.

41. Tokunaga, H. (1961) "On the roller straightener", *Bulletin of the JSME*, 4(15), 605-611.

42. Tselikov, A.I., Smirnov, V.V. (1965) *Rolling Mills*, Pergamon, p. 254-278.

43. Utrata, D. (1989) "Residual stress distributions measured along rail lengths", Appendix VII of minutes of AREA 4 meeting, Spring 1989, Sept-Îles, Québec.

44. Vorozhishchev, V.I., Kisil', B.S., Babich, A.P., Ermolaev, V.N., Lysenko, I.K., Yudin, N.S. (1983) "Heat-treating and improving the quality of rails at the Kuznetsk metallurgical combine", *Metallurgist*, **26**(7-8), 296-298.

45. Wineman, S.J., McClintock, F.A. (1987) "Rail web fracture in the presence of residual stresses", *Theor. Appl. Fracture Mech.*, **8**, 87-99.

46. Wunderlich, W., Brünig, M., Obrecht, H. (1988) "Theoretisch-numerische Modellbildung und rechnerische Simulation zur Entstehung von Eigenspannungen beim Rollenrichten von Schienen", Abschlußbericht zum Projekt 153 der Studiengesellschaft für Anwendungstechnik von Eisen und Stahl e.V., Düsseldorf, unter Verwendung von Versuchsergebnissen der Krupp Stahl AG, Werk Rheinhausen, Qualitätswesen und Forschung, (unpublished report), December 1988.

2.10 Appendix 1: Comments on parameter selection

Table 5 shows the straightener parameters and their relative importance. Reasons for these choices are given below.

A. Material

1. The straightening temperature is assumed room temperature for the first approximation. In some mills, the rails are warmer than this (but not glowing). Near room temperature, the effect on mechanical properties should be small but for warmer rails may be significant.The effects of the elevated temperature should be included in a more thorough study but will be neglected in the first approximation.

2. Highly non-proportional loading occurs as the flange of the rail passes under the roll. The difference between a conventional kinematic hardening material model and one which includes effects of non-proportional loading bears consideration, but is beyond the scope of this study. Also, the bilinear kinematic hardening stress-strain behavior, which is an option in the program ABAQUS, is itself an approximation to the actual, more rounded stress-strain curve.

3. and 4. Rails with different yield strengths and hardening behavior will develop different residual stresses after straightening. The effects of these properties should be studied but are beyond the scope of this work.

B. Rail geometry

1. Initial curvatures affect the final straightness in light straightening. In heavy straightening, they have little effect on final straightness. Initial curvatures may be important for study, but it was felt more important to focus on more controllable aspects such as the straightener settings.

2. Different rail proportions (e.g. different head/web thickness) may have an effect on the deformation under the rolls and therefore the residual stresses produced. Although study of this effect is not practical in the sense that the rail rolling dimensions cannot be changed appreciably, it may shed light on the residual stresses produced in different types of rail.

3. Changing the rail size with respect to the straightener is the same as changing

the straightener parameters with respect to the rail, and therefore need not be treated separately.

C. Inside the straightener

1. Roll loads or imposed displacements affect the magnitudes of contact stresses and the bending and shear stresses in the rail. Therefore they are of prime importance for study.

2. Roll spacings affect the bending and shear stresses in the rail and are of prime importance.

3. Lateral loadings are negligibly small, since the flanges are allowed to spread.

4. Larger roll diameters create lower contact stresses and are important for study.

5. The roll-rail contact geometry is important in that it affects the contact stresses. However, generally the rolls start out contoured to the rail and wear over time. Also, although the base rolls actually do not contact the full base width, the length of contact corresponds roughly to the contacting length with anticlastic curvature of the flange tips. Therefore flat rolls, head, and base should be sufficient for a first approximation.

6. As a first approximation, friction will be neglected. The coefficient of friction between roll and rail, and the resulting longitudinal forces, are insufficient to develop inter-roll stresses which are significant compared to yield.

7. Sequencing of roll loads and deformations may be very important, especially if residual stresses can be reduced, say, by using heavier or lighter passes in the last few rolls. However, 5 rolls or more are needed for study of sequencing effects.

8. Since as a first approximation the rail is treated as being at room temperature, strain rate effects should be neglible. Therefore the overall feed velocity should not be important. (With warmer rails, this may become more important.)

9. For typical coefficients of friction, the longitudinal frictional forces accompanying typical roll loads are too small to cause significant longitudinal stresses in the rail. Therefore different speeds from roll to roll in the straightener should not be able to build up significant stresses between rolls and are not important for study.

40

D. External to the straightener

1. and 2. The start and end boundary conditions (guide rolls and vertical straightener) are not thought to cause the rail to yield in the straightener. They will not be considered as parameters in the straightening study.

Table 1. Composition, yield strength, tensile strength, and Brinell hardness (BHN, kg/mm^2) of typical rail steels (from Schmedders 1979, Orringer, Morris and Steele 1984).

Alloy	Composition (wt%)						Yield Strength (MPa)	Tensile Strength (MPa)	BHN
	C	Mn	Si	Cr	Mo	V			
Carbon (North America)	0.69-0.82	0.70-1.00	0.10-0.25	-	-	-	480	920	255
Carbon (Europe)	0.40-0.60	0.80-1.20	0.05-0.35	-	-	-		690-830	
Carbon (Japan)	0.65-0.75	0.70-1.10	0.10-0.30	-	-	-		780	
High-Si	0.75	0.80	0.65	-	-	-	520	980	285
Cr-V	0.70	1.00	0.70	1.00	-	0.10	640	1080	325
1% Cr	0.75	0.65	0.25	1.15	-	-	650	1100	320
Cr-Mo	0.75	0.81	0.26	0.69	0.18	-	790	1210	350

Table 2. Curvature and longitudinal residual stress magnitudes before and after roller-straightening.

	Before Straightening	After Straightening
Curvature (max. deflection)	wide range of magnitude and sense	$\leq$ 19 mm over 11.9 m (AREA 1975) $\leq$ 20 mm over 20 m (ORE 1987) $\leq$ 12 mm over 25 m (Babich 1982)
Typical longitudinal residual stress through cross-section	max. of $\pm$50 MPa	max. of $\pm$100-300 MPa; typical U-shape

Table 3. Roller-straightener parameters.

Roll diameter	550-1200 mm
Roll spacing	1140-1800 mm
Maximum applied displacement[1] (displacement-controlled machines)	8-25 mm
Decrement of applied displacement between lower rolls (displacement-controlled machines)	2-7 mm
Maximum applied force[1] (force-controlled machines)	980-1470 kN (100-150 tonnes)
Decrement of applied force between lower rolls (force-controlled machines)	$\approx$295 kN ($\approx$30 tonnes)

[1] Depends on type of rail section and severity of initial curvatures.

Sources: ORE 1987, Schweitzer et al. 1985, Botschen and Steck 1982, Babich 1982, Konyukhov Rabinovich et al. 1969, Frommann 1965, and private communications with mill operators.

Table 4. Comparison of experimental (ORE 1987) and finite element (static loading) results for 9-roll straightener.

Roll	1	2	3	4	5	6	7	8	9
Nominal displacement (mm)		0	17	0	9	0	7	0	4
Approximate actual displacement (mm)			14		6		4		1
Measured loads: rolling (kN)			1080-1190		1400-1420		980-970		
stopped (kN)			940-1060		770-860		710-750		
F.E. loads: (static, kN) plane stress elements	(0.004)	-387	1138	-1428	1272	-1110	864	-443	94
beam elements	(0.004)	-396	1166	-1476	1321	-1134	865	-435	88

Note: For the finite element models, rolls 2, 4, 6, and 8 were assumed to have zero vertical deflection and roll 1 (a guide roll) was given a load of 0.004 kN.

Table 5. Selection of straightener parameters.

Parameters	Most important	Secondary	Neglect
A. Material			
1. hot rail (properties not stable)		X	
2. Material other than kinematic hardening; non-proportional loading		X	
3. different amounts of hardening		X	
4. different yield strengths		X	
B. Rail geometry			
1. initial curvatures/kinks		X	
2. different rail proportions (w.r.t. 136RE rail)		X	
3. diff. rail proportions (w.r.t. straightener)			(X)
C. Inside the straightener (macro-loadings on rail)			
1. roll load or imposed displacement	X		
2. roll spacing	X		
3. lateral loadings			X
(affect local contact)			
4. roll diameter	X		
5. roll-rail contact geometry		X	
6. friction/lubrication		X	
(as rail passes through)			
7. sequencing of loads and deformations (need at least 5 rolls)		X	
8. overall velocity			X
9. relative roll speed			X
D. External to straightener			
1. cooling bed and guide rolls (before str.)			X
2. vertical straightener (after str.)			X

Table 6. Settings for a straight rail (curvature within AREA guidelines), 4-roll beam element model.

average displacement $(u_1 + u_3)/2$ (mm)	slope $(u_3 - u_1)$ (mm)	u_1 (mm)	u_3 (mm)	F_1 (kN)	F_2 (kN)	F_3 (kN)	F_4 (kN)
15.	-30.33	30.165	-0.165	462.21	-1206.4	1105.9	-361.71
20.	-46.769	43.3845	-3.3845	503.43	-1302.7	1181.2	-381.95
30.	-77.24	68.62	-8.62	618.24	-1507.5	1294.9	-405.68
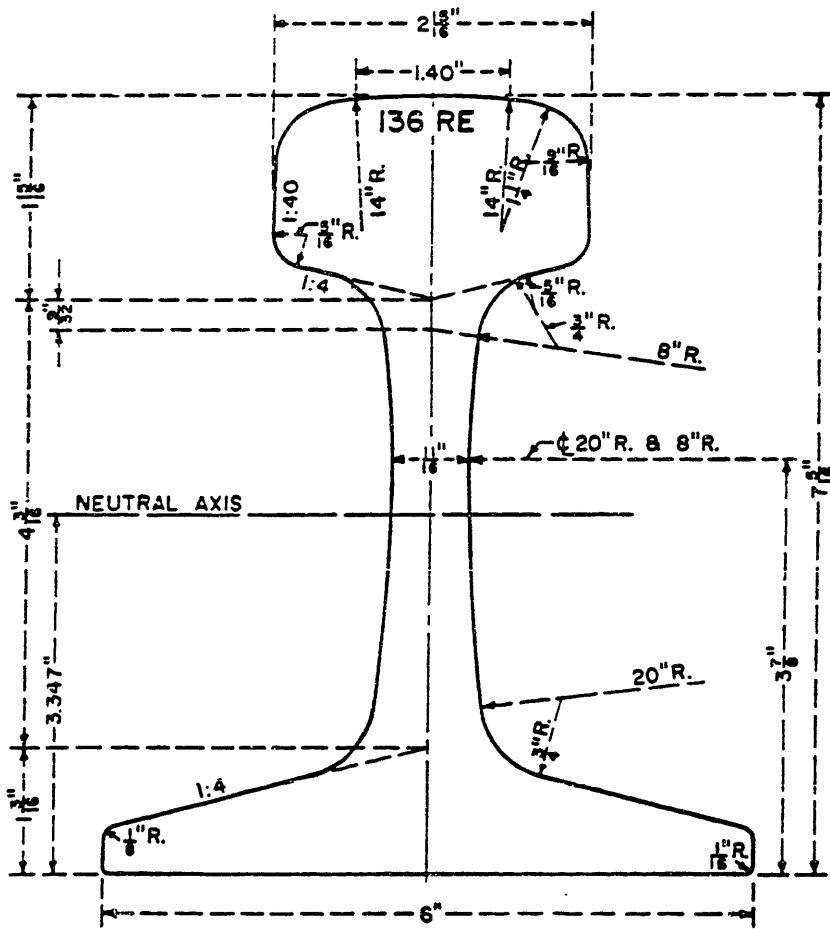
	Area Sq In	Percent	
Head	4.86	36.4	Moment of inertia 94.9
Web	3.62	27.1	Section modulus, head 23.9
Base	4.87	36.5	Section modulus, base 28.3
			Ratio m.i. to area 7.11
	———	———	Ratio s.m. head to area 1.79
			Ratio height to base 1.22
Total	13.35	100.0	Calculated weight, lb per yd 136.2

Fig. 6—136 RE rail section.

Fig. 1. 136RE rail section (AREA 1978).

48
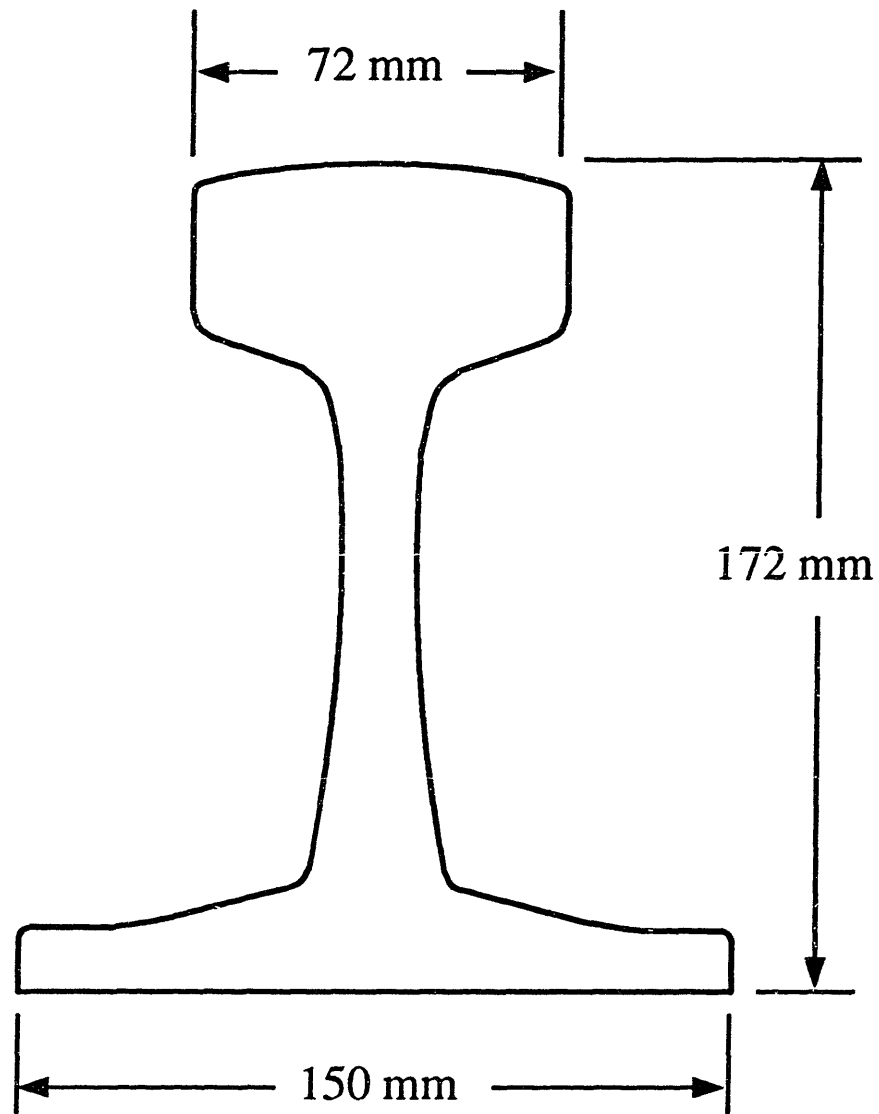
Fig. 2. UIC60 rail section (US DOT/TSC, private communication, 1990).
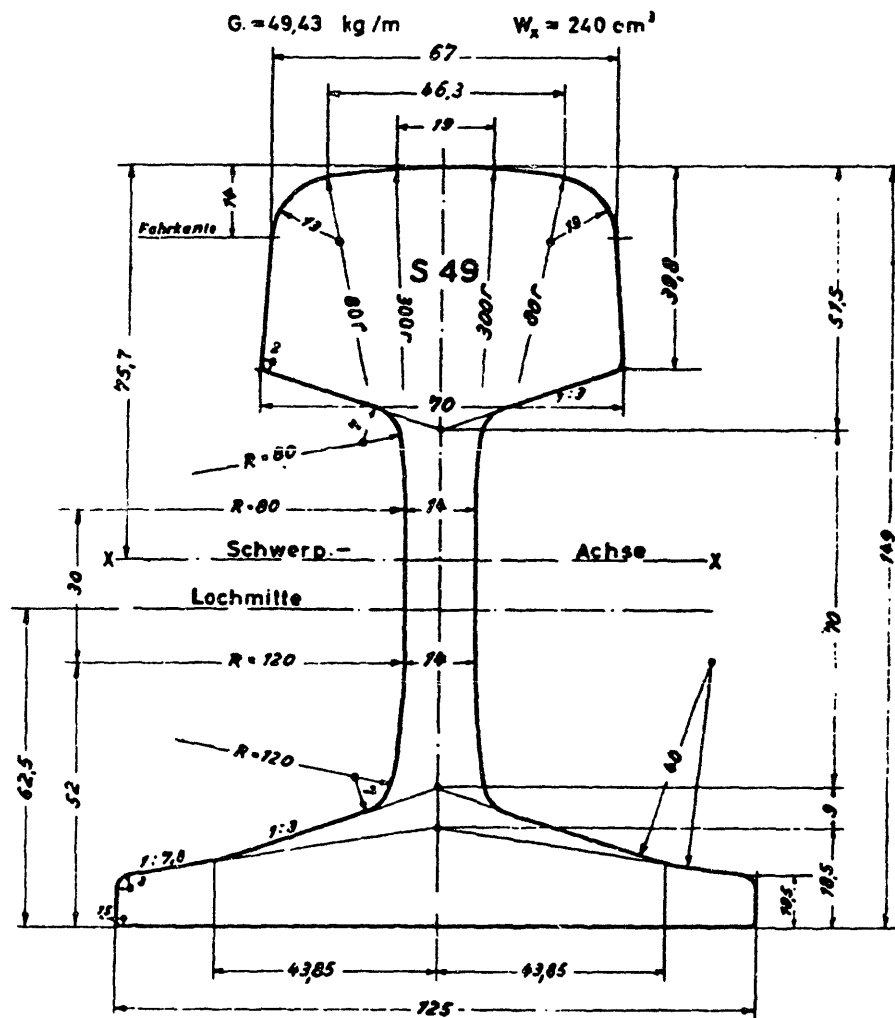
Bild 14. Schiene S 49 (Deutsche Bundesbahn).

Fig. 3. S49 rail section (Frommann 1965).
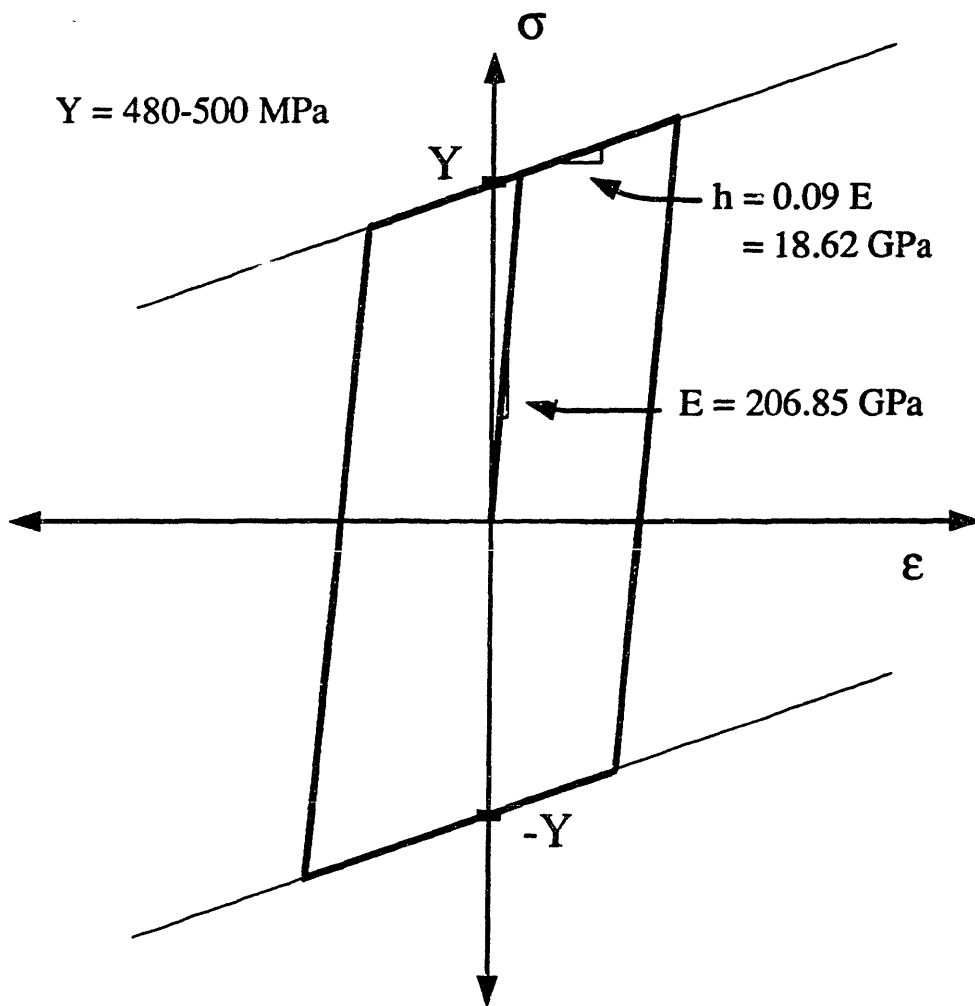
Fig. 4. Bilinear kinematic hardening approximation for behavior of carbon rail steel.

51
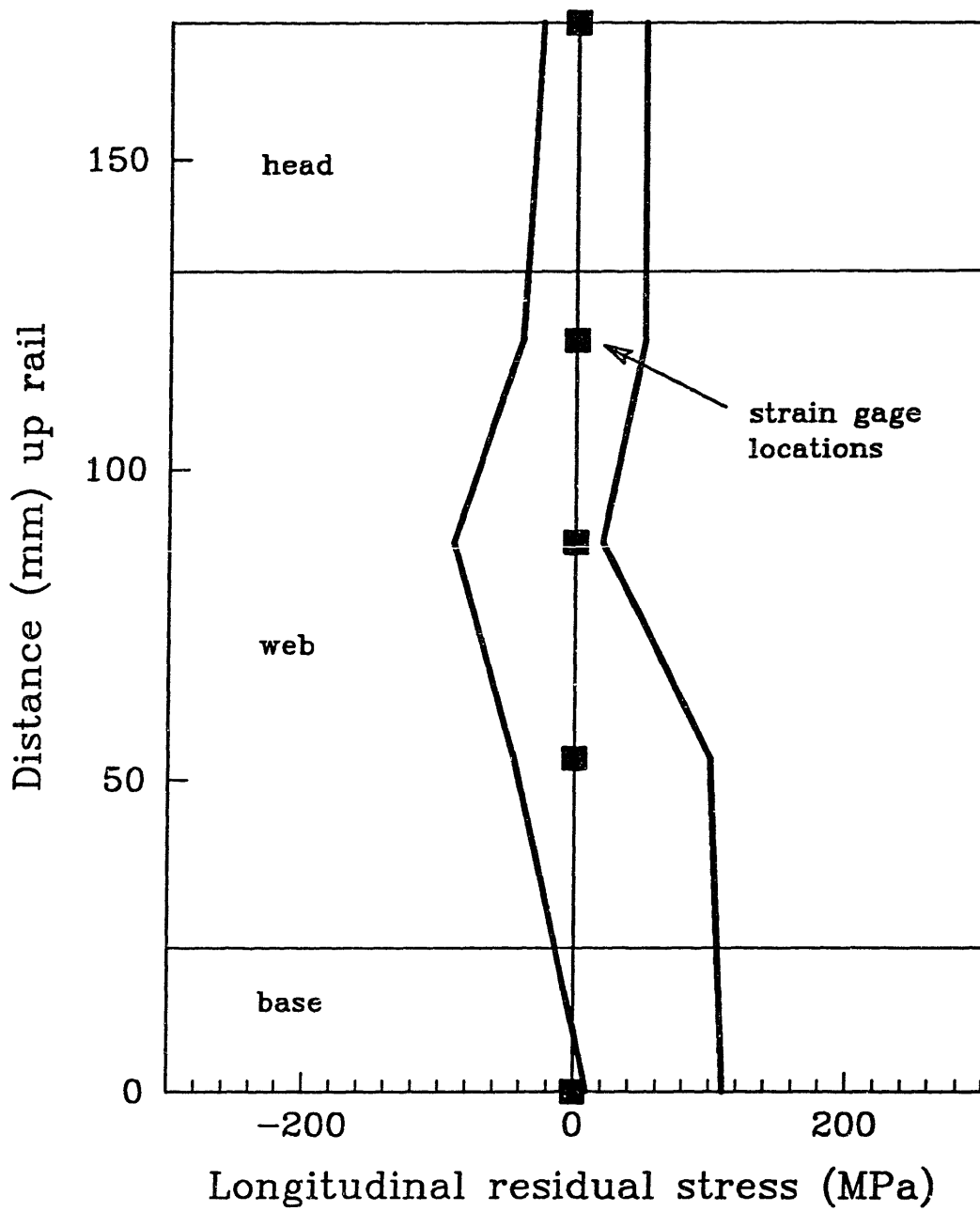
Fig. 5. Scatterband of measured longitudinal residual stress for unstraightened carbon and alloy rail (from ORE 1984).
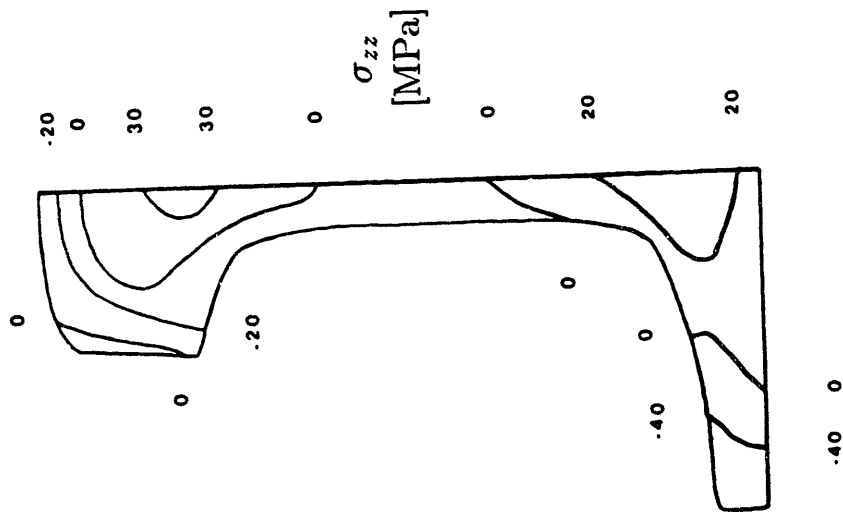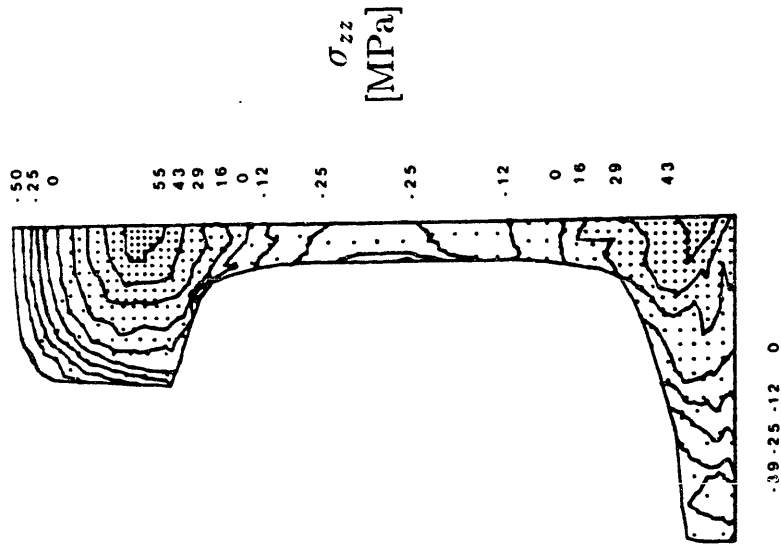
Fig. 6. Contours of calculated longitudinal residual stress from cooling (Marcelin, Abouaf, and Chenot 1986).
a) Elasto-plastic model. b) Elasto-viscoplastic model.
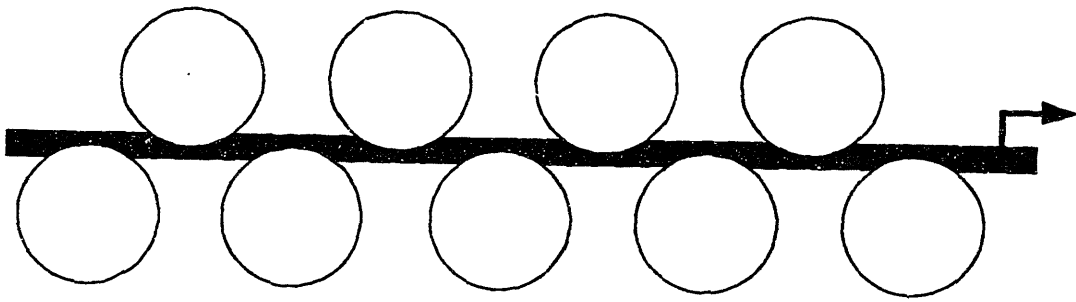
a) Europe and North America
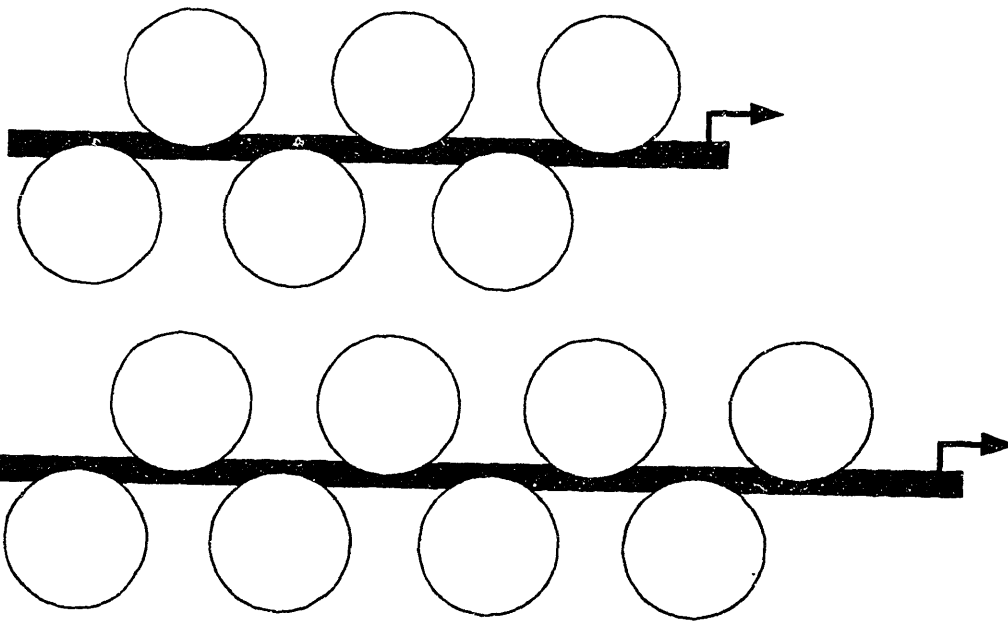
b) Soviet Union

Fig. 7. Roller-straightener configurations used in Europe, North America, and the Soviet Union (sources: ORE 1987, Schweitzer, Flügge and Heller 1985, Botschen and Steck 1982, Babich 1982).

54
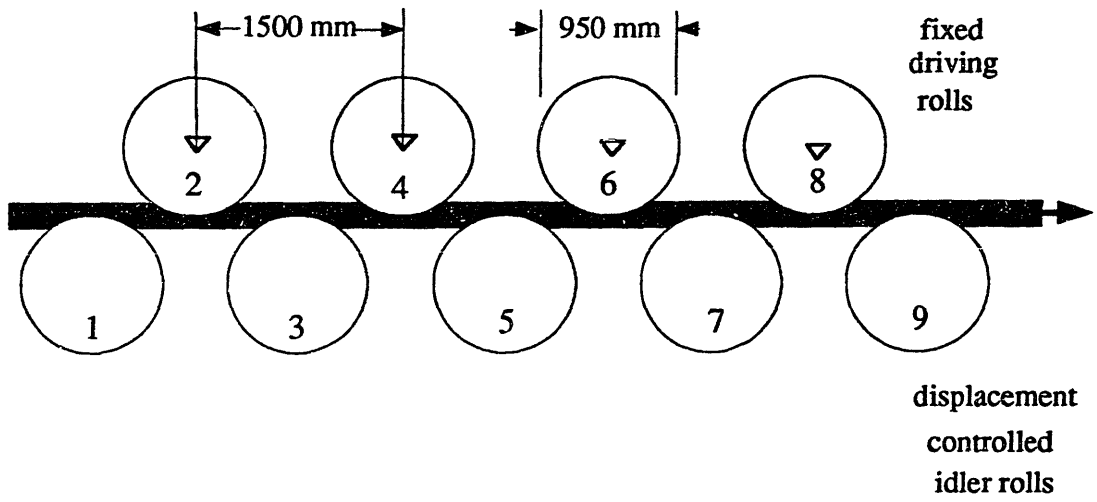
Fig. 8. Roller-straightener used for modelling.
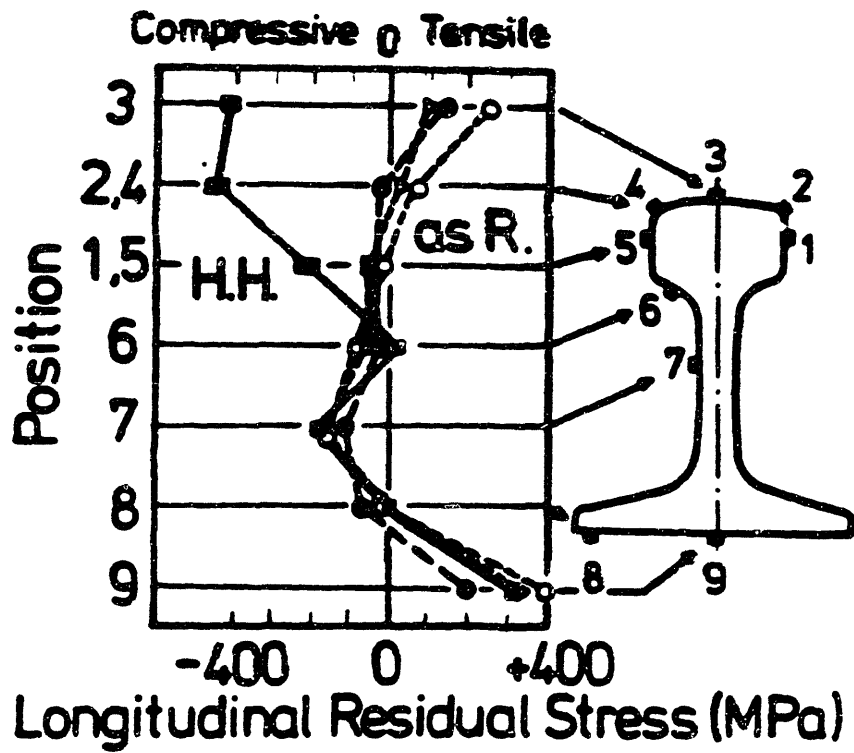
Fig. 9. Longitudinal residual stress on the surface of head-hardened or as-rolled rails (Masumoto et al. 1982).
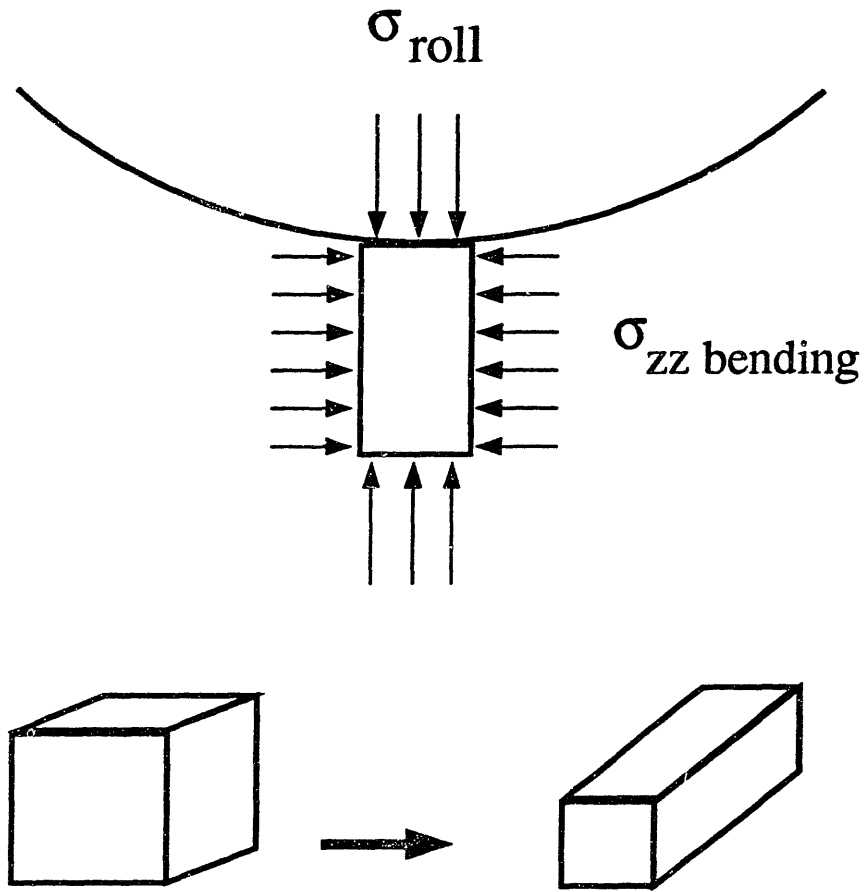
Fig. 10. Deformation of a small element in the flange as it passes beneath the roll, resulting in a decrease in length and height and an increase in width.

0.027 rail height

transition
region

1 rail height

zero
. . . ,
st.

-500   0   500

σ_{zz} residual after roll
(MPa)

σ_{zz} head

uniform
σ_{zz} web

σ_{zz} base
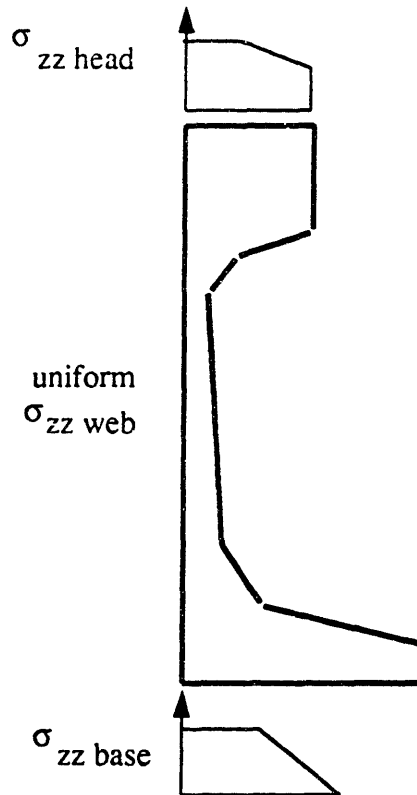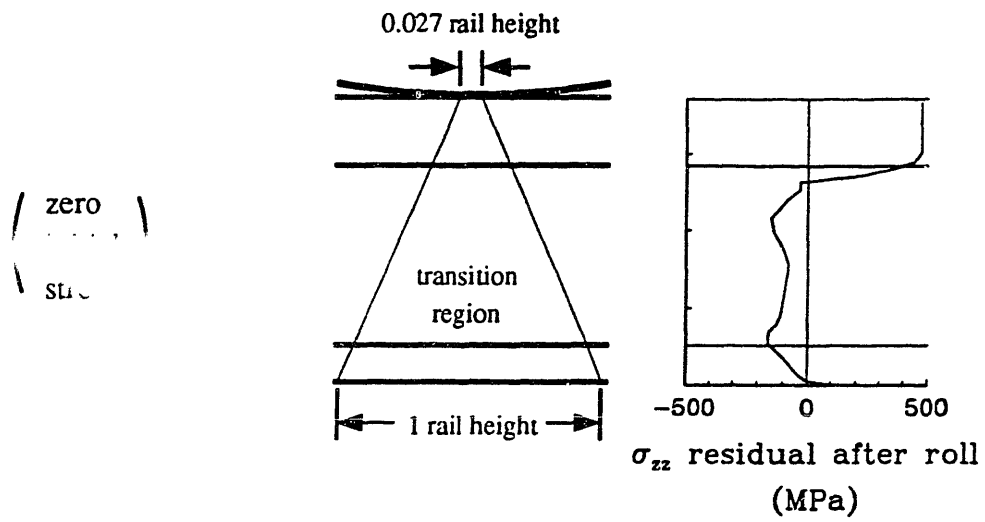
Fig. 11. Initial longitudinal residual stress for the finite element study of head loading.

σ_{zz} residual before roll (MPa)

1 rail height

transition region

0.027 rail height

σ_{zz} residual after roll (MPa)

σ_{zz} head

uniform σ_{zz} web

σ_{zz} base
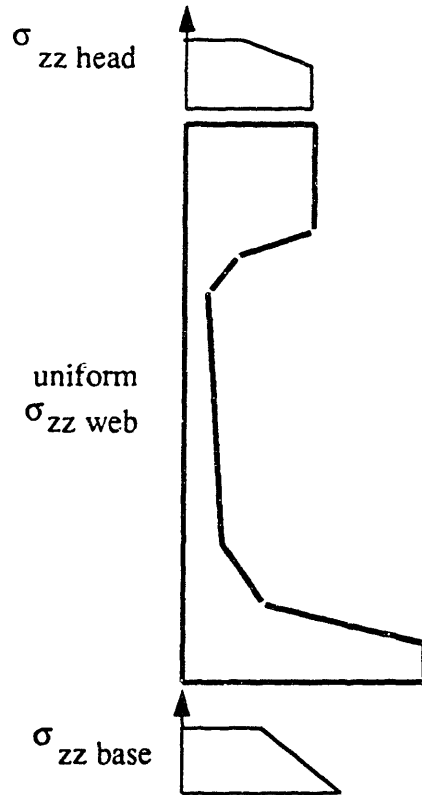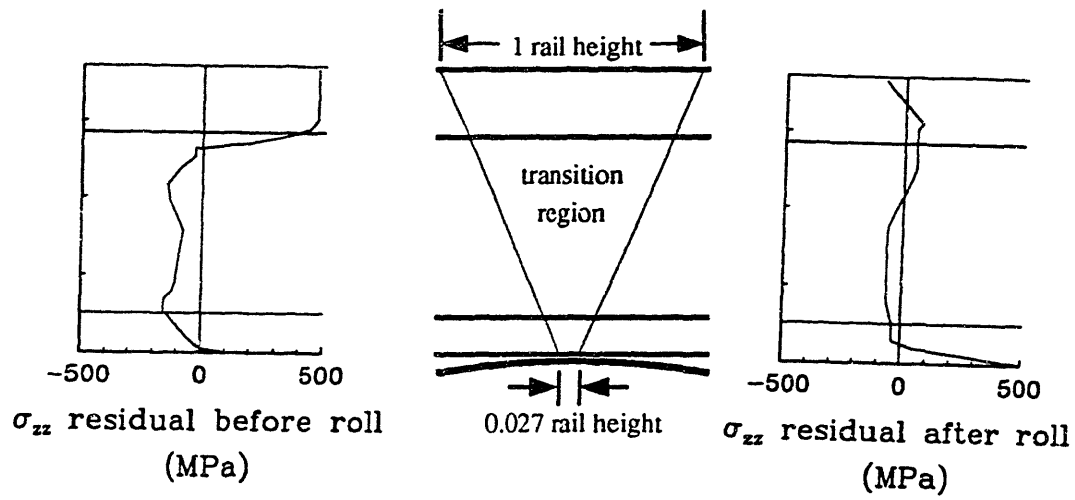
Fig. 12. Initial longitudinal residual stress for the finite element study of base loading.
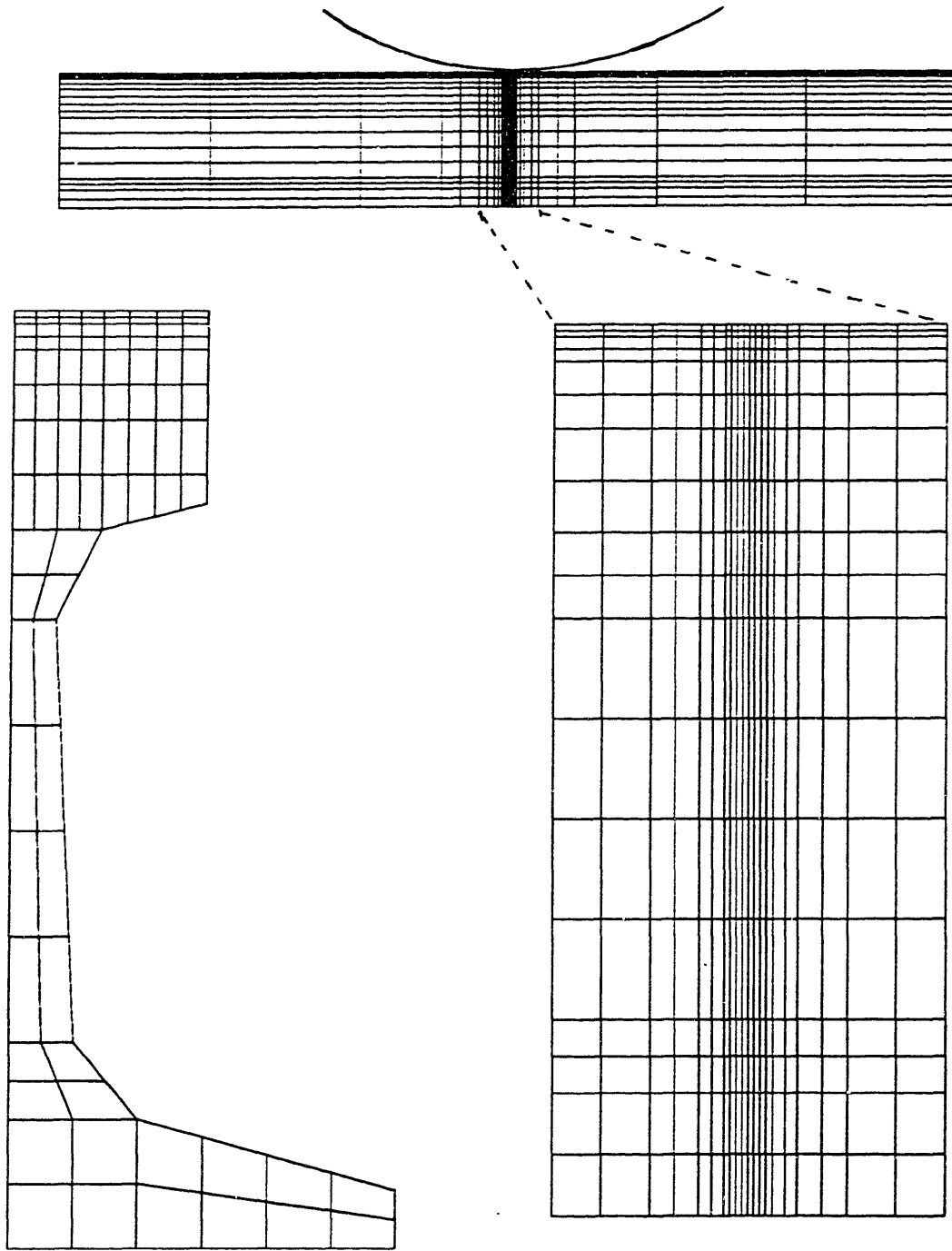
Fig. 13. Three-dimensional mesh for static loading of the rail head.
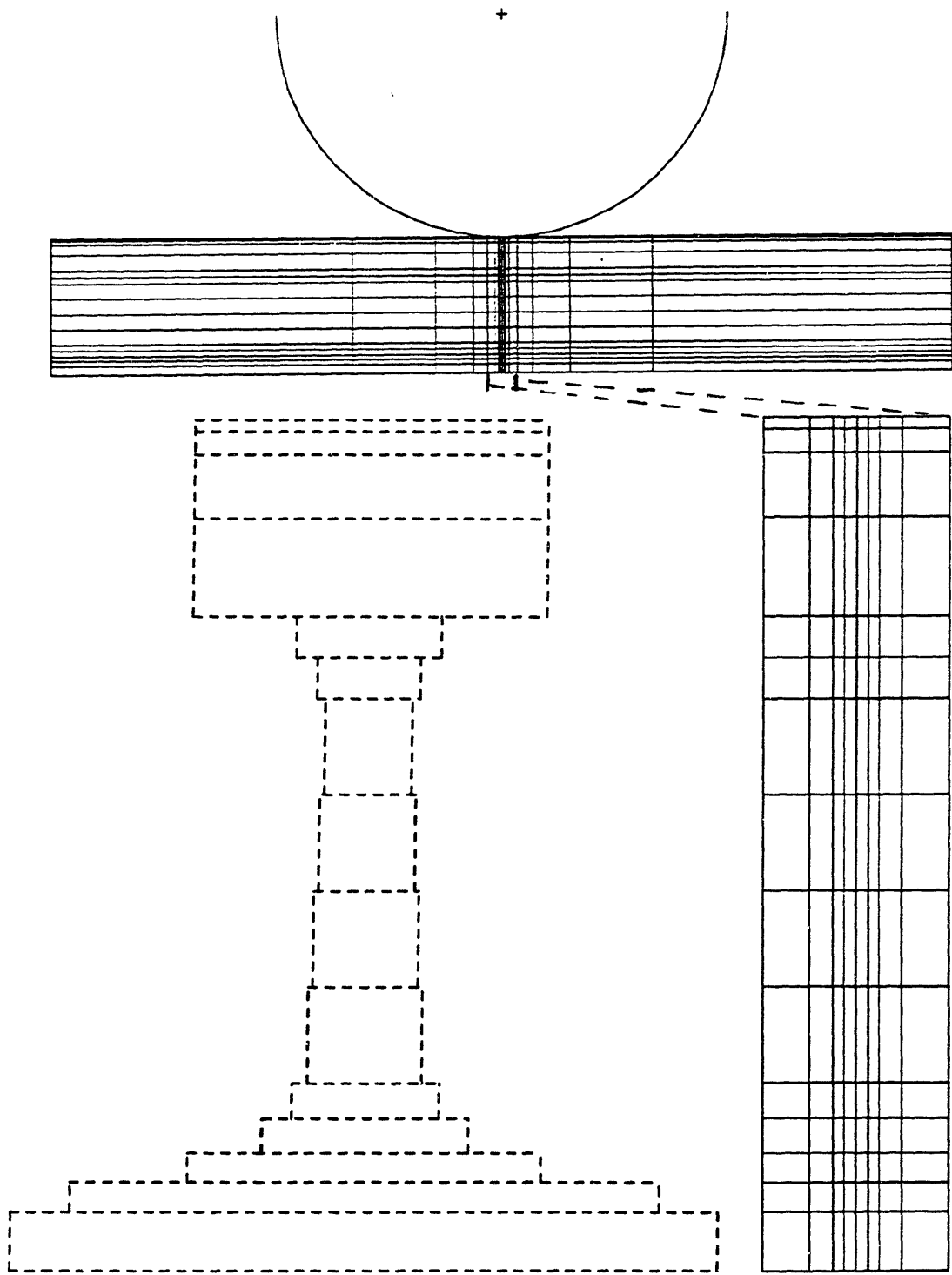
Fig. 14. Two-dimensional mesh for static loading of the rail head.
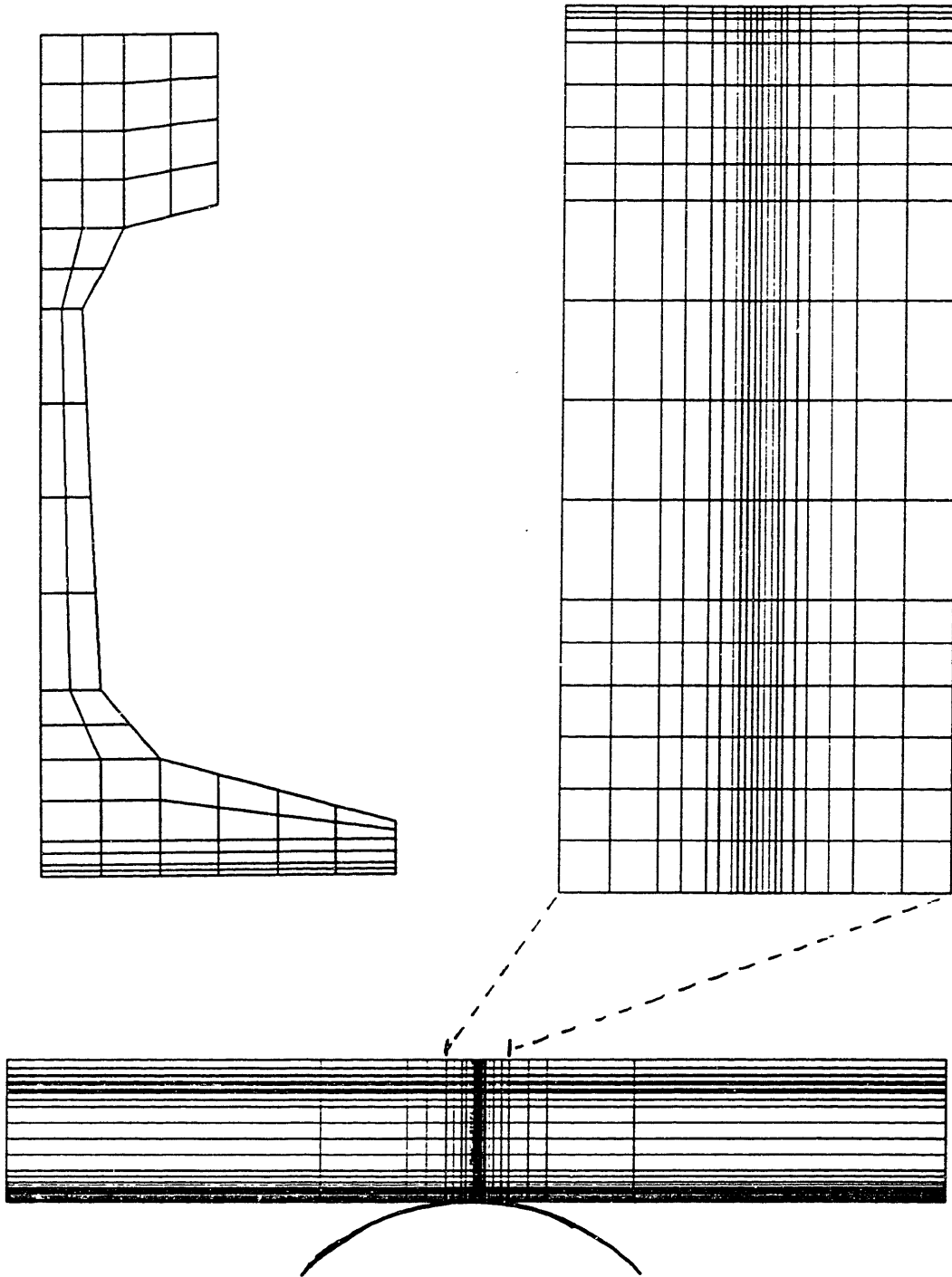
Fig. 15. Three-dimensional mesh for static loading of the rail base.

Fig. 16. Two-dimensional mesh for static loading of the rail base.

σ_{zz}

(MPa)	(ksi)
-966	-140
-276	-40
-138	-20
0	0
138	20
276	40
414	60
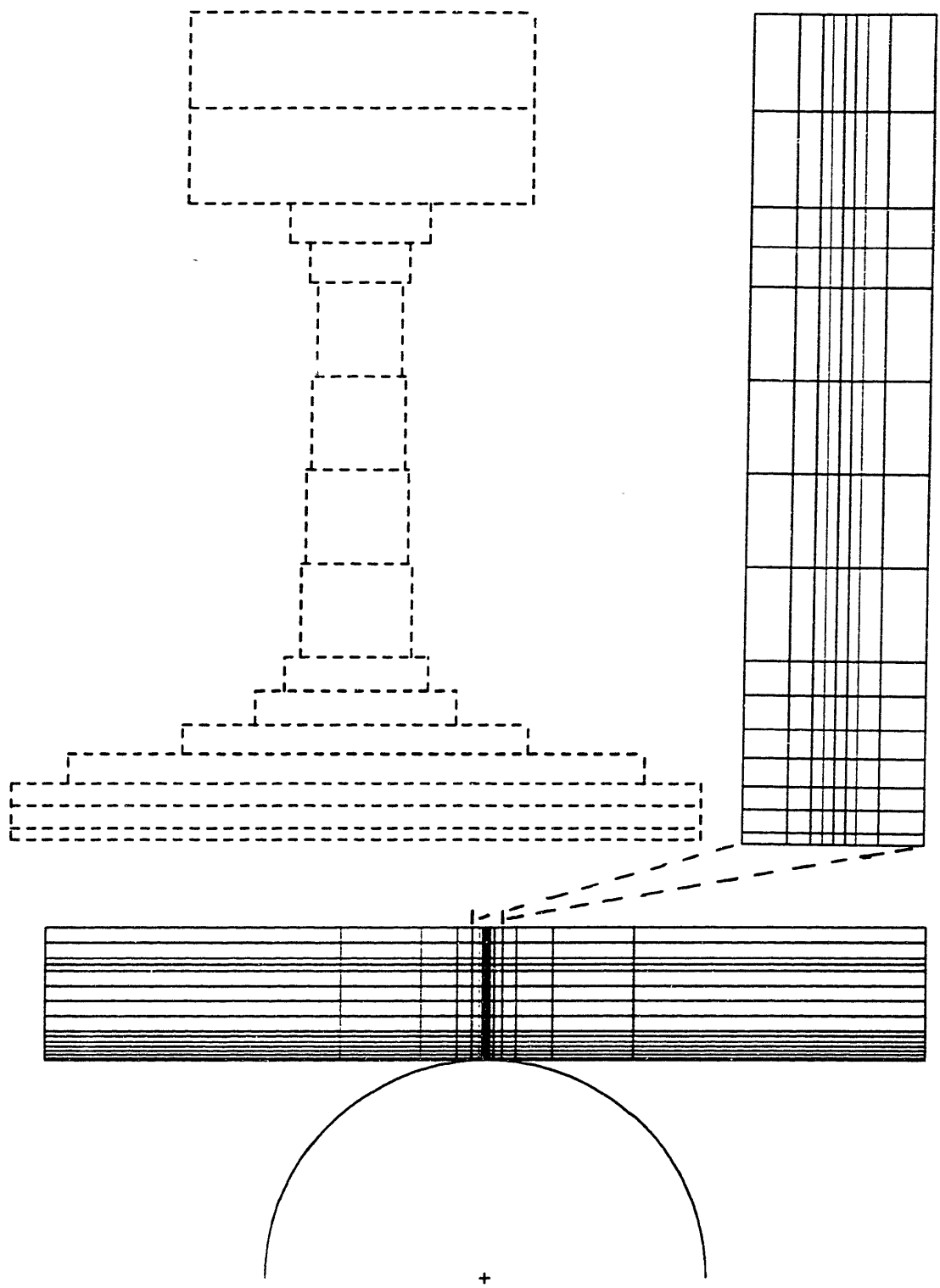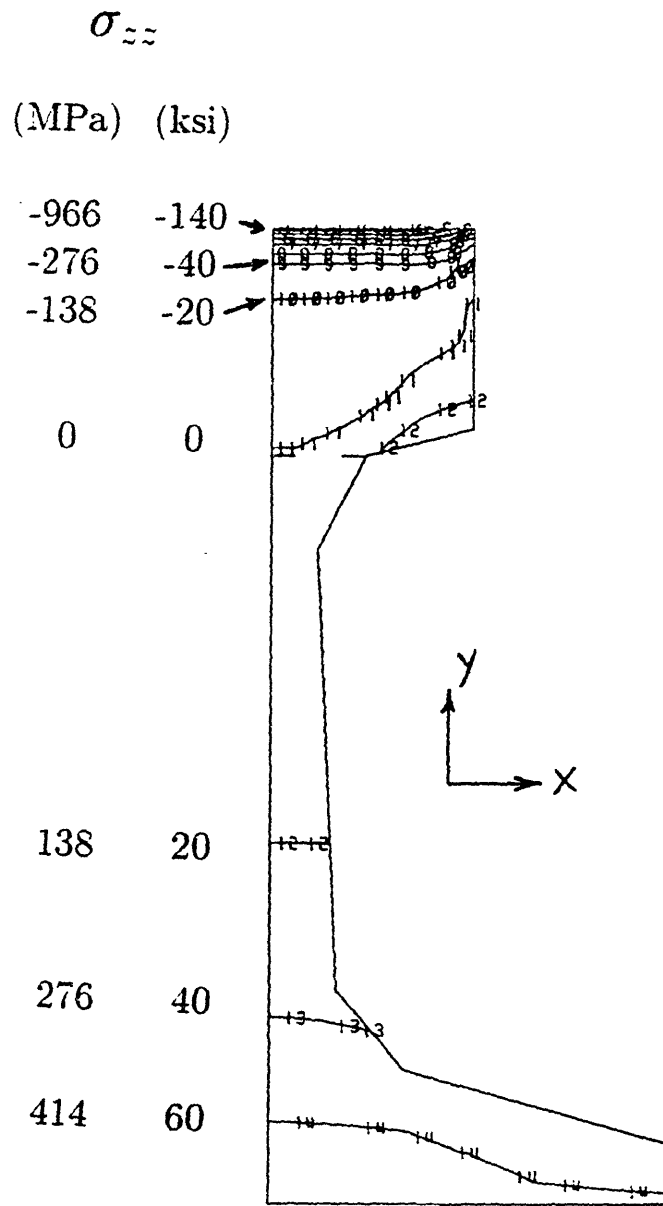
Fig. 17. Contours of longitudinal stress under the loaded roll, head static loading.
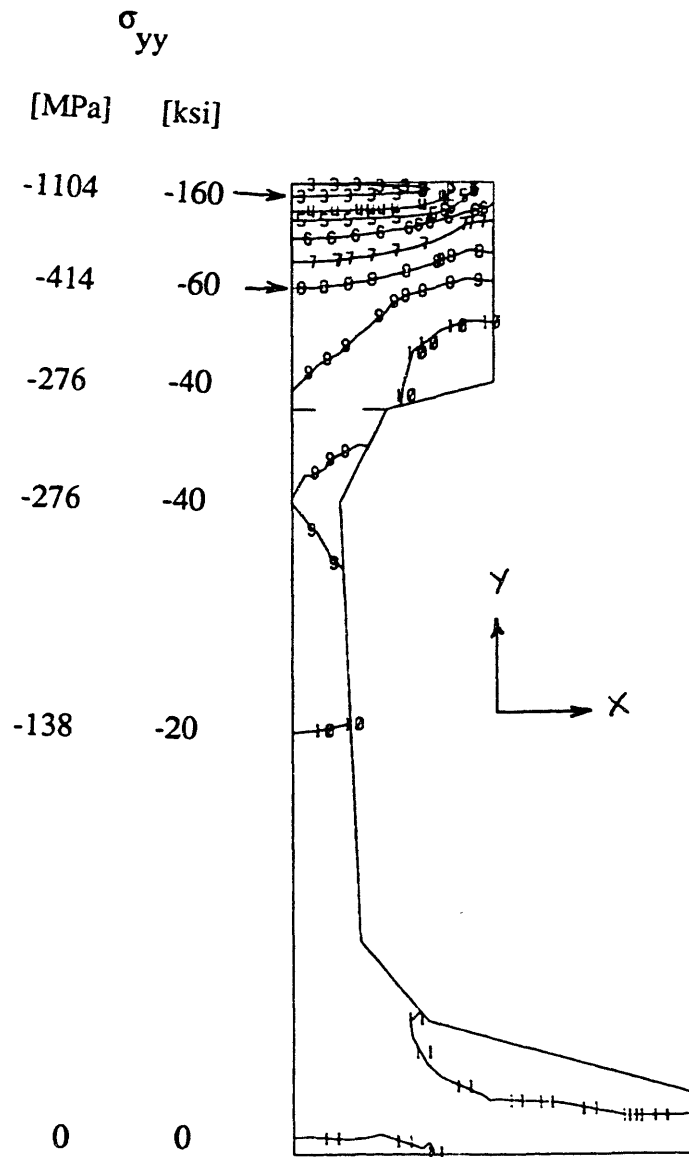
Fig. 18. Contours of vertical stress under the loaded roll, head static loading.
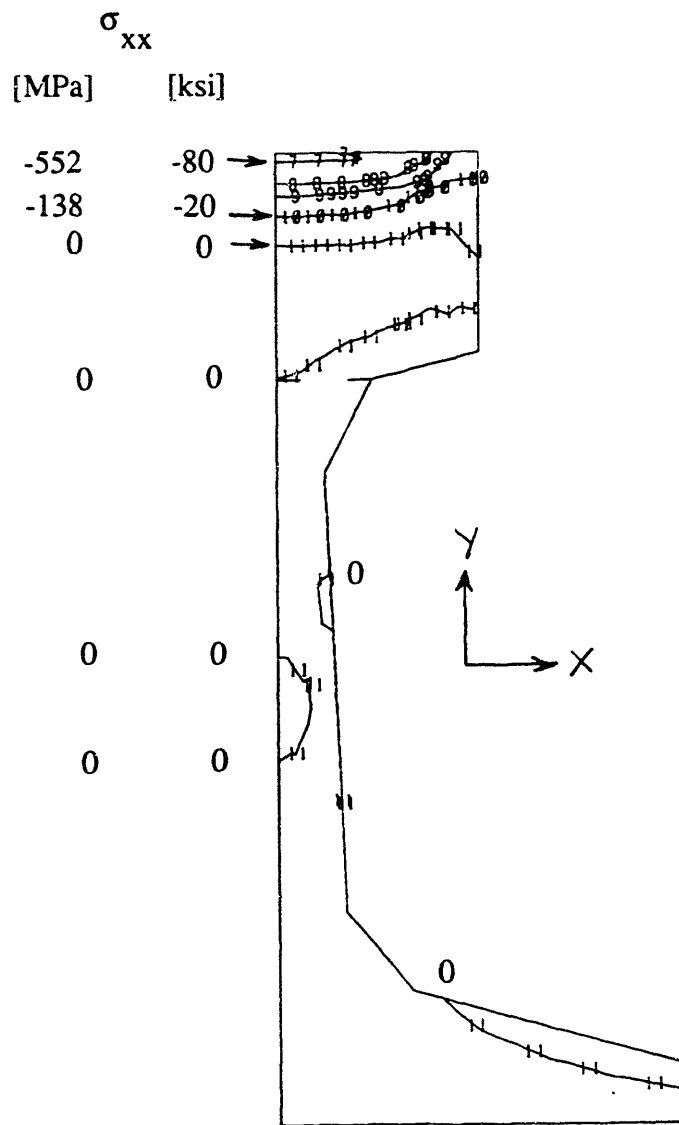
Fig. 19. Contours of transverse stress under the loaded roll, head static loading.
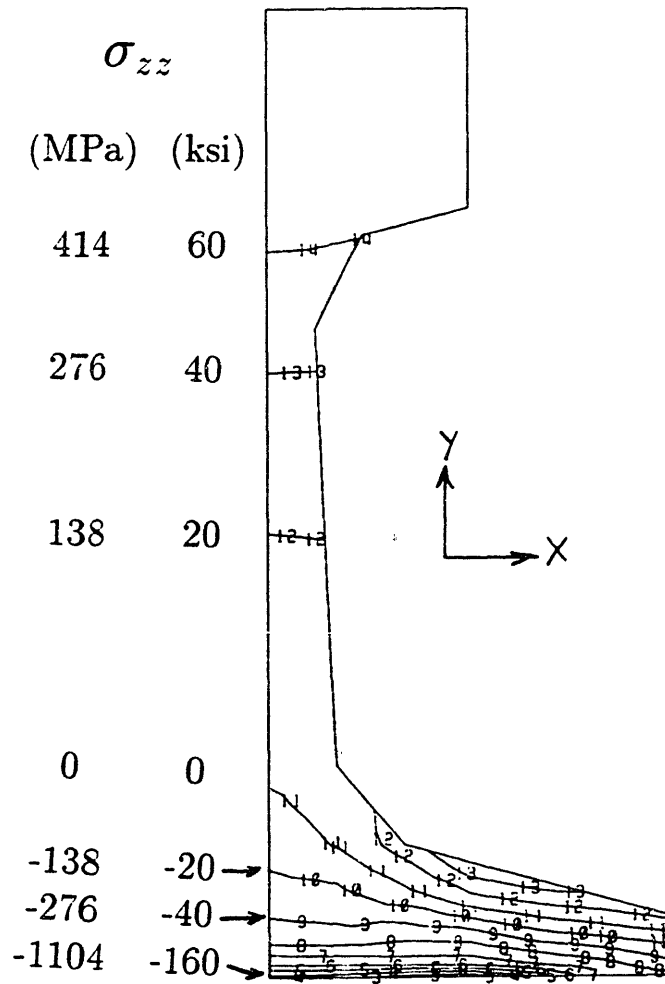
Fig. 20. Contours of longitudinal stress under the loaded roll, base static loading.

σ_{yy}
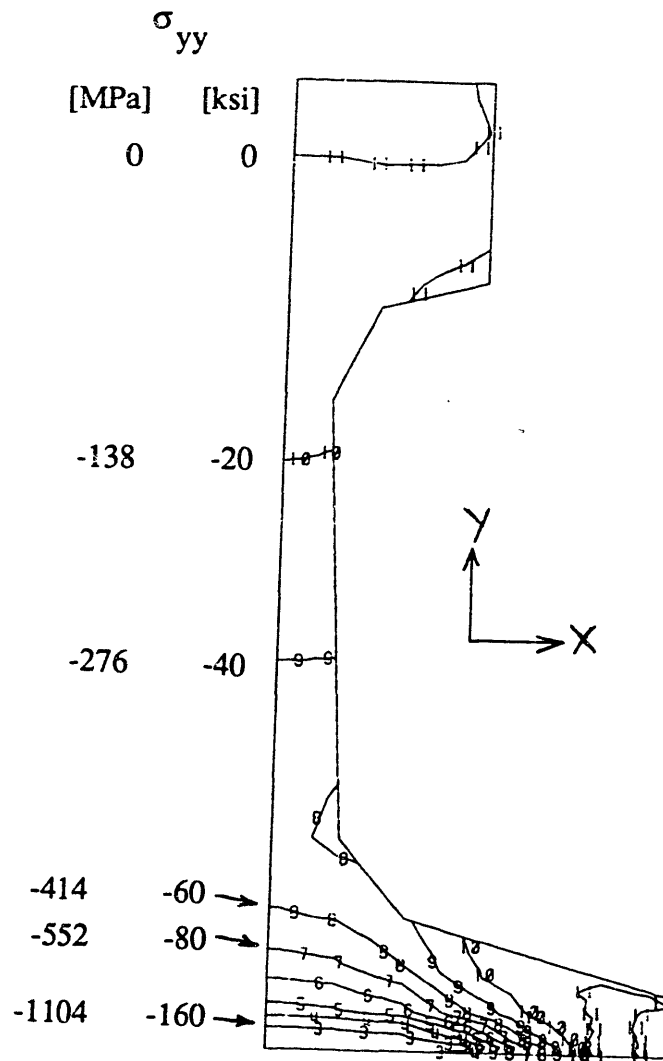
Fig. 21. Contours of vertical stress under the loaded roll, base static loading.
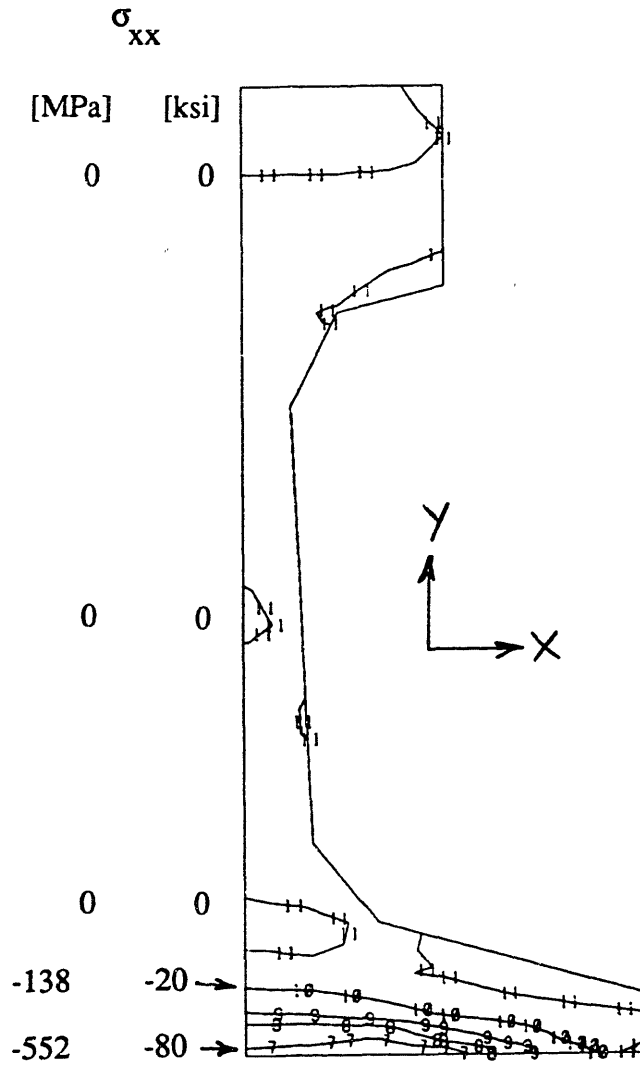
Fig. 22. Contours of transverse stress under the loaded roll, base static loading.
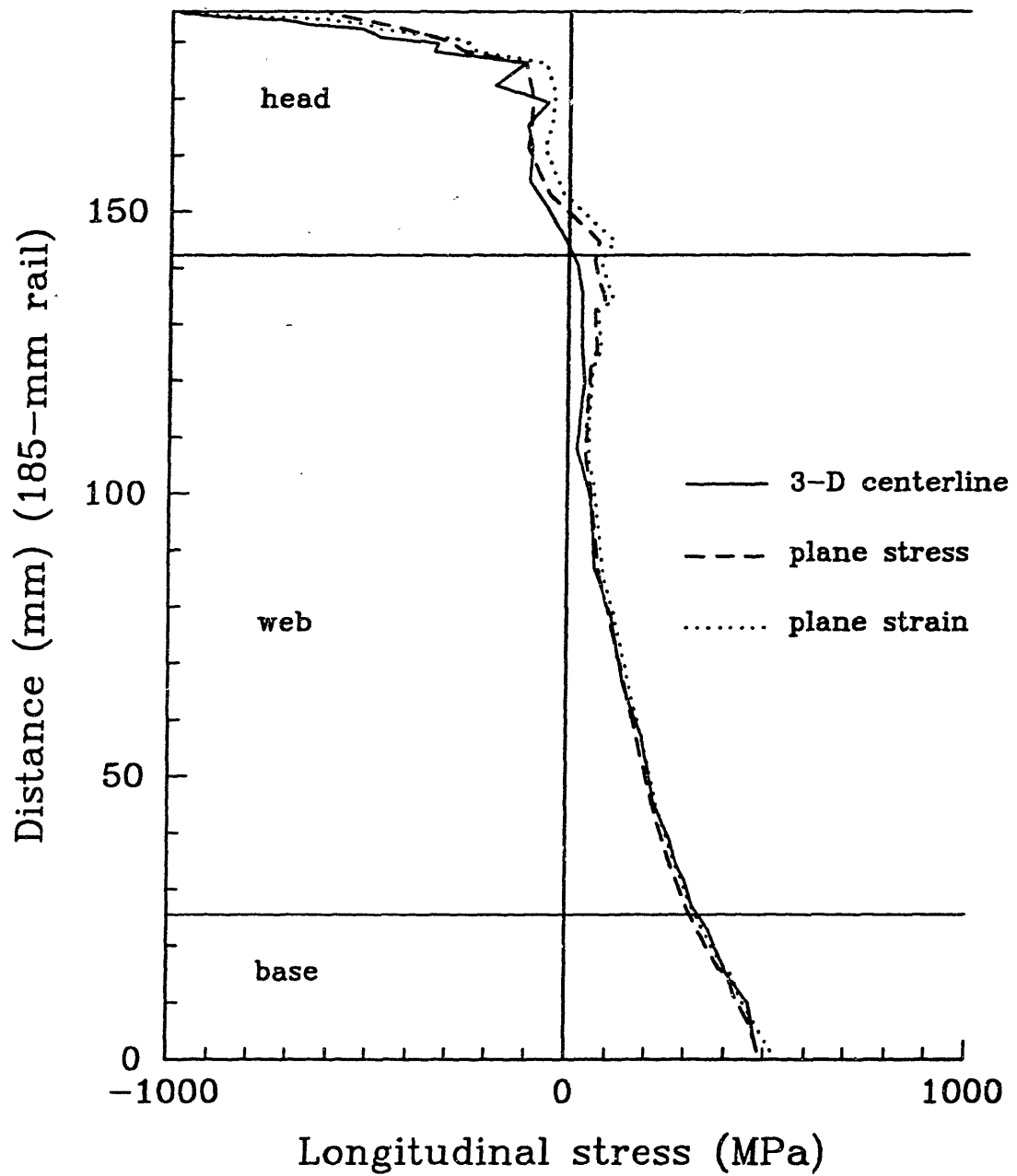
Fig. 23. Comparison of 3–D centerline longitudinal stress σ_{zz} with plane stress and plane strain results, static roll loading on the rail head.
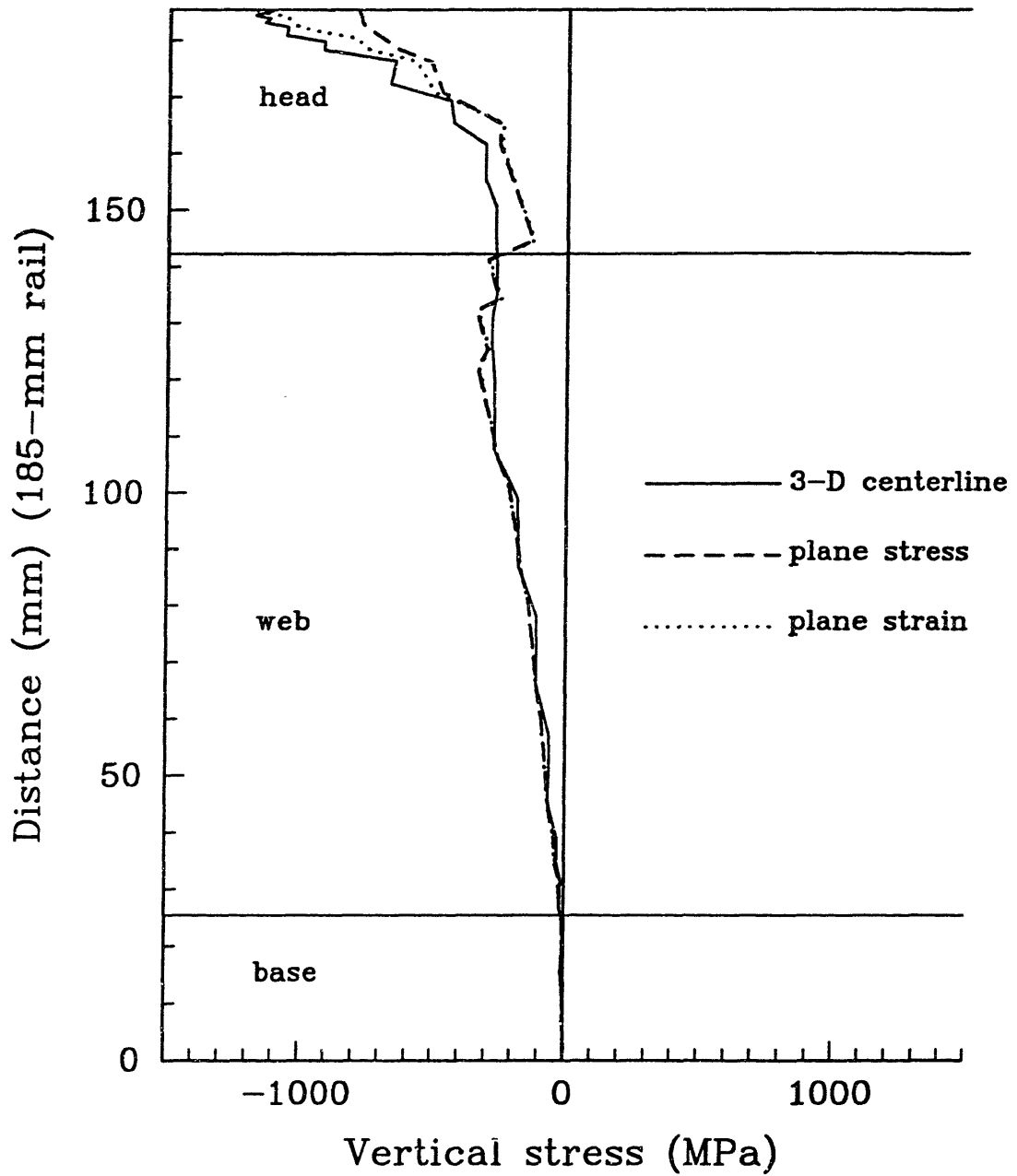
Fig. 24. Comparison of 3–D centerline vertical stress σ_{yy} with plane stress and plane strain results, static roll loading on the rail head.

71
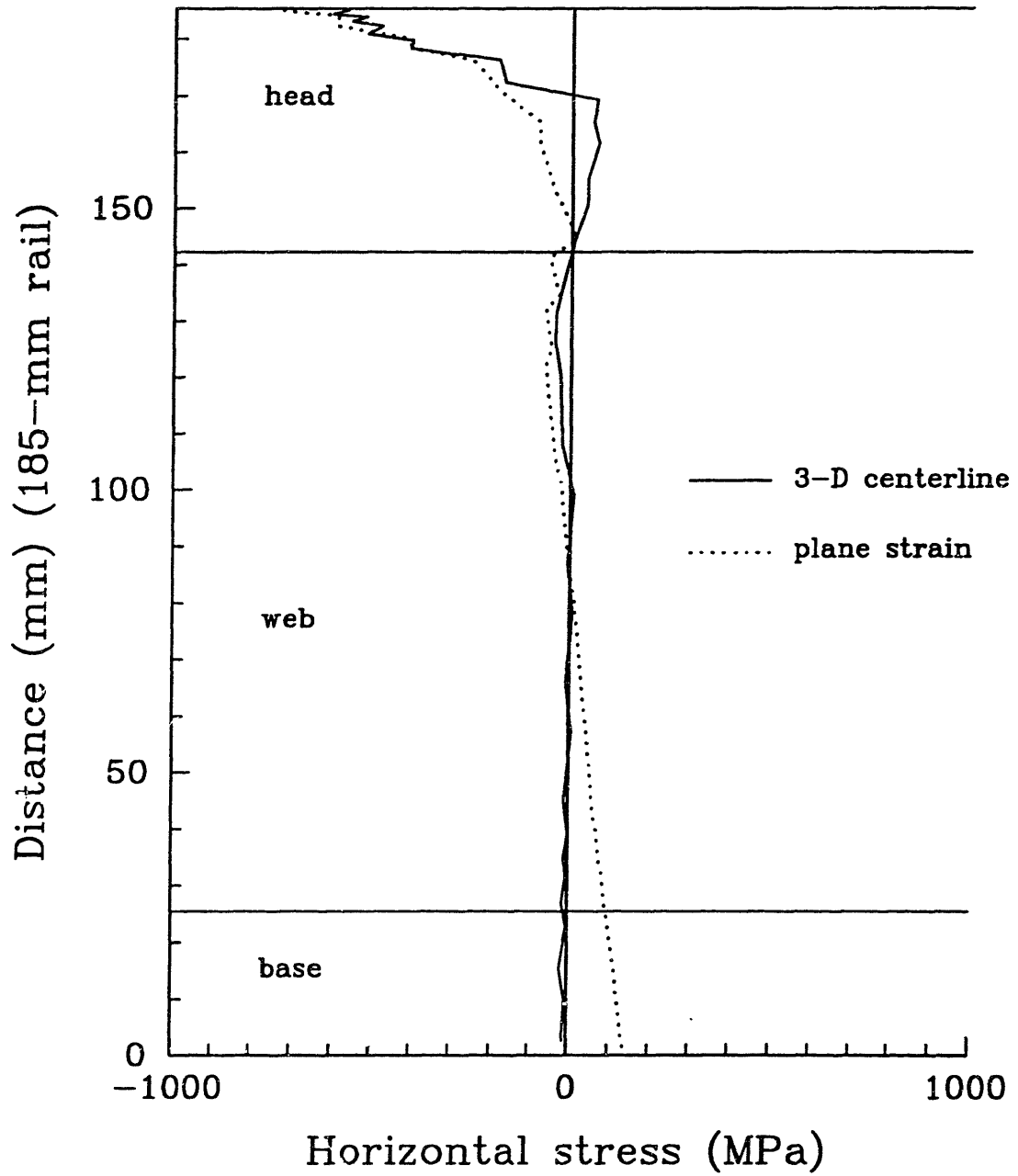
Fig. 25. Comparison of 3—D centerline horizontal stress σ_{xx} with plane strain results, static roll loading on the rail head.
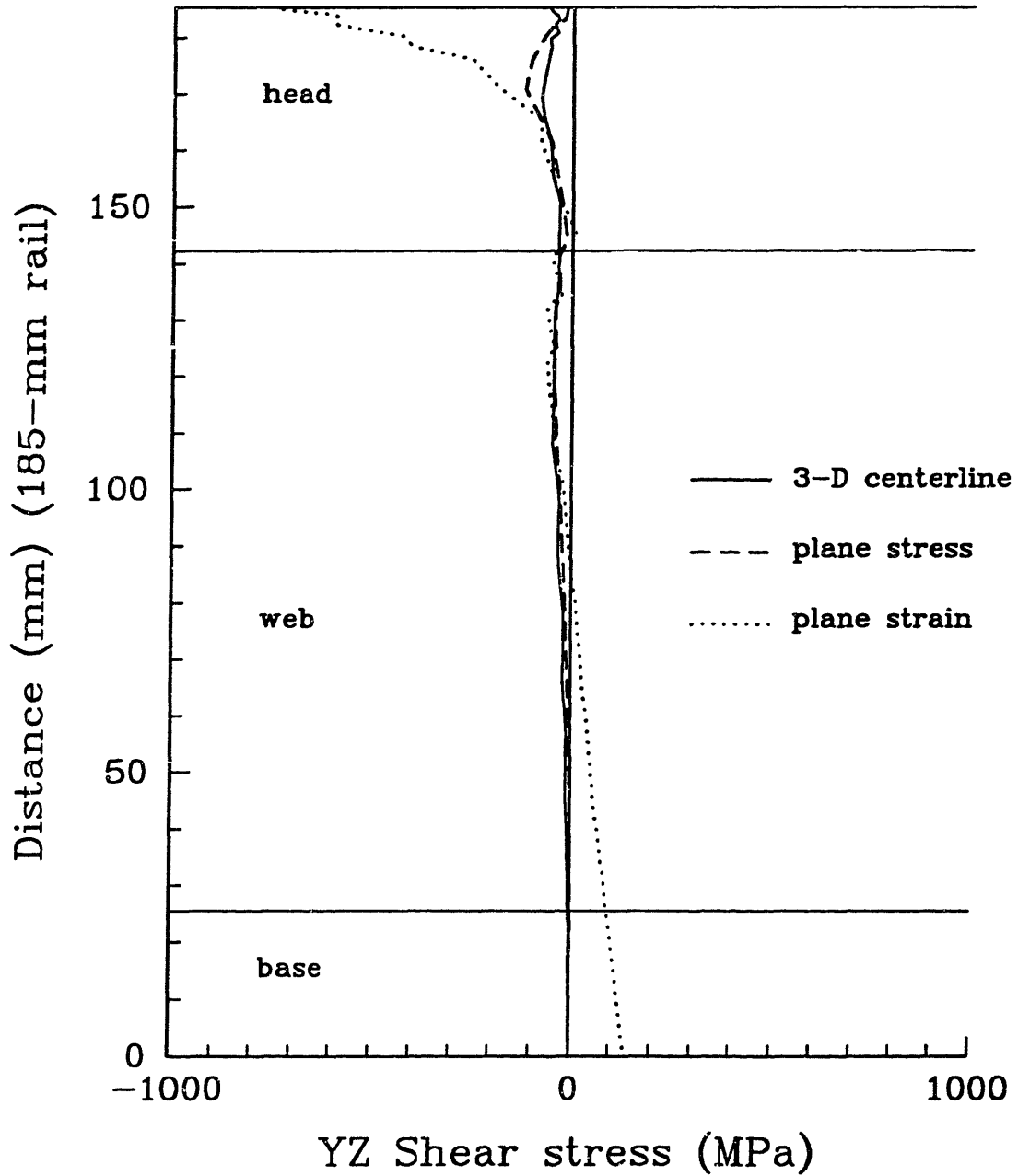
Fig. 26. Comparison of 3—D centerline shear stress σ_{yz} with plane stress and plane strain results, static roll loading on the rail head.
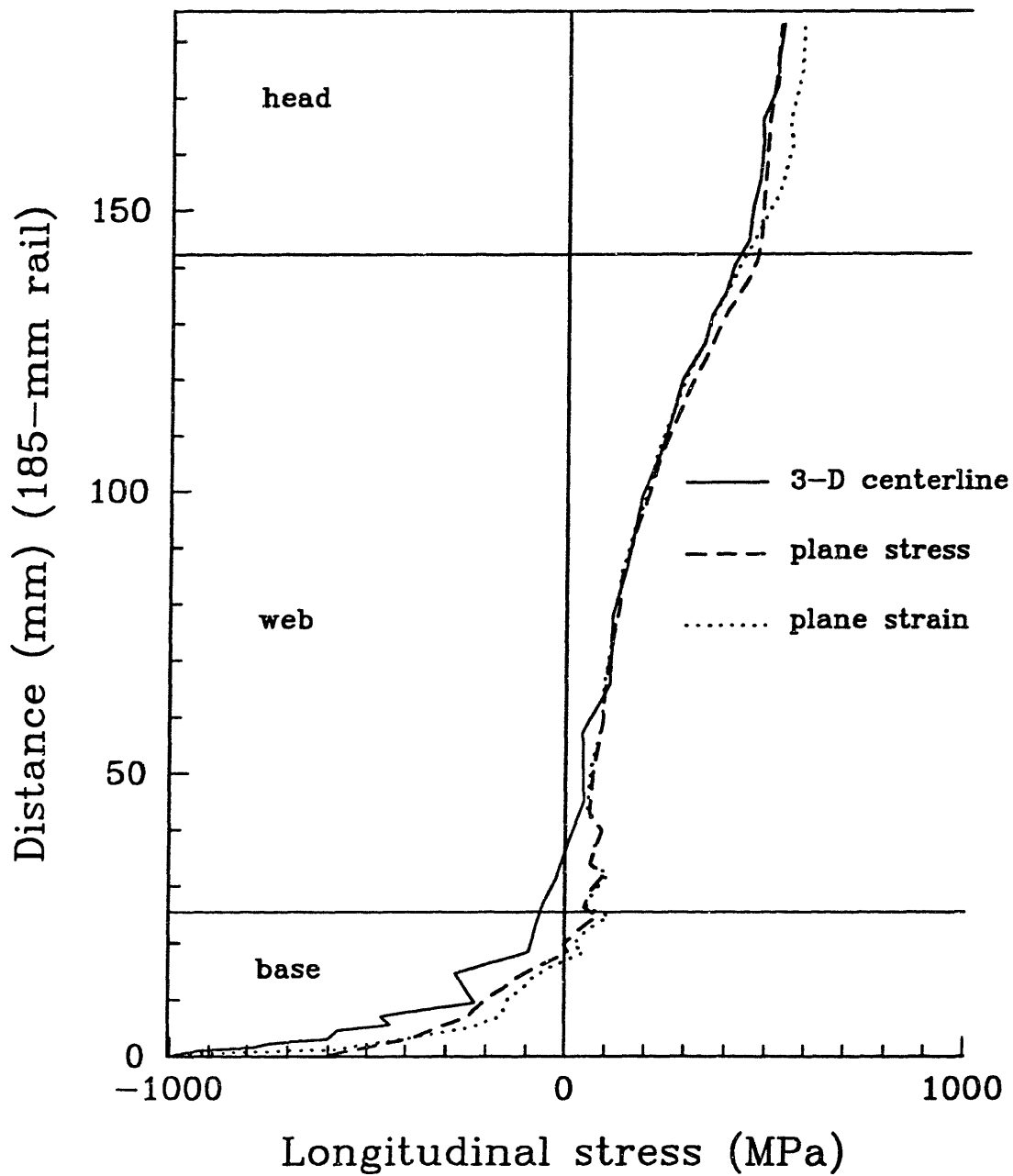
Fig. 27. Comparison of 3–D centerline longitudinal stress σ_{xx}
with plane stress and plane strain results, static roll loading
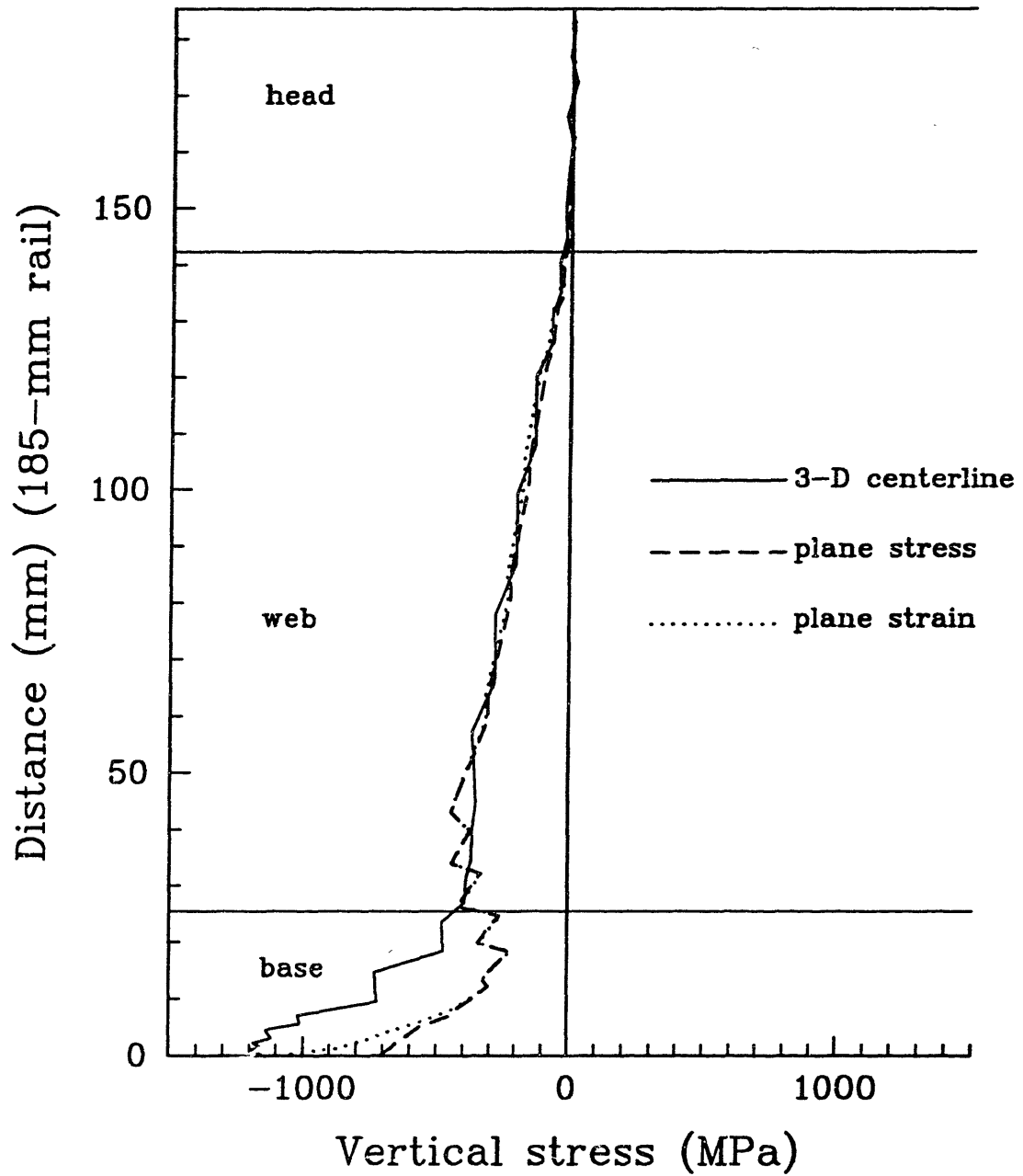on the rail base.

Fig. 28. Comparison of 3-D centerline vertical stress σ_{yy} with plane stress and plane strain results, static roll loading on the rail base.
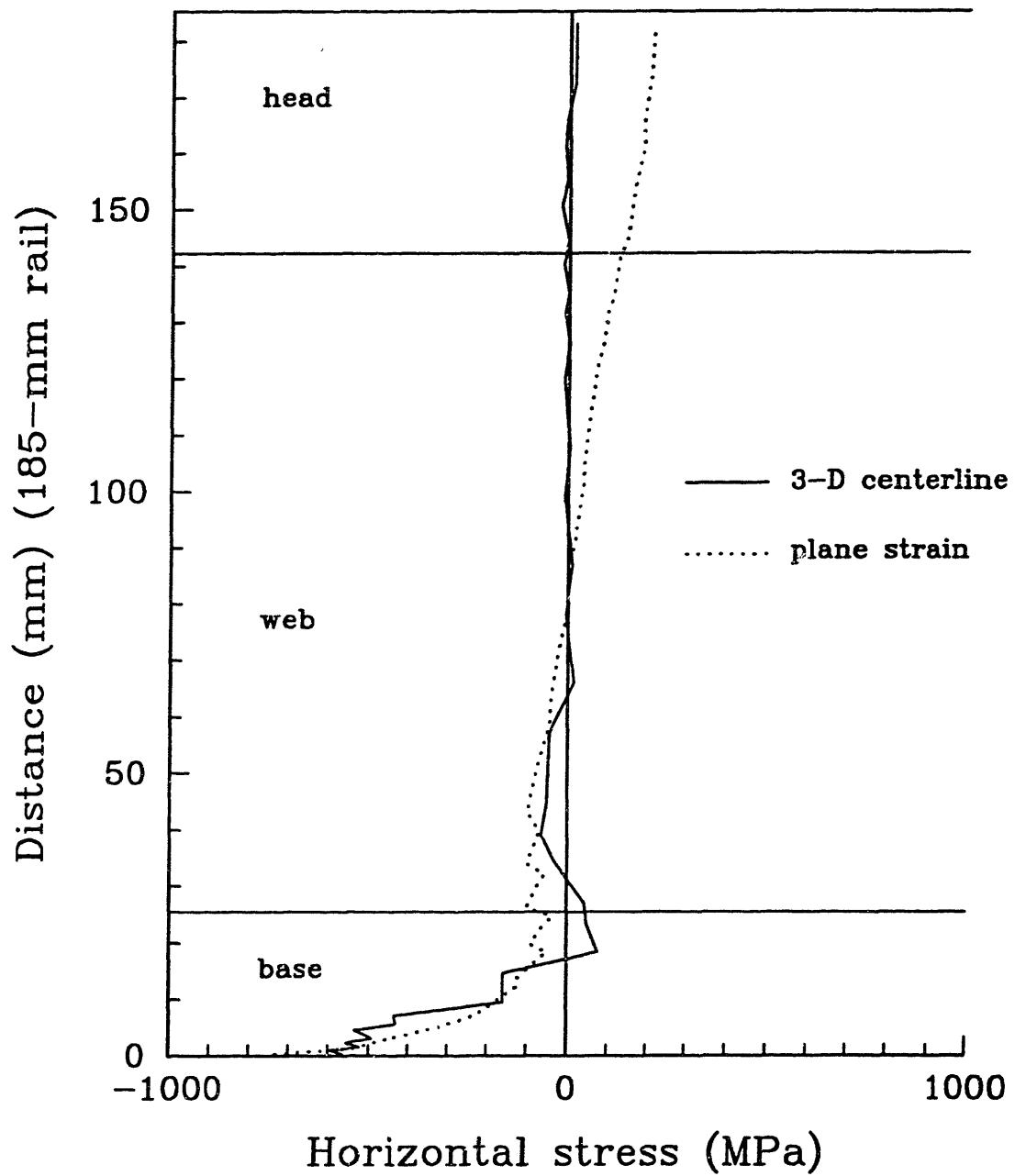
Fig. 29. Comparison of 3–D centerline horizontal stress σ_{xx} with plane strain results, static roll loading on the rail base.
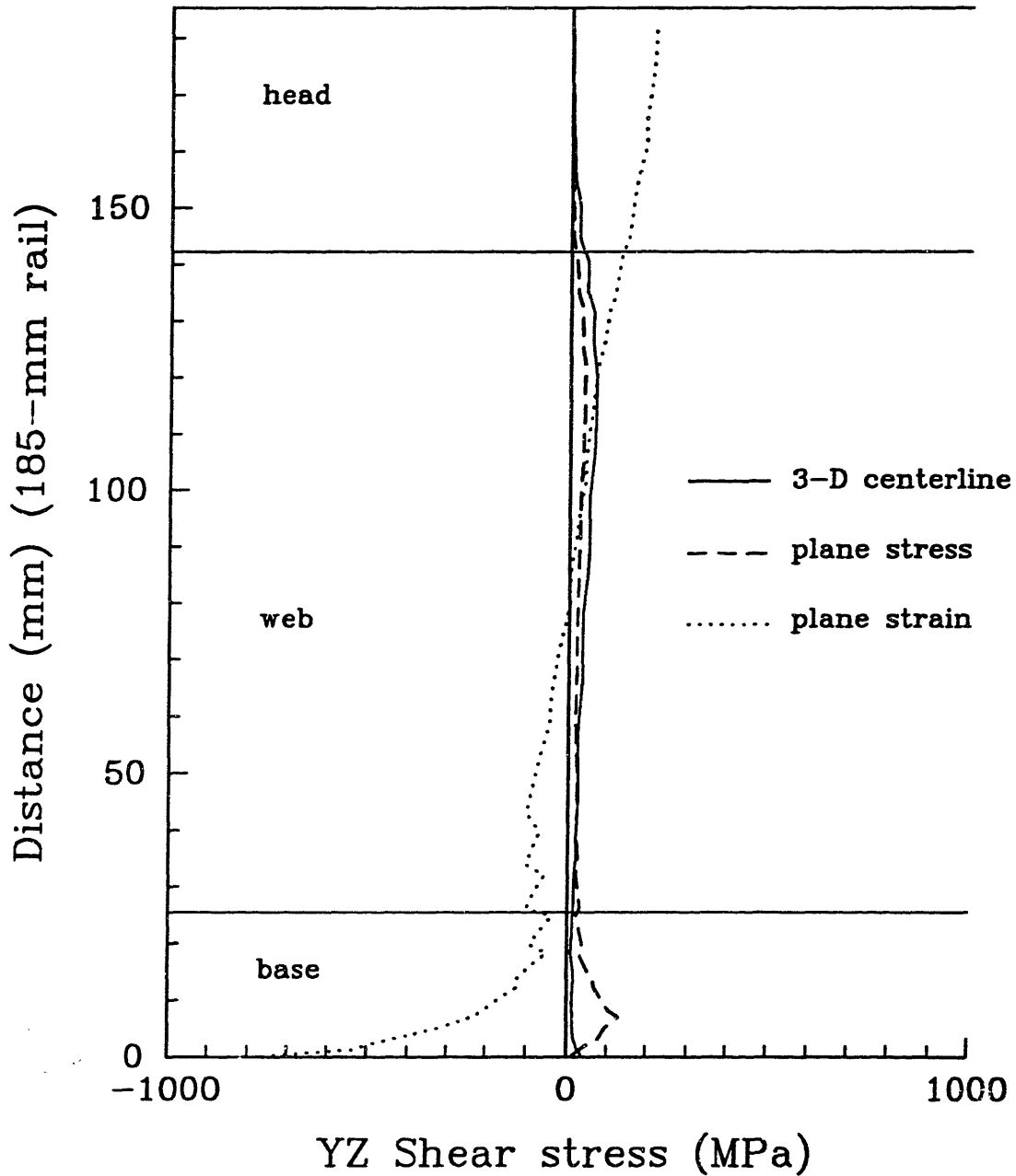
Fig. 30. Comparison of 3–D centerline shear stress σ_{yz} with plane stress and plane strain results, static roll loading on the rail base.
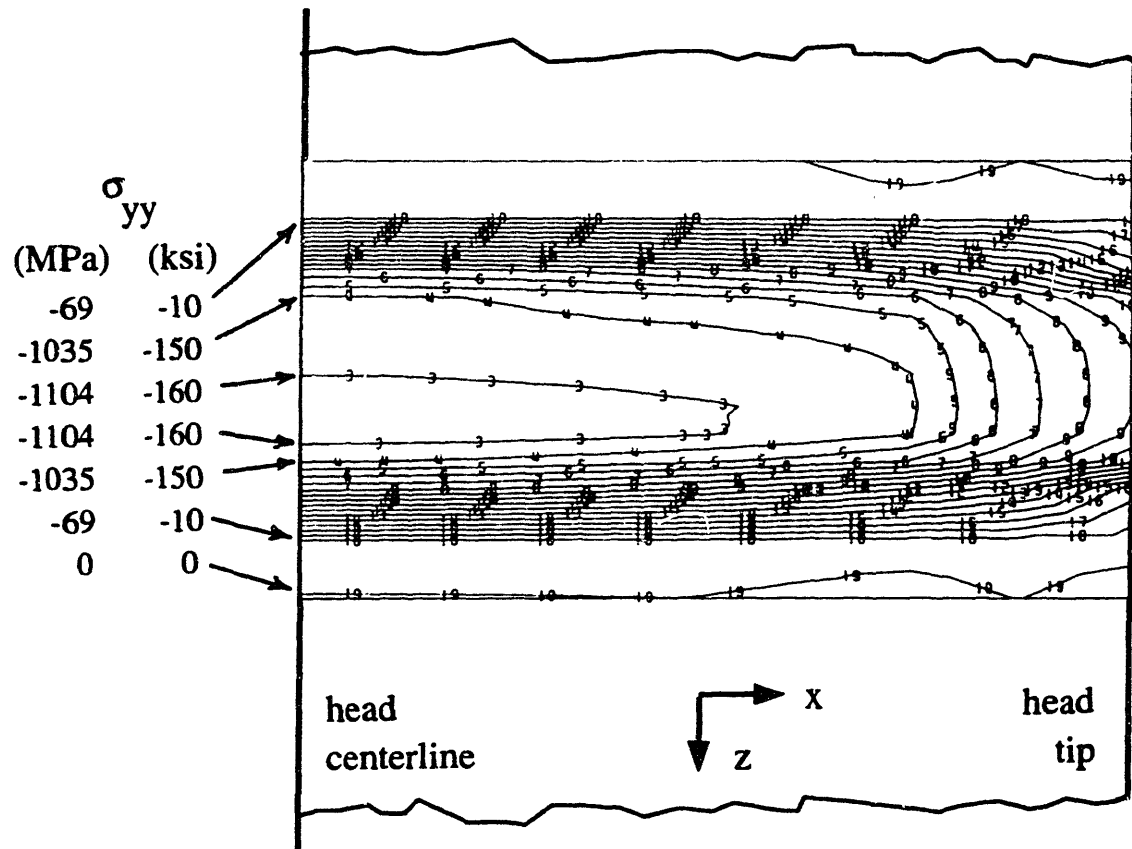
Fig. 31. Contours of vertical stress σ_{yy}, looking down on the top surface of the rail head under the loaded roll.
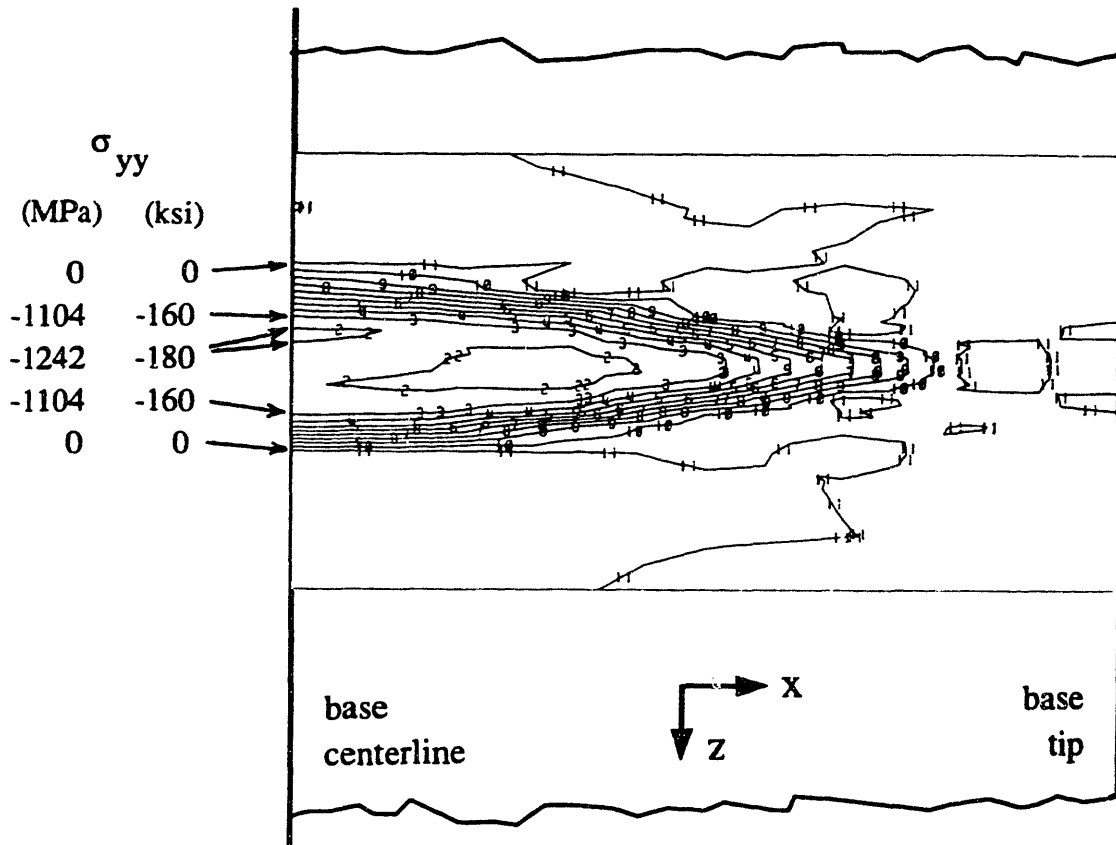
Fig. 32. Contours of vertical stress σ_{yy}, looking down on the top surface of the rail base under the loaded roll.

79

Fig. 33. Comparison of longitudinal residual stress σ_{zz} after head static loading, for 3-D centerline, plane stress, and plane strain results.
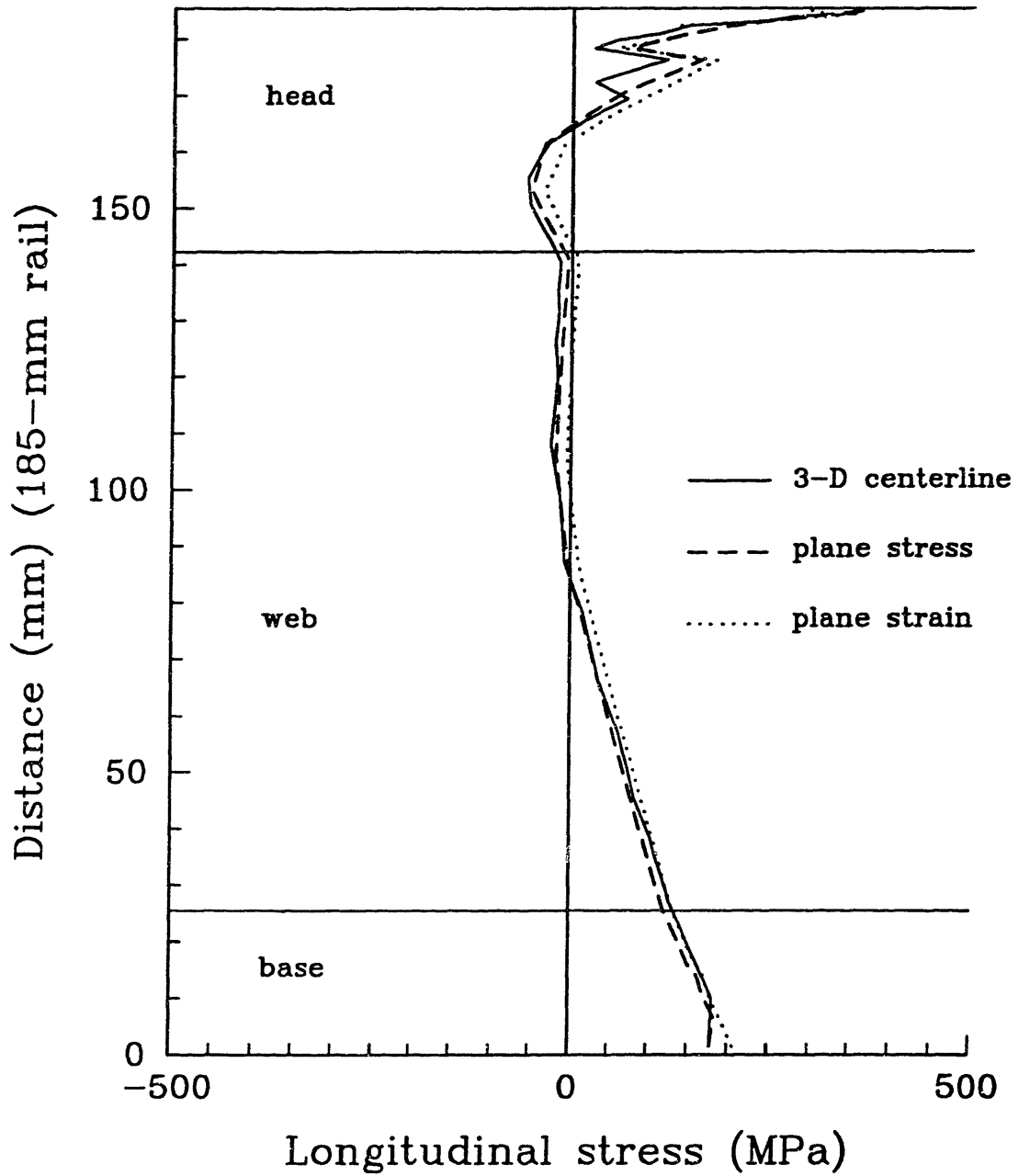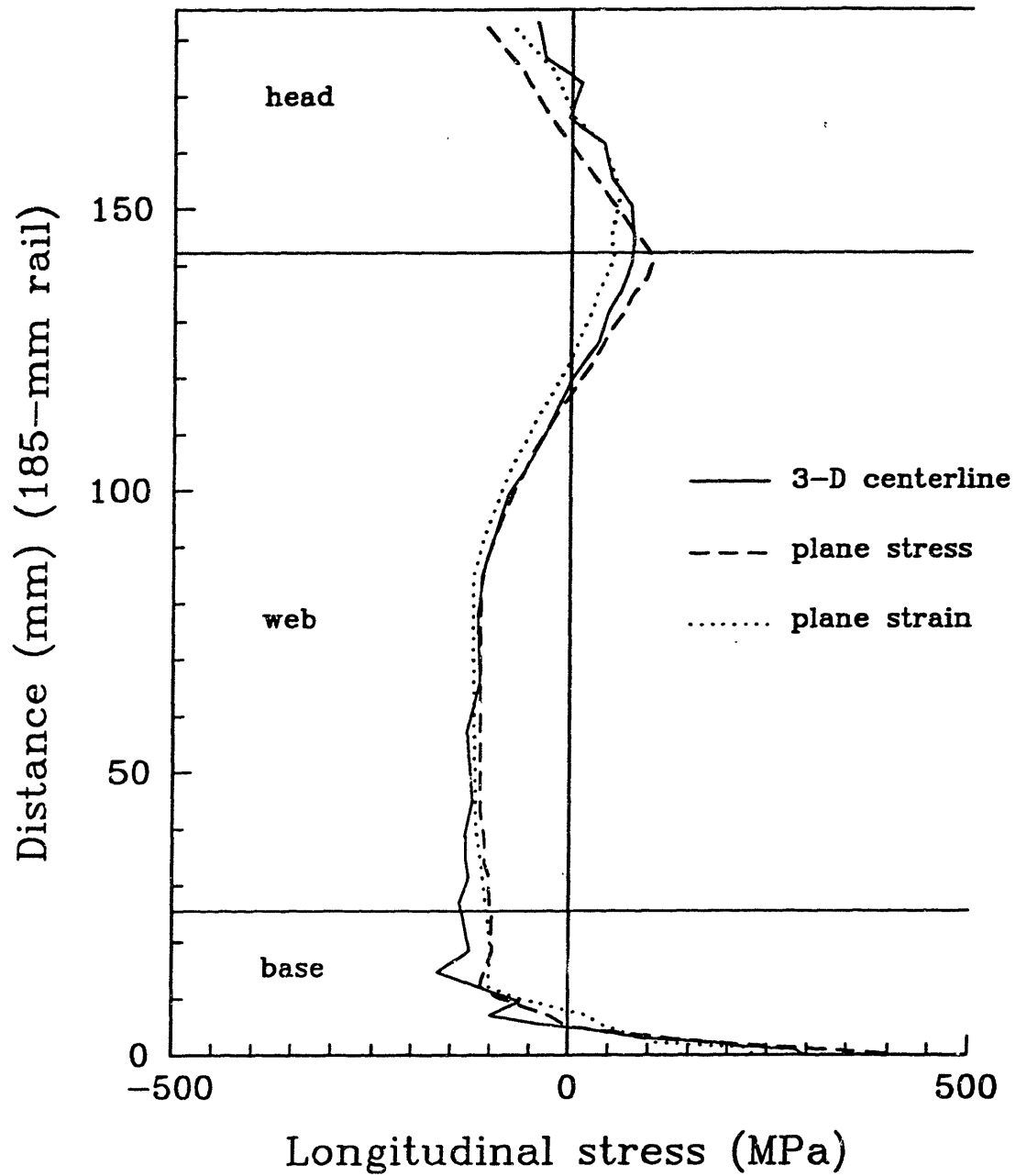
Fig. 34. Comparison of longitudinal residual stresses σ_n
after base static loading, for 3-D centerline, plane stress,
and plane strain results.
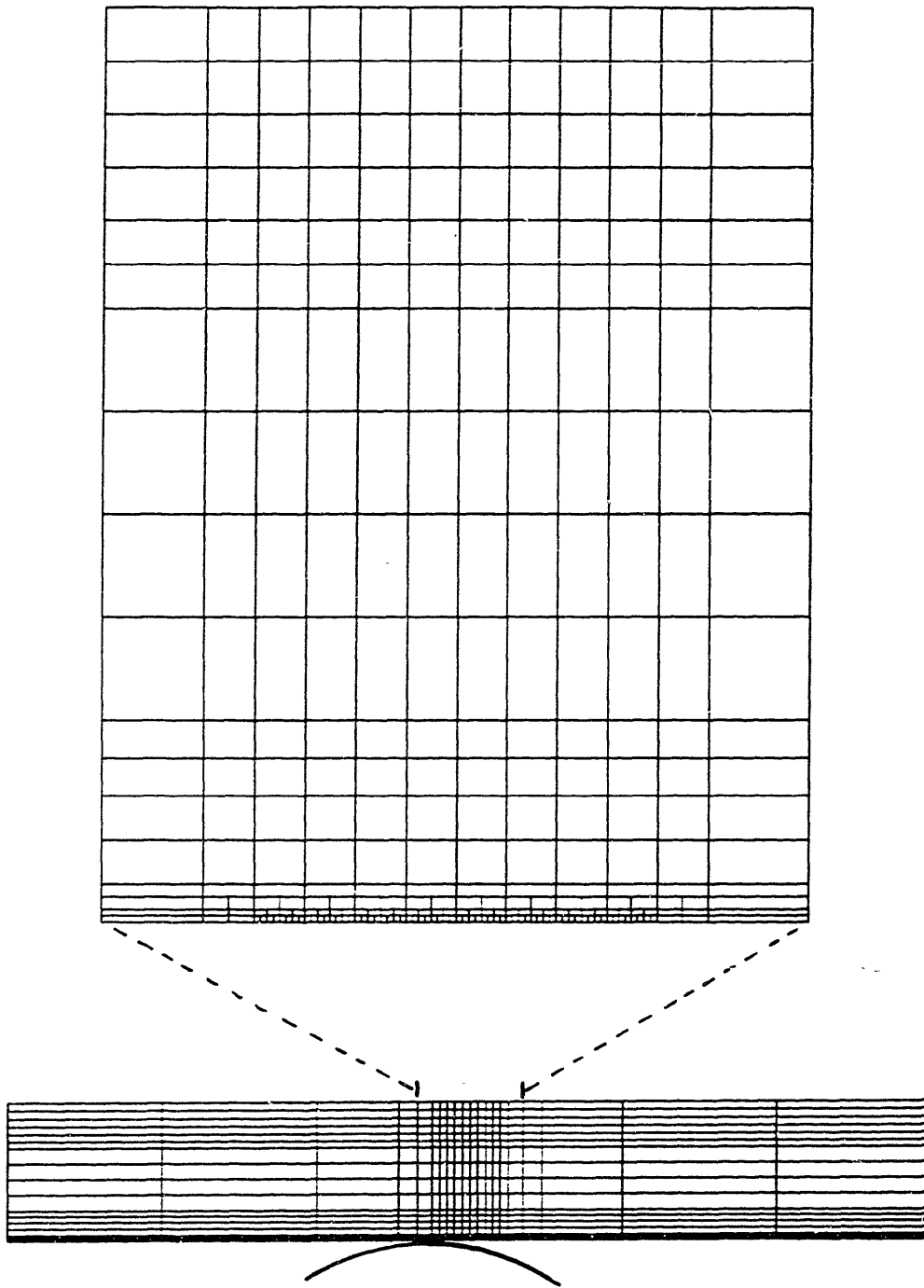
Fig. 35. Three-dimensional mesh for roll travel along the rail base.
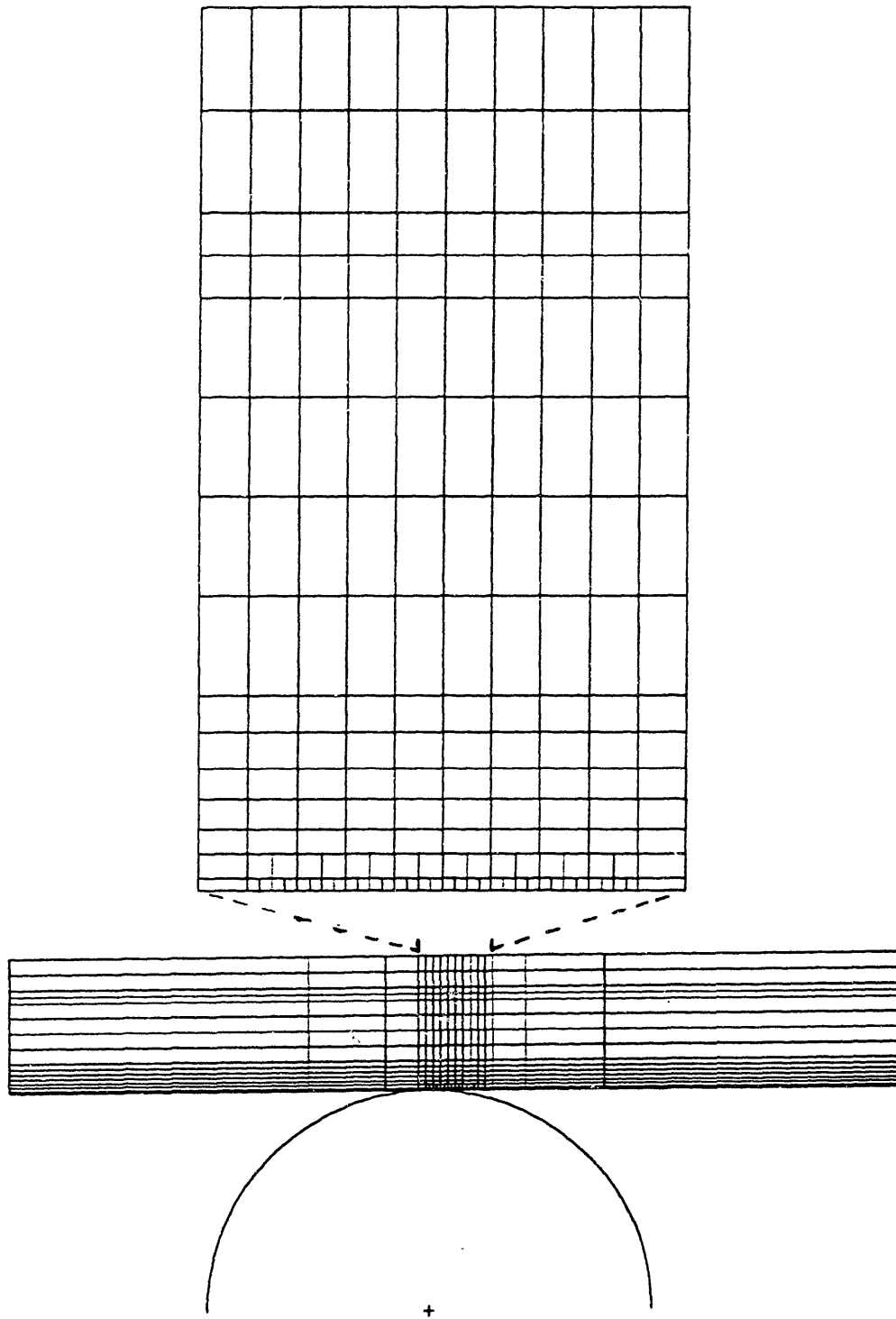
Fig. 36. Two-dimensional mesh for roll travel along the rail base.
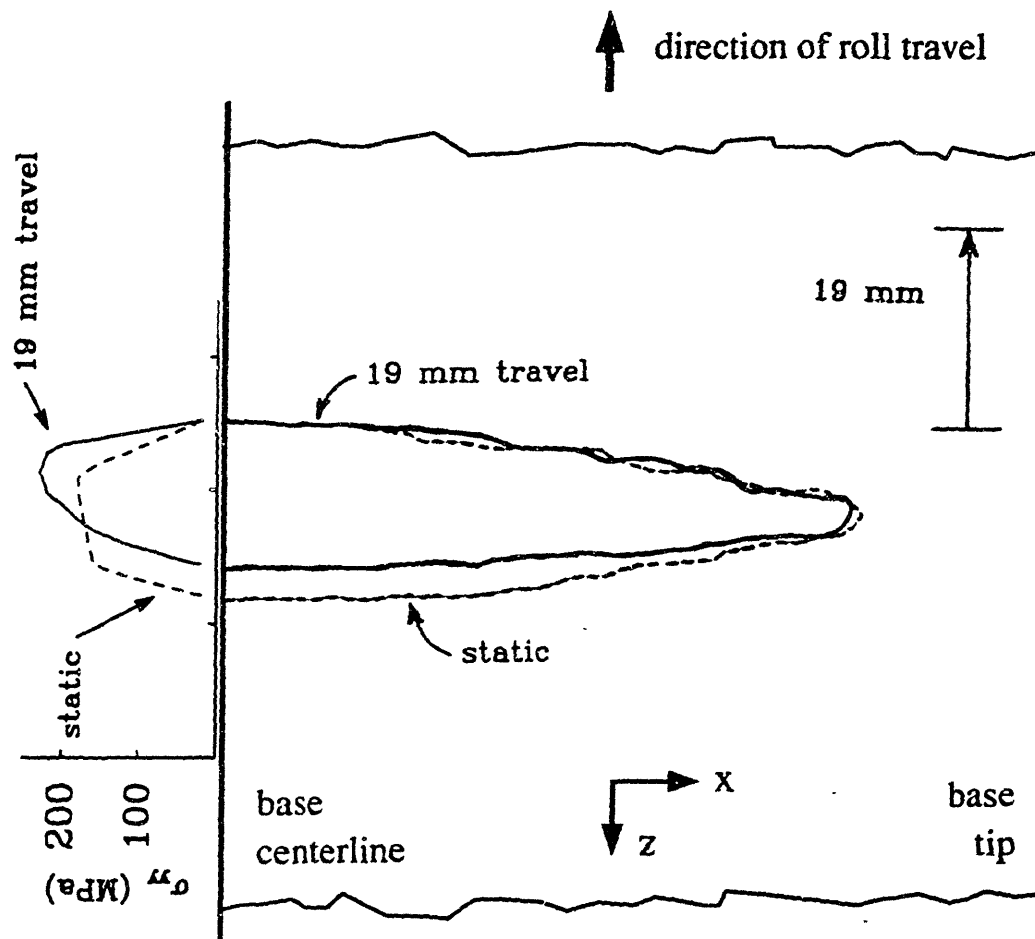
Fig. 37. Comparison of roll "footprints" for static loading and after 19 mm travel along the rail base.
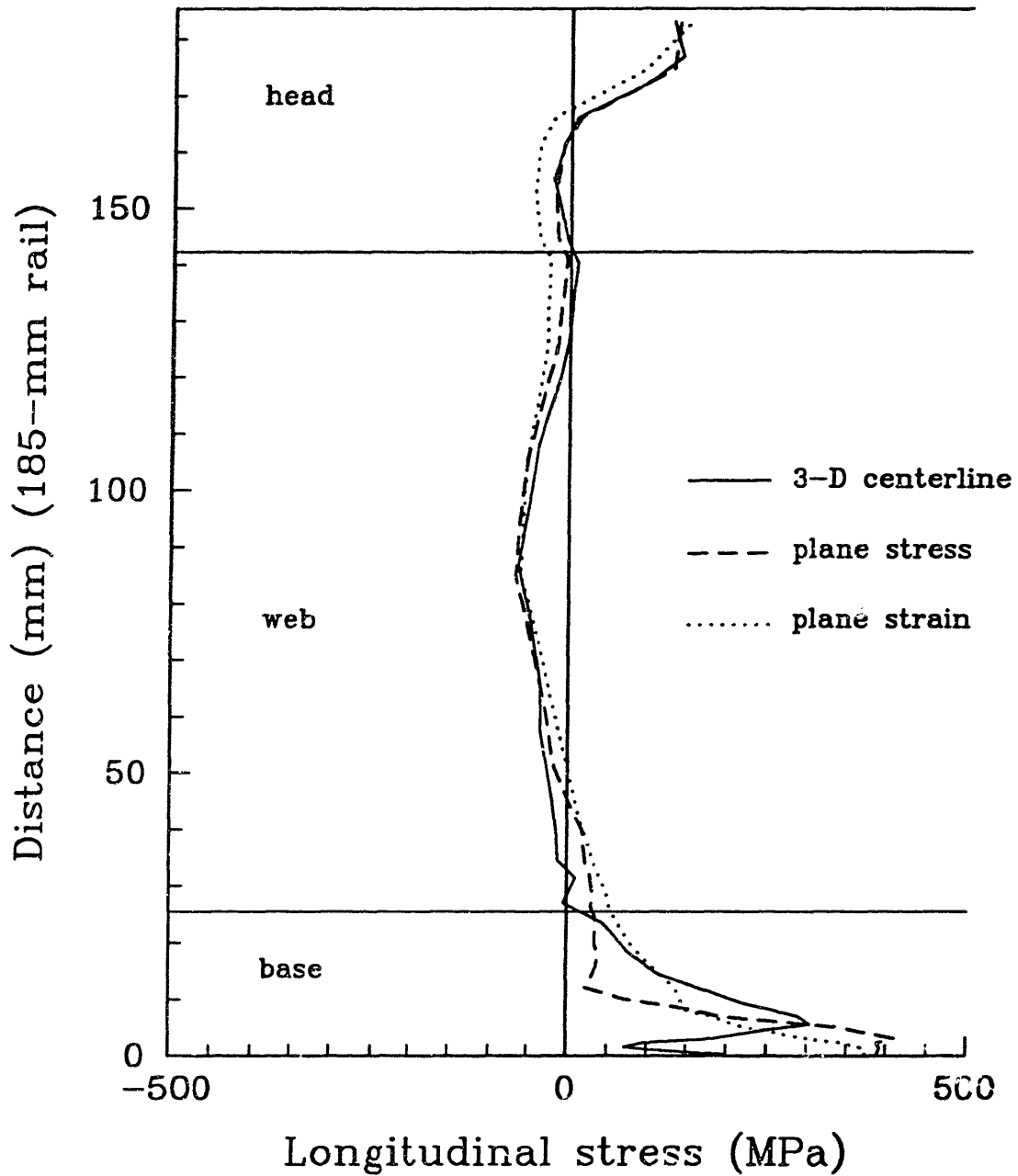
Fig. 38. Comparison of longitudinal residual stresses σ_{zz} in the roll wake after 19 mm base travel, for 3–D centerline, plane stress, and plane strain results.

85
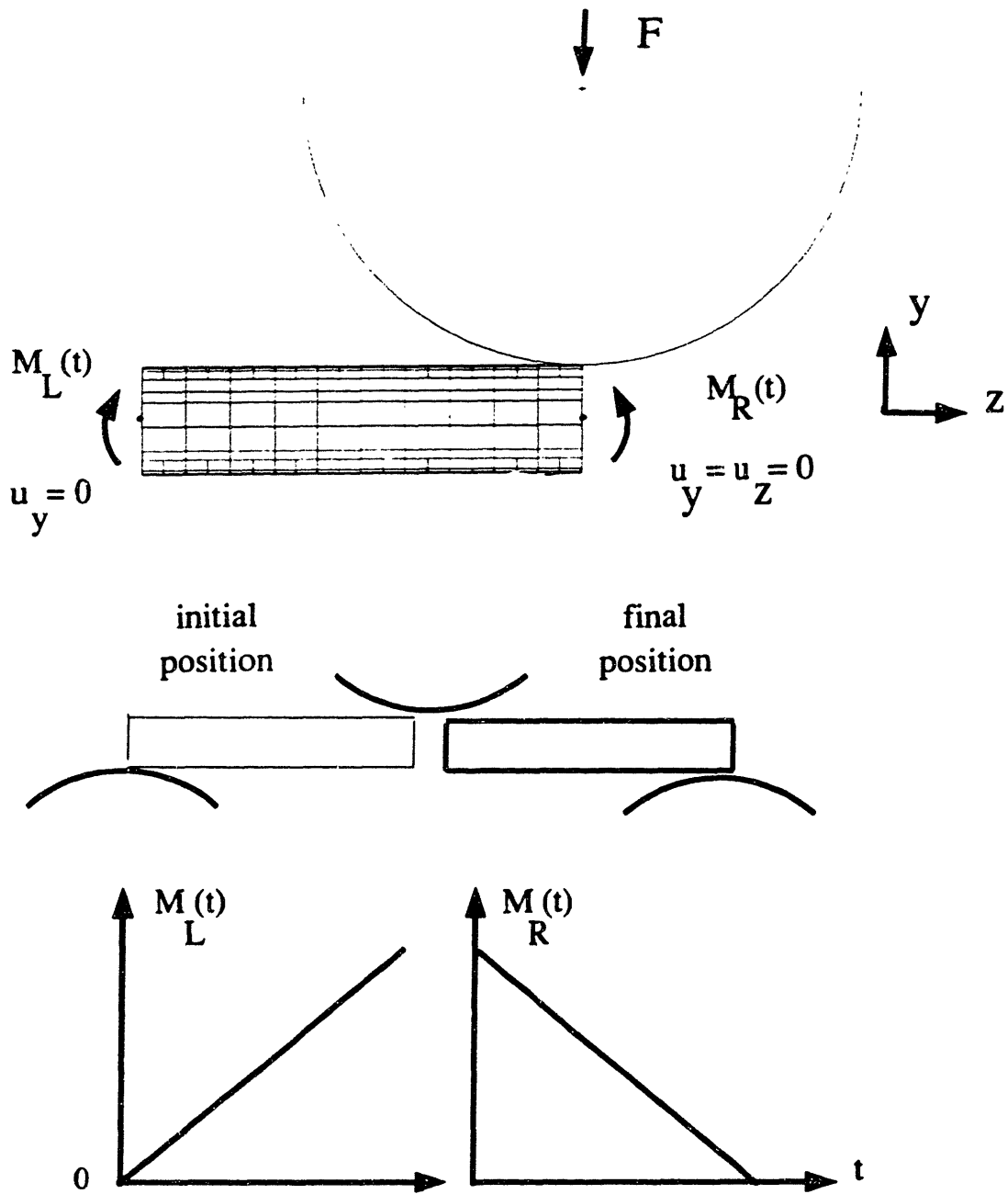
Fig. 39. "Single-roll" model for 3-roll straightener section.
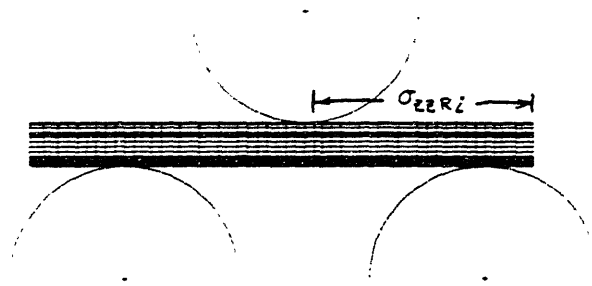
initial stresses (after top roll only)
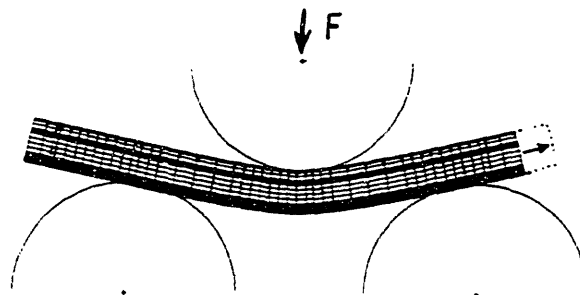
loading and 200 mm (1.1 rail heights) travel
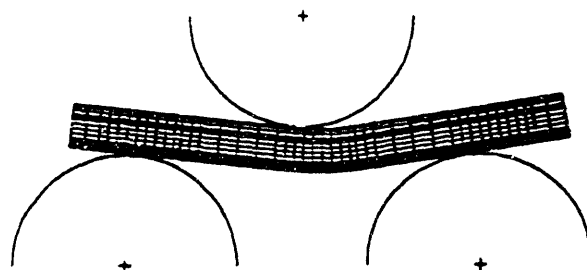
unloading

Fig. 40. "Quasi-Eulerian" model for 3-roll straightener section.
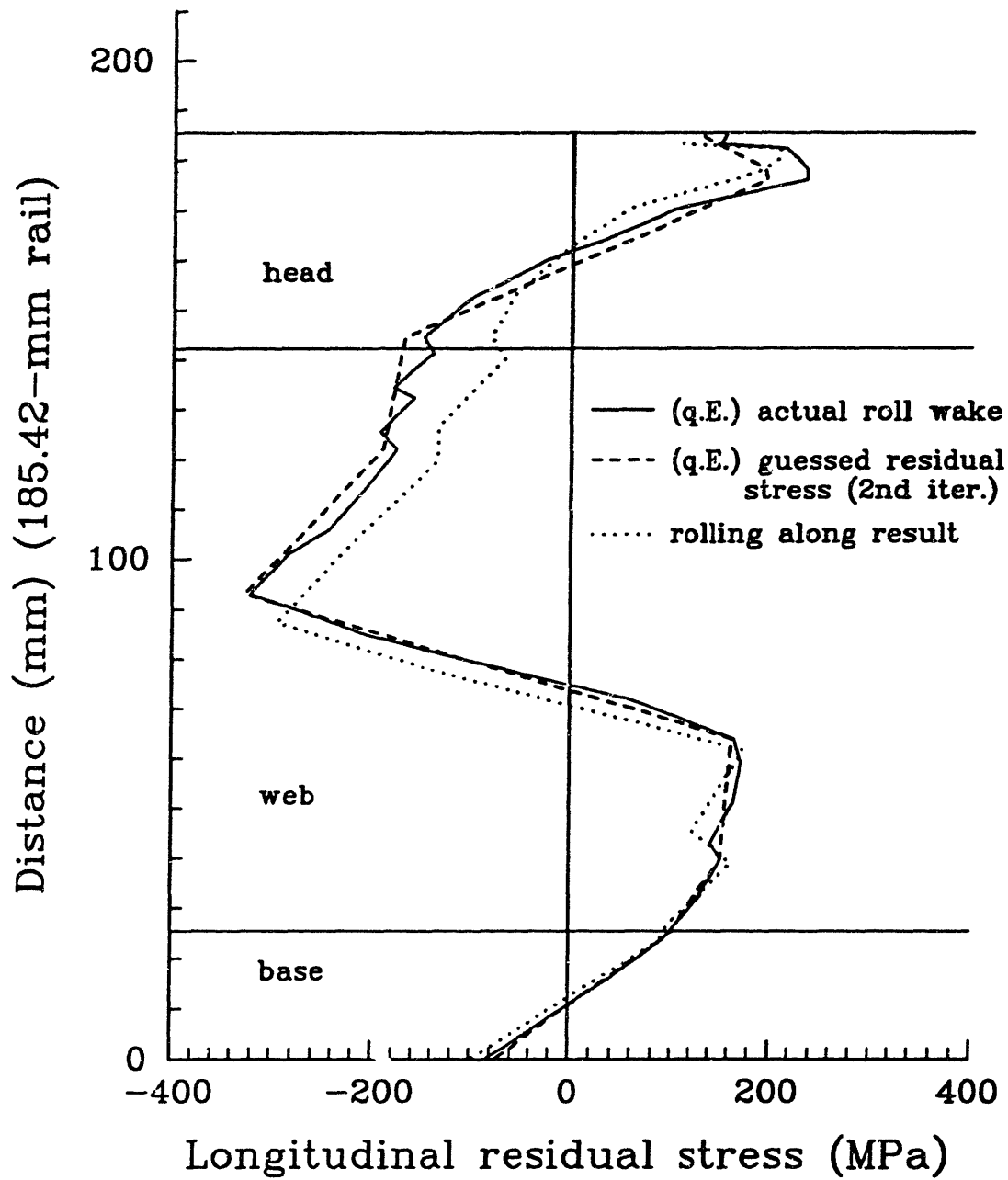
Fig. 41. Resulting residual stresses, quasi—Eulerian and single—roll models.
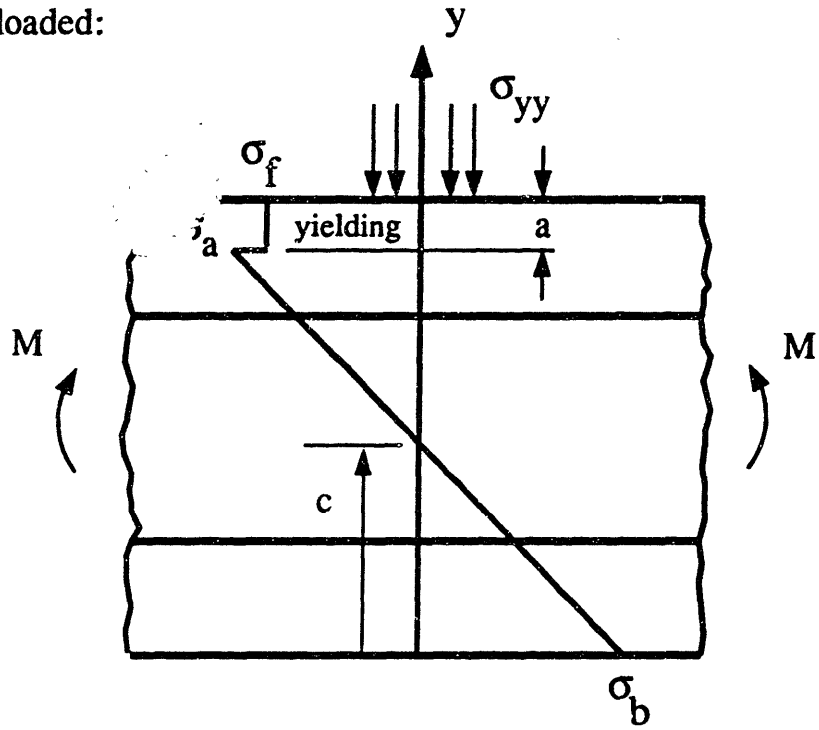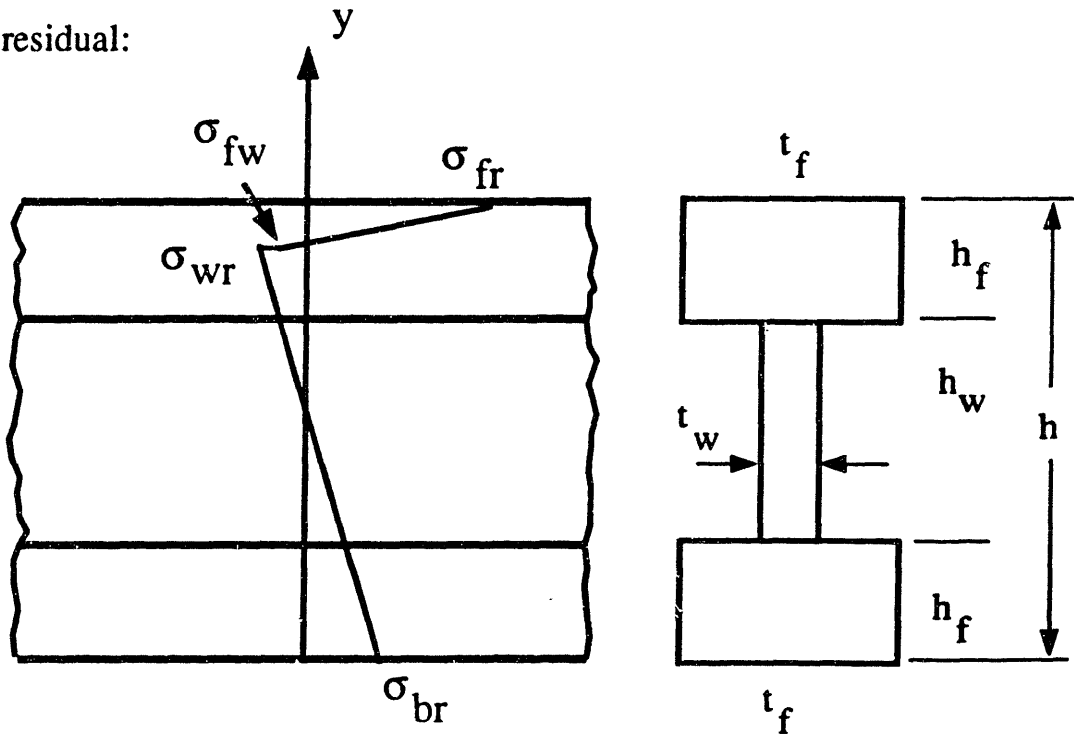
Fig. 42. Analytical model for residual stress creation.

loaded:

$\sigma_f = -0.854\ Y$

$\sigma_{yy} = -1.1Y$

$\sigma_a = -0.871\ Y$

a=0.05 h

M

$M = 0.95\ M_Y$

c =0.497 h

$\sigma_b = 0.955\ Y$

residual:

$\sigma_{fw} = 0.007\ Y$

$\sigma_{fr} = 0.1\ Y$

$t_f = 0.6\ h$

$\sigma_{wr} = -0.01\ Y$

$h_f = 0.2\ h$

$h_w = 0.6\ h$

$t_w = 0.15\ h$

h_f

$\sigma_{br} = 0.005\ Y$

t_f
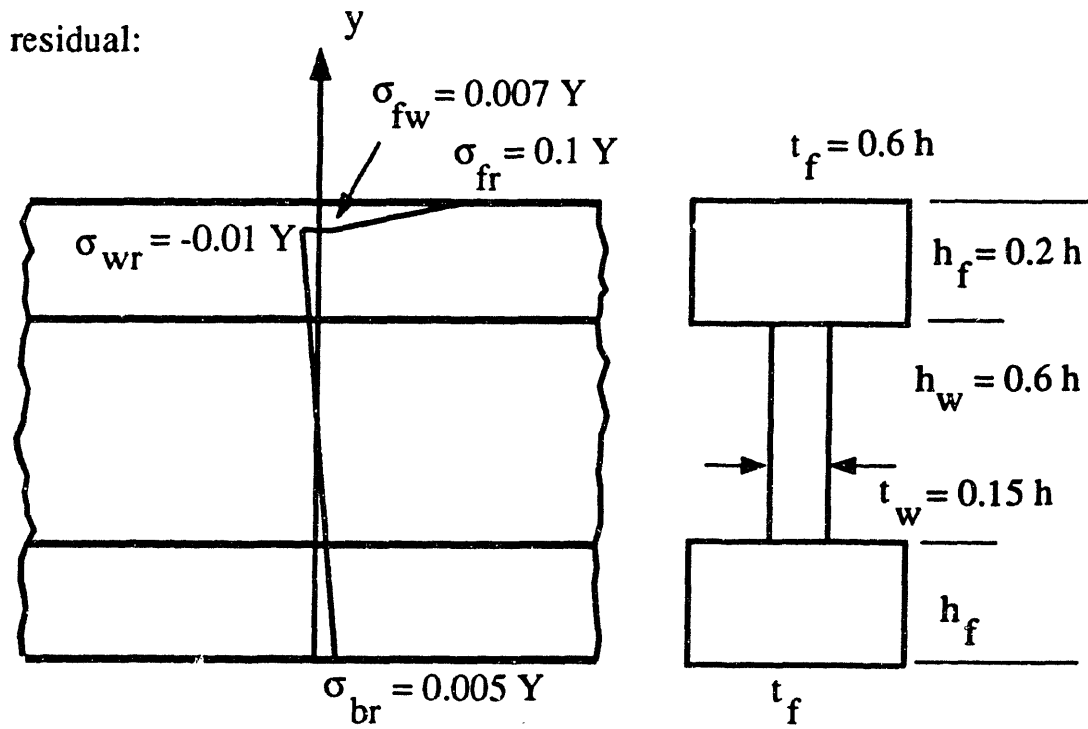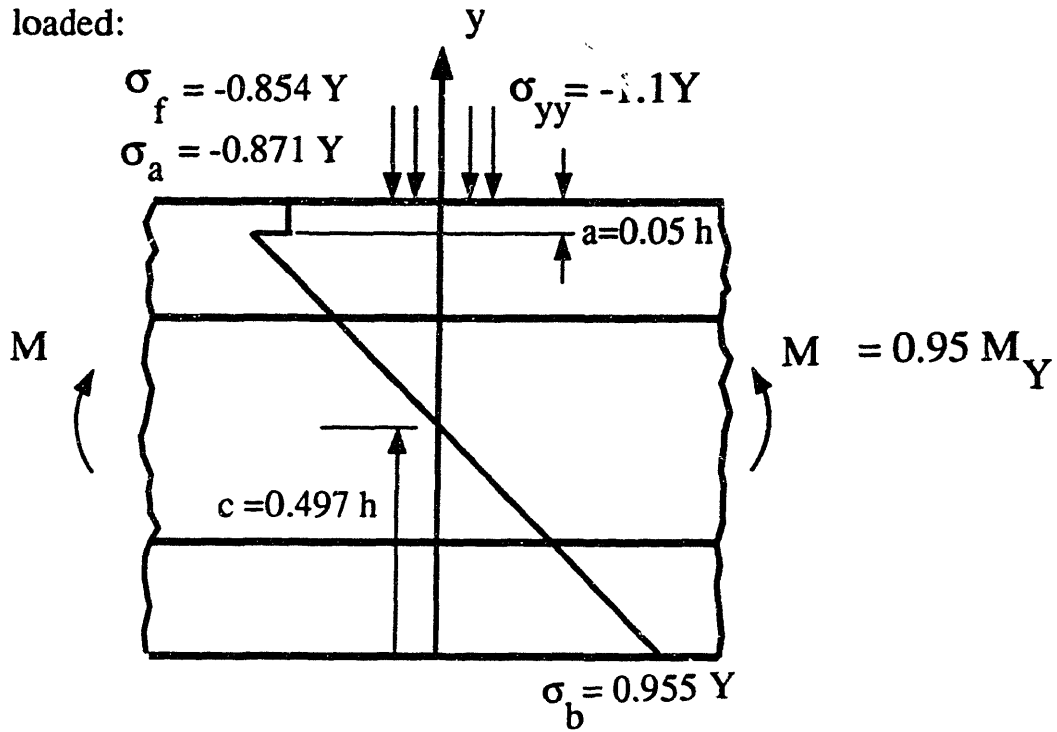
Fig. 43. Analytical model: numerical example giving tension-compression-tension residual stress distribution.

90
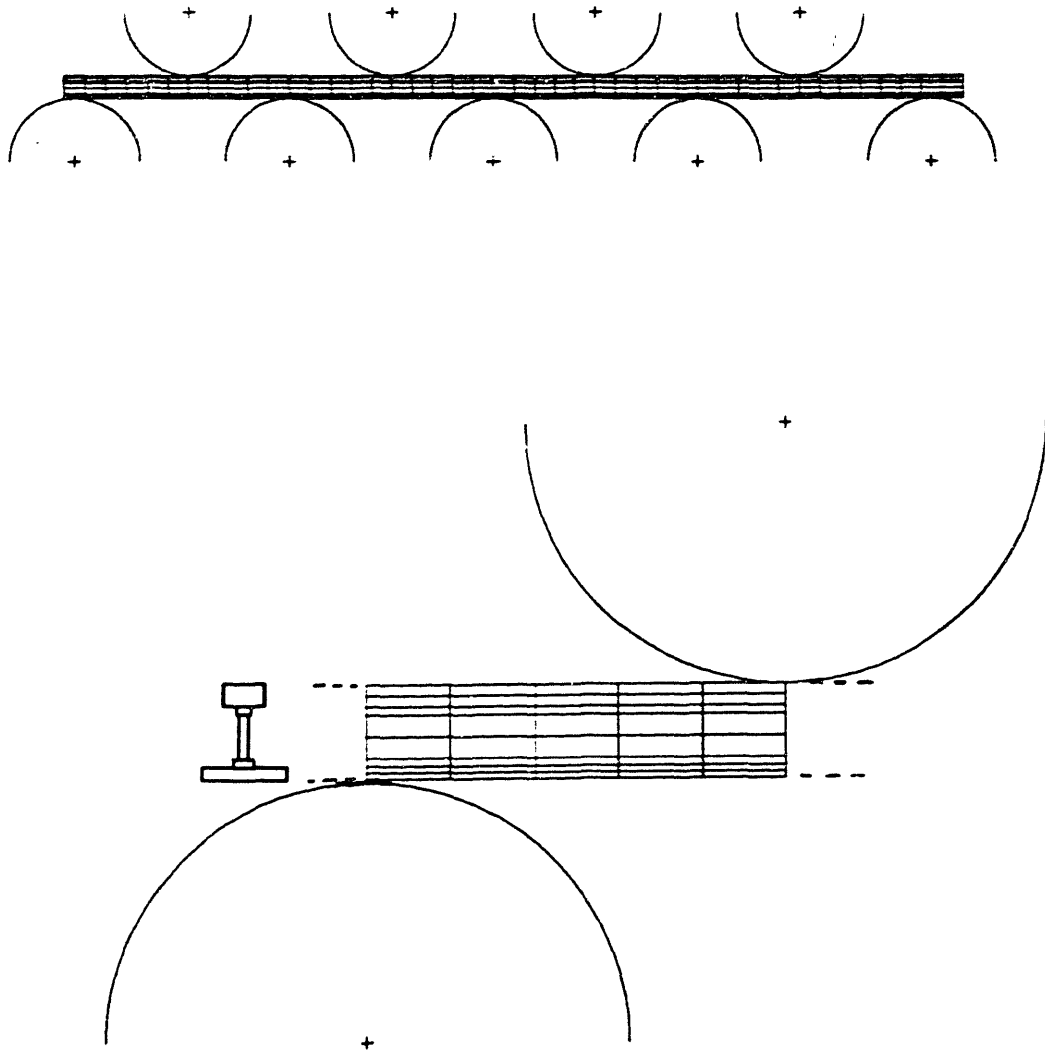
Fig. 44. Plane stress model of a 9-roll straightener.
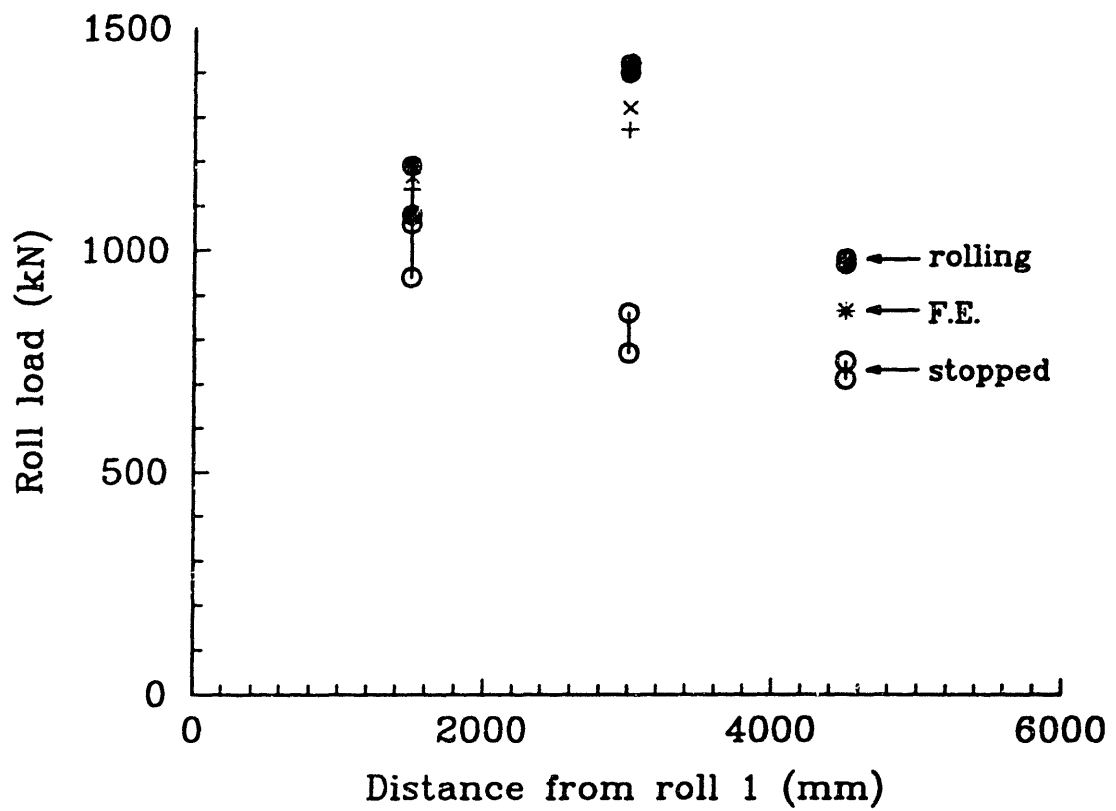
Fig. 45. Comparison of experimental roll loads (rolling and
stopped) with finite element loads.
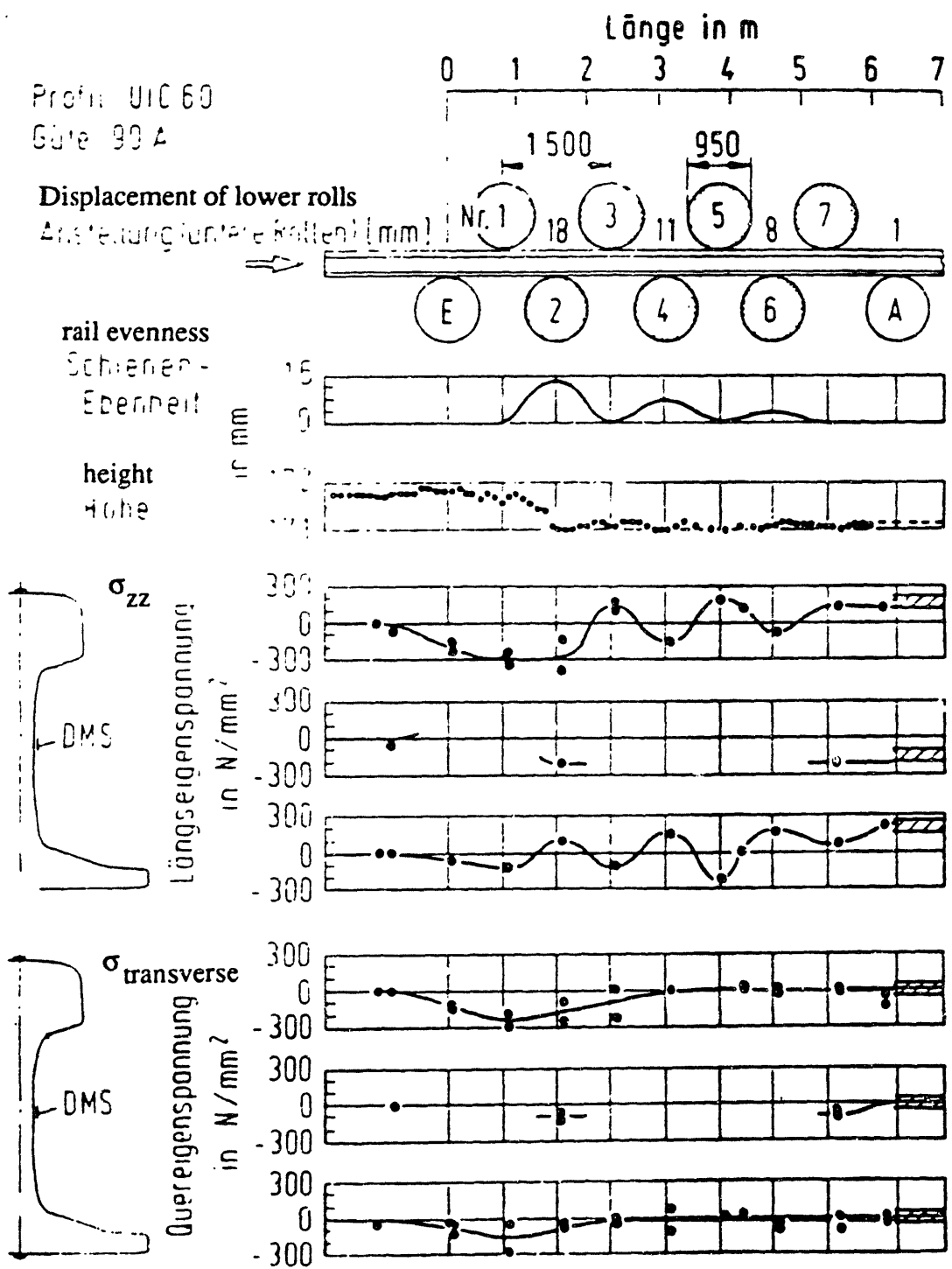
Fig. 46. Experimental data through the straightener. The straightener was stopped and intermediate values of rail deflection, height, and residual stresses were measured (from Schweitzer, Flügge and Heller 1985).

93
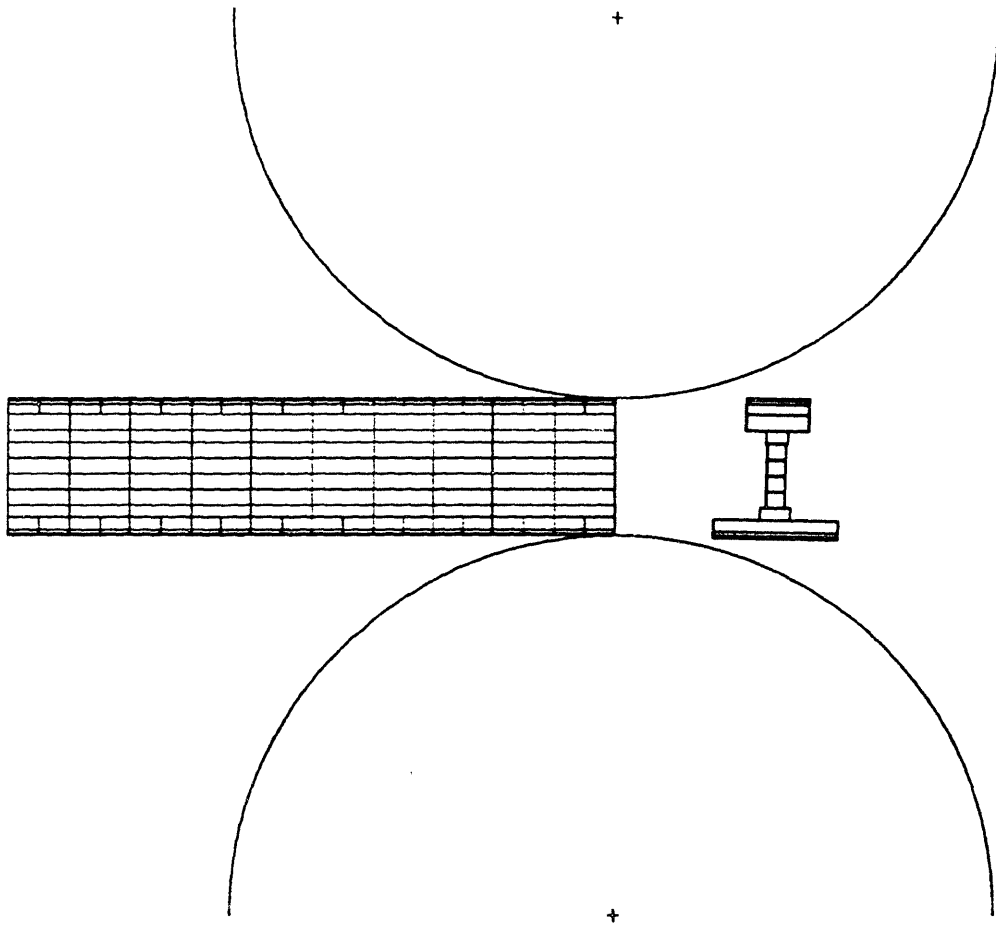
Fig. 47. Plane stress mesh for "single-roll" model, used for comparison with experimental data and for study of effects of increasing roll diameter.
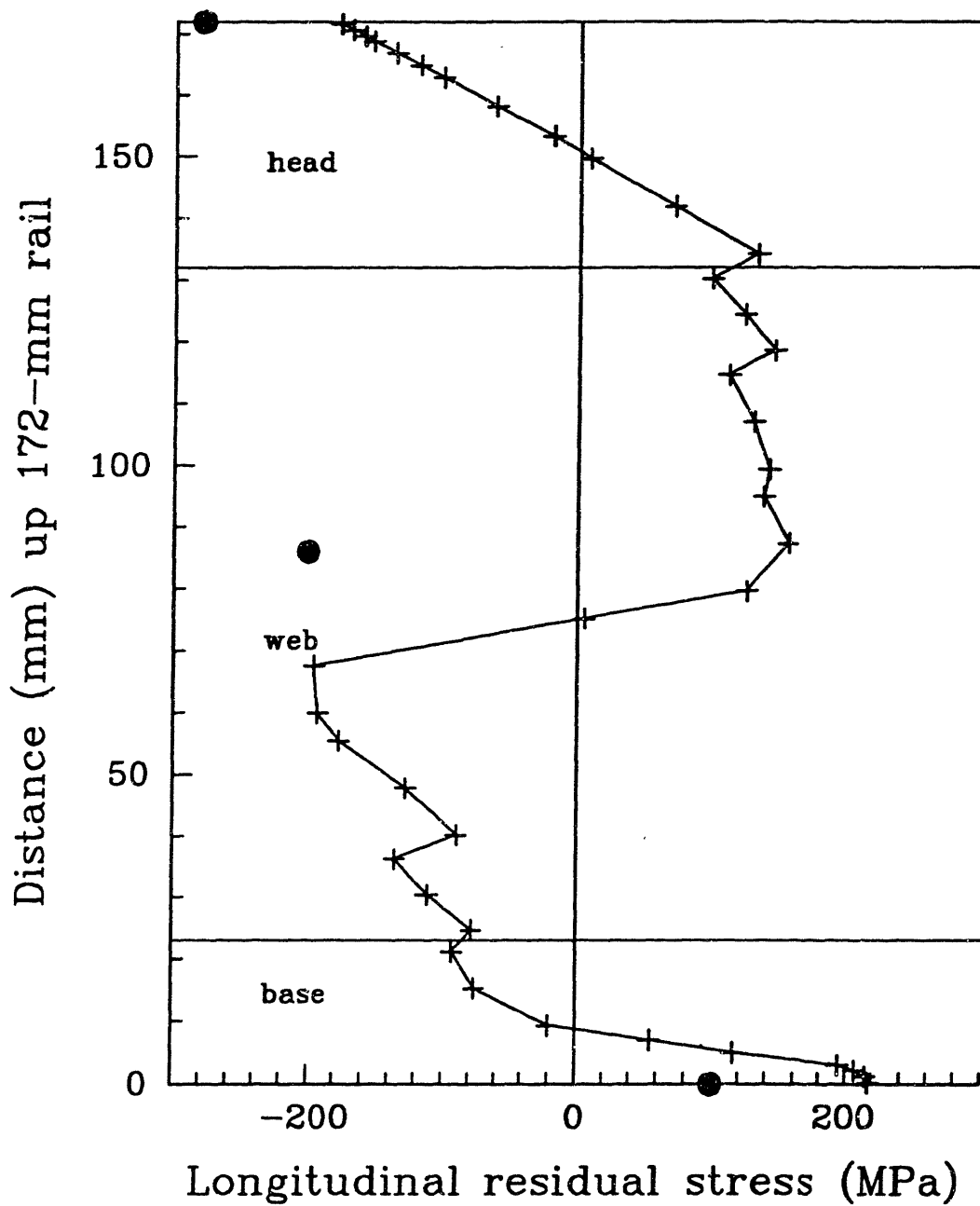
Fig. 48. Longitudinal residual stress after roll 2. Dark circles
represent strain gage measurements taken by Schweitzer
et al. (1985).
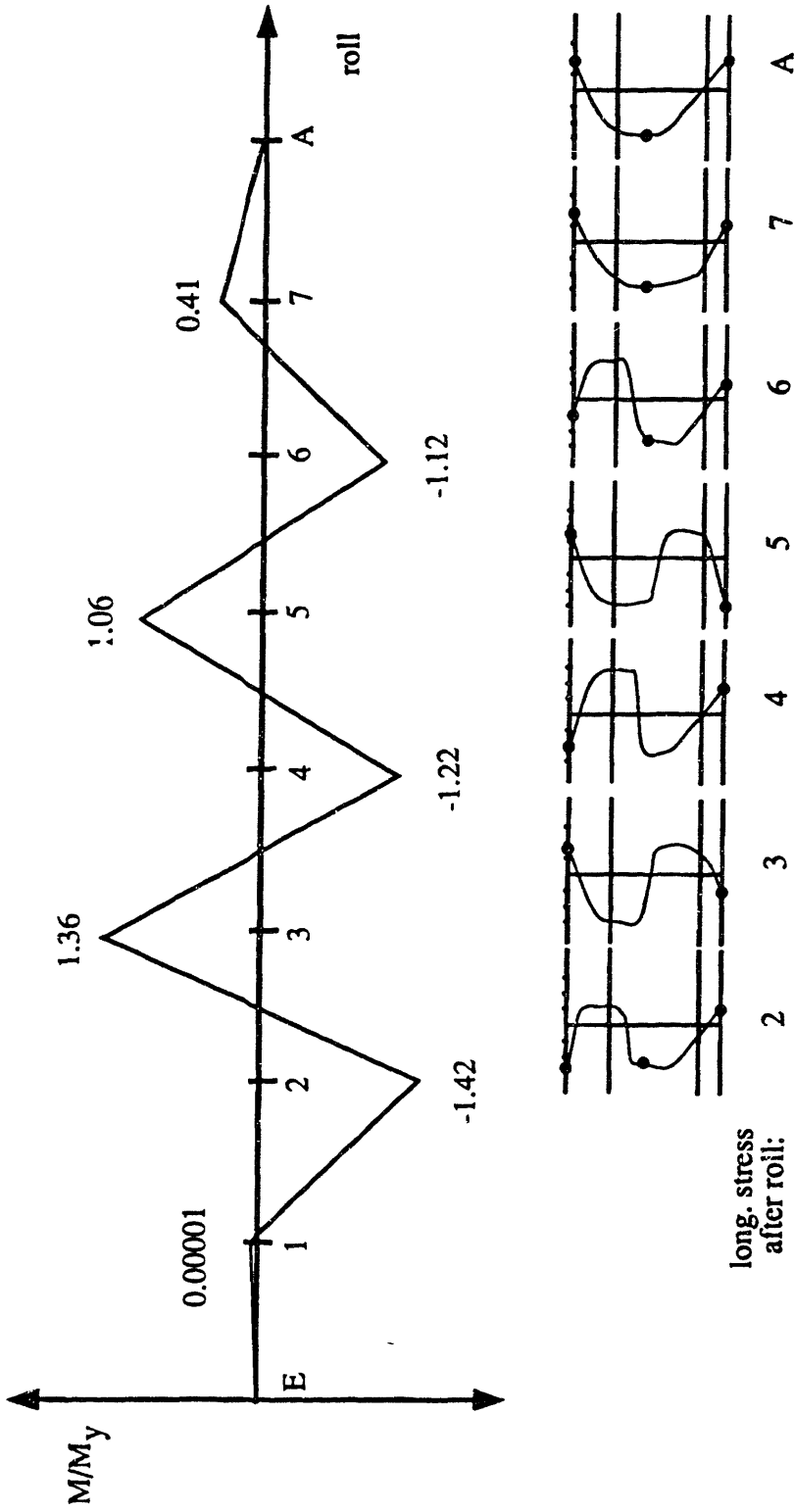
Fig. 49. Bending moment through the straightener and residual stresses after each roll. Bending moments correspond to loads given by a 9-roll static loading finite element model. Residual stress measurements, shown as dark circles, are from Schweitzer, Flugge, and Heller (1985). Postulated residual stress distributions are sketched between data points.

96
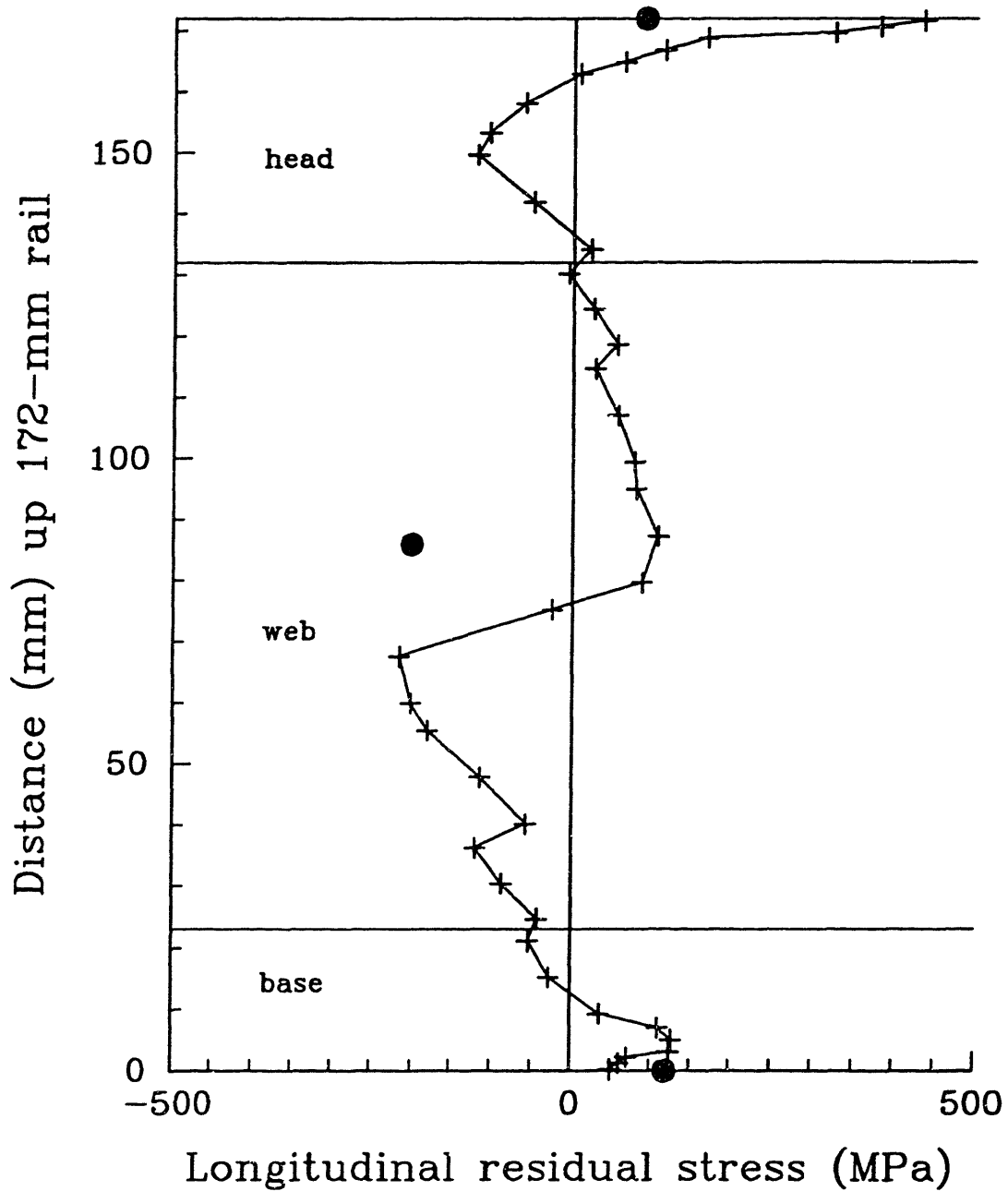
Fig. 50. Longitudinal residual stress after passes with rolls 1, 2, 6, and 7. Dark circles represent strain gage measurements after roll 7 taken by Schweitzer et al. (1985).
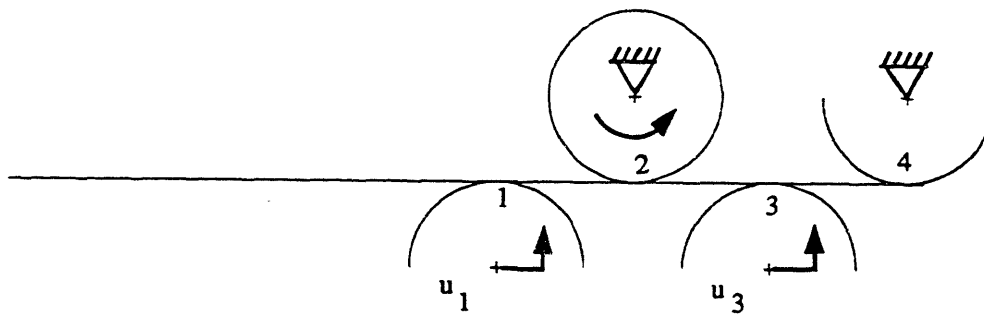
Fig. 51. Beam element model of a 4-roll straightener.
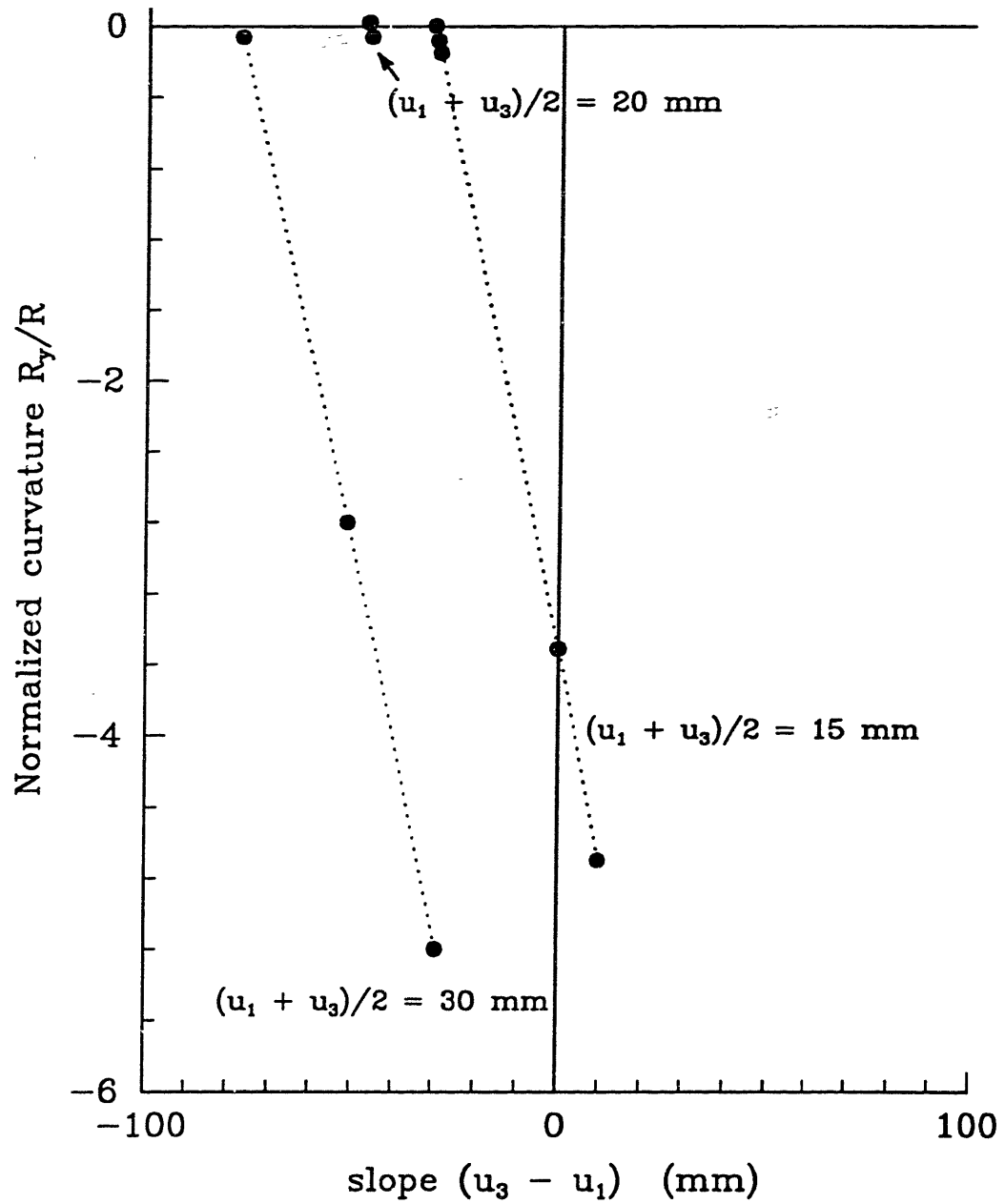
Fig. 52. Results of studies using 4-roll, beam element model.
Variation in final curvature R_y/R with slope ($u_3 - u_1$), for constant
values of average deflection ($u_1 + u_3$)/2.
(yield curvature $1/R_y = 22.61 \times 10^{-6}$ mm^{-1})
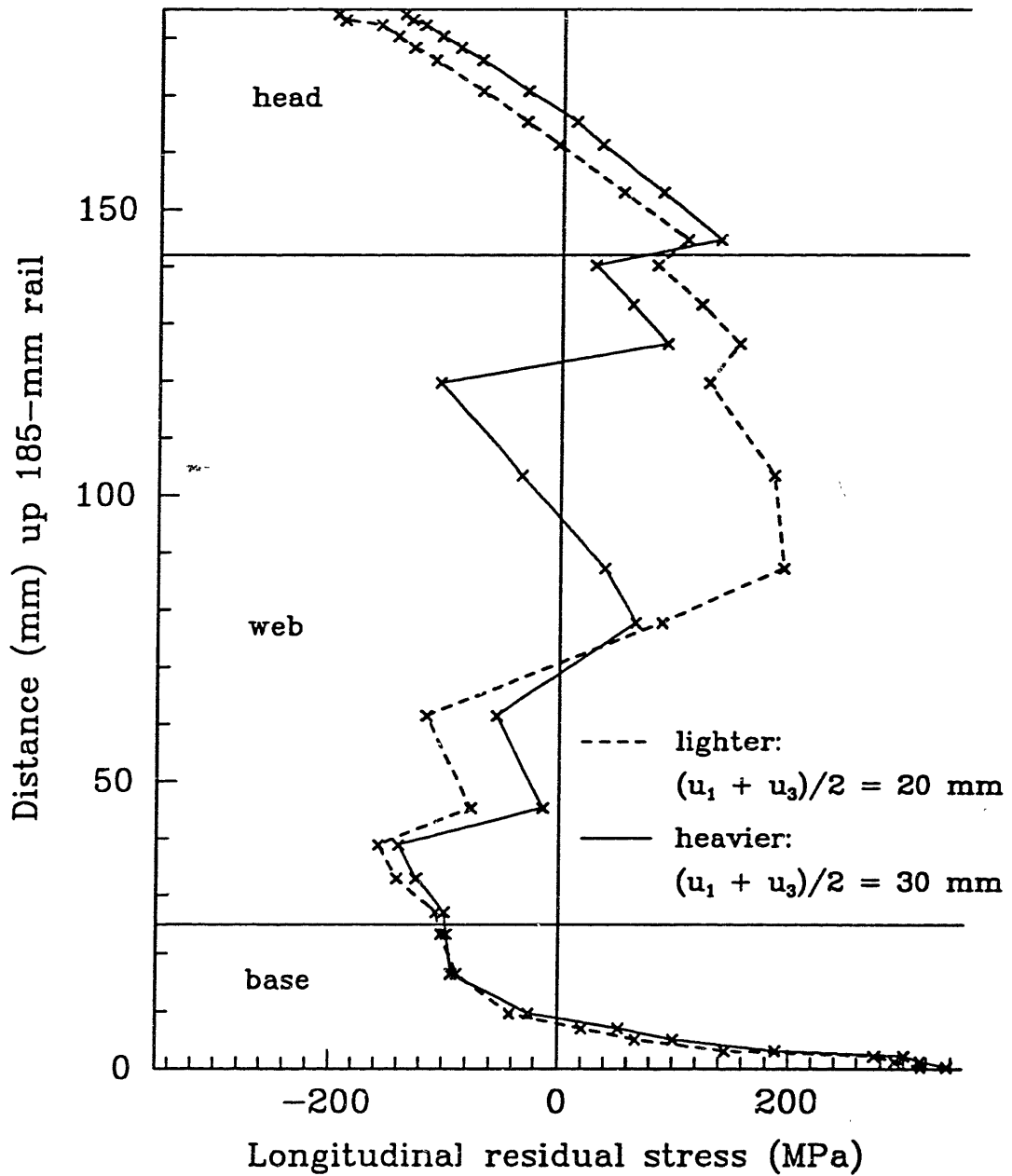
Fig. 53. Longitudinal residual stress after roll 2, for light and heavy straightenings. Results of single-roll model for a 4-roll straightener giving a straight rail.
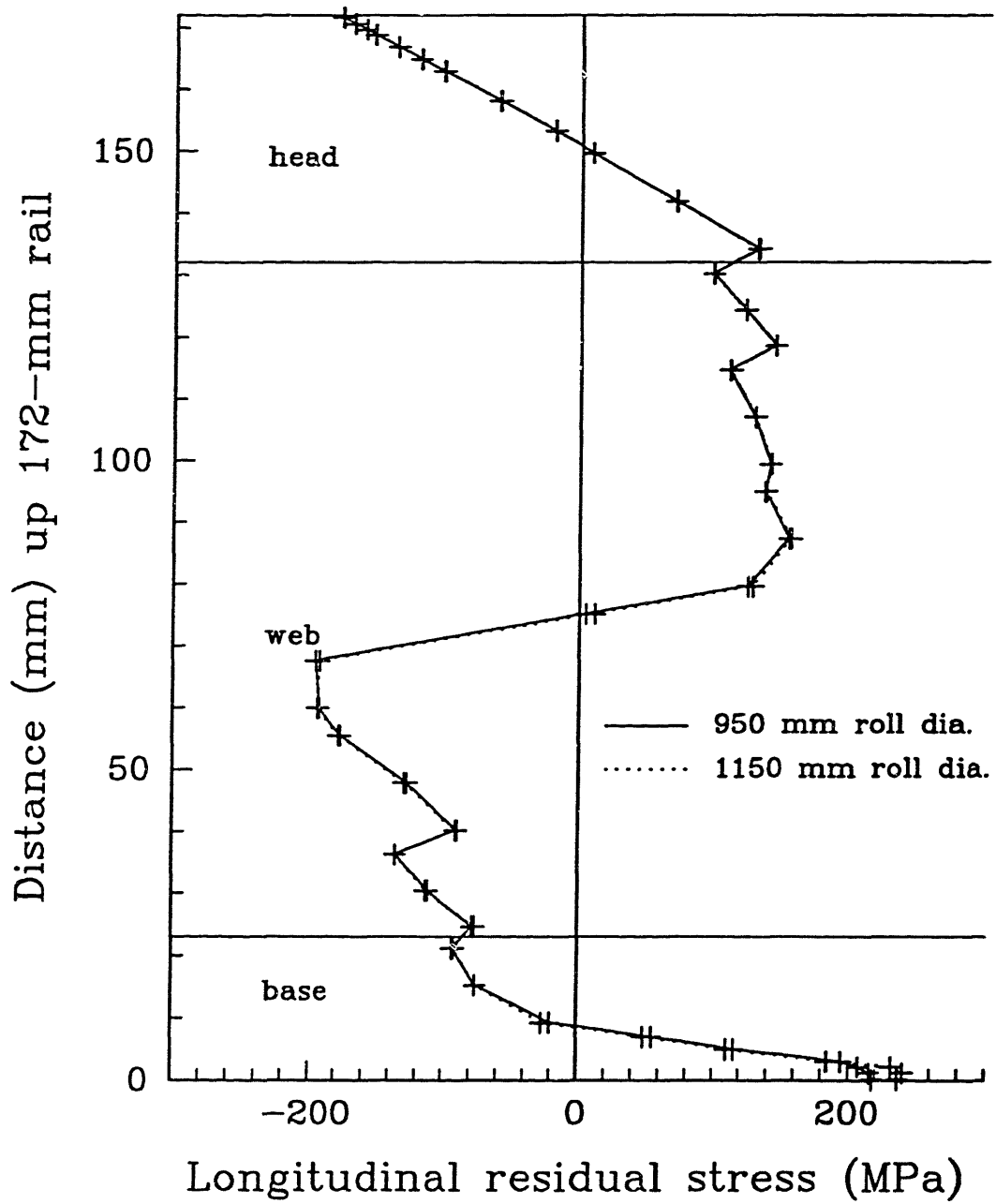
Fig. 54. Longitudinal residual stress after roll 2, for standard and 20% larger roll diameters.
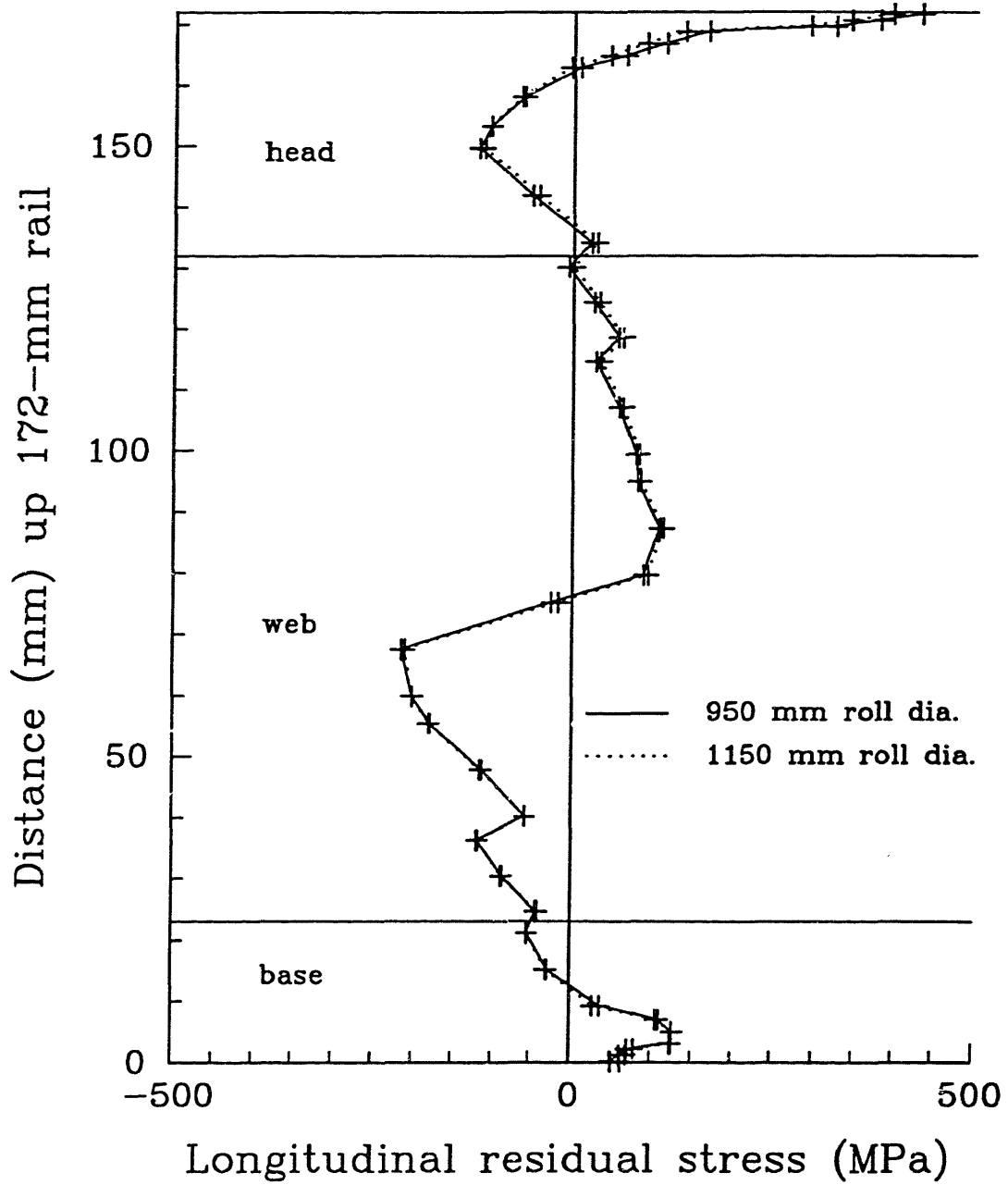
Fig. 55. Longitudinal residual stress after passes with rolls 1, 2, 6, and 7, for standard and 20% larger roll diameters.

Chapter 3

Residual stresses and short cracks at rail ends

3.1 Introduction

The longitudinal residual stress field found in roller-straightened rail can contain enough elastic strain energy to drive web fracture, as demonstrated by Wineman and McClintock (1987). However, near the rail ends this longitudinal residual stress must drop to zero, and for equilibrium there must be an accompanying rise of other residual stress components, such as vertical stress in the web. Knowledge of the length and character of these stress transients is necessary for predicting the behavior of cracks at and near rail ends.

The models discussed here apply to ends of rail which have been cut through the mid-rail stress field, such as may occur during installation or repairs. Mill ends of roller-straightened rail retain their as-rolled dimensions over the first 750-890 mm (30-35 inches) (Deroche et al. 1982), and therefore their end effects should be of this length or longer.

The objective of this work was first to determine the stress transients at a cut rail end for rail containing the longitudinal residual stress field found in roller-straightened rail. Several analytical models and a finite element model were developed and compared. Then the stresses near the end were used to determine the worst location for an end crack. A superposition of point load solutions was used to estimate the stress intensity K_I at the tip of a horizontal web crack in the

(uncracked) rail-end vertical residual stress field.

The stress transients predicted by these models agree with those of the finite element work of Joerms (1987). He reconstructed the residual stresses at the cut end of a roller-straightened rail by modelling the deformed rail resulting from a web saw-cut, then forcing the displacements at the saw-cut location back to zero. The resulting length to develop 95% of the mid-rail longitudinal residual stress was between 0.8 and 1.1 rail heights. The maximum vertical residual stress at the end was 0.96 of the maximum magnitude of longitudinal residual stress developed in mid-rail.

3.2   Models of a rail end

Figure 1 shows a scatterband of typical mid-rail longitudinal residual stress σ_{zz} for roller-straightened rail (ORE 1984, Deroche et al. 1982, Konyukhov, Reikhart, and Kaportsev 1973, Lempitskiy and Kazarnovskiy 1973, and Masumoto et al. 1982). Although residual stresses have been measured on the surface of the rail only, it was assumed in all calculations that the distribution of mid-rail longitudinal residual stress is constant through the rail thickness. The other mid-rail residual stress components, such as a transversely-varying vertical residual stress σ_{yy} in the web, were assumed zero since Wineman and McClintock (1987) demonstrated, based on Groom (1983) and ORE (1984), that their magnitudes and effects on web fracture are small compared with those of σ_{zz}.

The general character of changes in stress components near the rail end can be found from equilibrium. At a free rail end, the longitudinal residual stress σ_{zz} and the shear stress σ_{yz} must go to zero. If the stress gradients in the thickness direction are negligibly small($\partial/\partial x = 0$), the y- and z-direction differential equations of equilibrium require that there be vertical gradients of shear and vertical stress ($\partial\sigma_{yz}/\partial y$ and $\partial\sigma_{yy}/\partial y$) to compensate for longitudinal gradients near the end of longitudinal and shear stress ($\partial\sigma_{zz}/\partial z$ and $\partial\sigma_{yz}/\partial z$). Working through these stress changes keeping careful track of signs gives the general character of residual stress transients near a cut rail end: a longitudinal stress (σ_{zz}) decay to zero at the

end. a tensile vertical stress σ_{yy} at the end which is maximum near mid-web, and shear stresses σ_{yz} toward the end which change sign with y and have a maximum magnitude somewhere near the end, but not at it. In addition, because of thickness transitions at the head-web and web-base intersections, there are stress singularities at the rail end. As shown below, these singularities turn out to be weak even with abrupt thickness transitions; typical fillets make them weak enough to be ignored.

3.2.1 Analytical models

Three analytical models were used to estimate the distance from a cut end needed to develop 95% of the mid-rail residual stress field. Two of these, the beam-on-elastic-foundation model and the elasticity solution of Horvay, can also be used to estimate the maximum vertical stress developed at the end.

Beam on elastic foundation.

Modelling the rail head as a beam on the web as an elastic foundation can give an estimate of the length to reach the mid-rail residual stress and also of the maximum vertical residual stress at the rail end (see Hetényi (1962) or Orringer, Morris and Jeong (1986) for descriptions of beam-on-elastic-foundation models). Several different models were compared, using different definitions for the "beam" and "foundation". Both a free rail end and one whose base is restrained in the vertical direction were modelled. The models giving the best agreement with the finite element results were, for a free rail end, modelling the rail head plus half the web as the beam, on half the web as the foundation, and for a rail with fixed base, modelling the head plus half the web as the beam, plus the whole web as the foundation. In these models, the web or part of the web is behaving as both beam and foundation. The results of these models were within 30% of the finite element results.

It should be kept in mind that real cases of cut rail ends will never have a base which is rigidly constrained, since the spiking of the base to the ties is intermittent and there will always be some compliance in the ties and bed. However, the fixed-

base analytical and finite element models are still useful for estimates.

The length of stress transients at a cut rail end can be found from the characteristic length $1/\lambda$ of the differential equation for displacement of the beam (Hetényi 1962). For rail, the stiffness k of the elastic foundation can be written (Orringer Morris and Jeong 1986) in terms of the web thickness t_{web}, the height of web used as the foundation h_{found}, and the elastic modulus E:

$$k = \frac{t_{web}E}{h_{found}} . \tag{3.1}$$

Dominance by the exponential in the solution for beam displacement means that the length L_{ss} to reach 95% of the mid-rail residual stress field is three times the characteristic length:

$$L_{ss} = 3 \left(\frac{1}{\lambda}\right) = 3 \left[\frac{4EI_{yy}}{k}\right]^{1/4} = 3 \left[\frac{4h_{found}I_{yy}}{t_{web}}\right]^{1/4} . \tag{3.2}$$

Here, I_{yy} is the centroidal moment of inertia of the part of the rail modelling the beam.

The maximum vertical residual stress in the web at a cut end can be estimated from the vertical deflection w at the end of a semi-infinite beam subject to an end moment M_o(Hetényi 1962):

$$w(z = 0) = \frac{-2M_o\lambda^2}{k} = -\frac{M_o}{E}\left[\frac{h_{found}}{t_{web}I_{yy}}\right]^{1/2} . \tag{3.3}$$

The moment M_o was taken to be that acting above the rail centroid for a fourth-order, self-equilibrating polynomial stress distribution representing the longitudinal mid-rail stress.

The vertical stress σ_{yy} in the web at the end is then related to the dimensions and residual moment by

$$\sigma_{yy}(z = 0) = E\epsilon_{yy} \approx E\left(\frac{w(z = 0)}{h_{found}}\right) = -M_o\left[\frac{1}{t_{web}h_{found}I_{yy}}\right]^{1/2} . \tag{3.4}$$

106

Saint-Venant (Horvay).

Saint-Venant's principle suggests that for a uniform-thickness bar, 95% of the steady-state residual stress field will be attained one or two bar heights away from the cut end. Horvay (1957) has solved a related problem for stresses near a self-equilibrated, parabolic distribution of end loads on a uniform-thickness, semi-infinite rectangular strip. From superposition, the stress changes should be the same for end stresses going to zero in mid-strip as for mid-strip stresses going to zero at a free end. For the rail, these stress transients will be changed somewhat by the non-uniform thickness, but Horvay's solution is still useful as a comparison.

From plots of the stress components given in the reference, the length L_{ss} (normalized by the strip height h) to reach 95% of the longitudinal residual stress is:

$$\frac{L_{ss}}{h} \approx 1.8 . \tag{3.5}$$

The maximum tensile stress σ_{yy} in the web at the end, normalized by the maximum longitudinal stress σ_{zz}, is:

$$\frac{\sigma_{yy}}{\sigma_{zzmax}} \approx 0.7 . \tag{3.6}$$

Shear lag.

A shear-lag model (Fig. 2) predicts the length to attain the mid-rail residual stress field by idealizing the rail as a composite of a web and two equal flanges, with transition regions between the web and flanges. In the web and flanges, longitudinal displacement is assumed to be constant vertically and to vary longitudinally. In the transition regions, longitudinal displacement varies linearly with y and also varies longitudinally. All other displacement components are assumed zero. This means that the web and flanges are in a state of longitudinal compression and tension, respectively, and the transition regions are mostly shear. It is useful when analyzing the model to think in terms of *changes* in stress and displacements from the mid-rail field. That is, in mid-rail the displacement changes Δu and the stress changes $\Delta \sigma$ are zero. At the free end, the displacement and stress changes are nonzero, with the

107

stress changes at the end being the same in magnitude and opposite in sign to the original mid-rail stress field. The length to reach 95% of the mid-rail stress field, then, is the length for 95% of the displacement and stress changes to decay to zero.

Equilibrium for a differential element dz in the web can be written in terms of the longitudinal stress change $\Delta\sigma_{zzw}$ in the web, the shear stress change $\Delta\sigma_{yzt}$ in the transition region, and the height h_{wi} of the idealized web (the transition regions are the same thickness as the web):

$$\frac{d\Delta\sigma_{zzw}}{dz} = -\frac{2\Delta\sigma_{yzt}}{h_{wi}}. \tag{3.7}$$

Equilibrium for a differential element in the flange can be written in terms of the longitudinal stress change $\Delta\sigma_{zzf}$ in the flange, the shear stress change $\Delta\sigma_{yzt}$ in the transition region, the flange height h_f, and the web and flange thicknesses t_w and t_f:

$$\frac{d\Delta\sigma_{zzf}}{dz} = \frac{\Delta\sigma_{yzt}t_w}{h_f t_f}. \tag{3.8}$$

Combining these into one equation gives

$$\frac{d}{dz}(\Delta\sigma_{zzf} - \Delta\sigma_{zzw}) = \left(\frac{t_w}{h_f t_f} + \frac{2}{h_{wi}}\right)\Delta\sigma_{yzt}. \tag{3.9}$$

The stress changes can be expressed in terms of displacement changes via the following relations, where h_t is the height of the transition region and E and G are the elastic and shear moduli, respectively:

$$flange: \quad \Delta\sigma_{zzf} = Ed(\Delta u_{zf})/dz. \tag{3.10}$$

$$\tag{3.11}$$

$$web: \quad \Delta\sigma_{zzw} = Ed(\Delta u_{zw})/dz. \tag{3.12}$$

$$\tag{3.13}$$

$$transition\,region: \quad \Delta\sigma_{yzt} \approx G(\Delta u_{zf} - \Delta u_{zw})/h_t. \tag{3.14}$$

This results in a differential equation of the form

$$\frac{d^2}{dz^2}(\Delta u_{zf} - \Delta u_{zw}) = \frac{1}{L^2}(\Delta u_{zf} - \Delta u_{zw}) \tag{3.15}$$

108

where

$$L = \left[\frac{E}{G} \frac{h_t h_{wi} h_f t_f}{(h_{wi} t_w + 2h_f t_f)} \right]^{1/2} , \tag{3.16}$$

and boundary conditions

$$(\Delta u_{zf} - \Delta u_{zw}) \to 0 \quad as \quad z \to \infty , \tag{3.17}$$

$$(\Delta \sigma_{zzf} - \Delta \sigma_{zzw}) = -(\sigma_f - \sigma_w) \quad at \quad z = 0 . \tag{3.18}$$

Here, σ_f and σ_w are the flange and web stresses in the idealized original mid-rail residual stress field.

The solution to the above differential equation is an exponential with characteristic length L. The length L_{ss} to reach 95% of the mid-rail stress field, then, is three times this length:

$$L_{ss} = 3 \left[\frac{E}{G} \frac{h_t h_{wi} h_f t_f}{(h_{wi} t_w + 2h_f t_f)} \right]^{1/2} . \tag{3.19}$$

Choosing h_t so that L_{ss} is maximized, remembering that $h_{wi} + 2h_t = h_w$ (the actual web height) gives:

$$h_t = (h_w - h_{wi})/2 \tag{3.20}$$

$$h_{wi} = \frac{1}{t_w} [4h_f^2 t_f^2 + 2h_f t_f h_w t_w]^{1/2} - \frac{2h_f t_f}{t_w} . \tag{3.21}$$

3.2.2 Finite element model

To obtain a more complete description of stress transients at the rail end, a plane-stress finite element model with elements of different thickness for the head, web, and base was run using the finite element program ABAQUS (1985). The final mesh of 8-node elements (Fig. 3) represented a 610 mm (24 in) long section of rail. At one end, the longitudinal displacements of all nodes and the vertical displacement of the node nearest to the centroid were constrained to simulate attachment to the rest of the rail. For the case imitating a rail spiked to fixed ties, the bottom nodes were also constrained. Residual stresses were introduced by specifying a self-equilibrating

initial stress distribution in the form of a fourth-order polynomial with maximum values of ± 138 MPa (± 20 ksi), and letting the program bring this to equilibrium.

The element size in the final mesh was chosen by estimating the curvature of the stress contours over several elements, and choosing the element size so that the error due to approximating these curved contours by linearly-varying-stress elements was less than 5% of the maximum longitudinal residual stress σ_{zzmax}. Assuming the local curvatures within an element are small and approximately constant, the error can be estimated as follows. Let $\partial^2 \sigma_{ij}/\partial x_k^2$ be the estimated curvature of a stress component in the x_k direction (y or z direction), and Δx_k be the element size. Then the error can be estimated as half the maximum distance between the curved stress contour and its mid-point tangent:

$$error \equiv \frac{1}{2} \left[\frac{1}{2} \left(\frac{\partial^2 \sigma_{ij}}{\partial x_k^2} \right) \left(\frac{\Delta x_k}{2} \right)^2 \right] \quad (no\ summation\ over\ x_k). \quad (3.22)$$

Singularities at thickness transitions. In the variable-thickness mesh, singularities in stress exist at the rail end at the thickness transitions. The strength of such singularities can be found by modelling the different thicknesses as different shear moduli: $G_1/G_2 \approx t_1/t_2$, and using Bogy's solution (1970) for two elastic quarter-planes with different moduli. The stresses vary as $r^{-\ell}$, where r is the distance from the intersection of the planes at the free surface. The exponent ℓ can be found from a plot in Bogy's paper, in terms of Dundurs' parameters α and β (functions of the elastic constants of the two quarter-planes). For the head-web and web-base intersections, the stress distributions can be written in terms of the radial distance r, the angle θ from the interface, and the exponent ℓ:

$$\sigma_{ij} = r^{-\ell} f(\theta), \quad where \quad \ell = \ 0.10 \ (head - web) ,$$

$$0.15 \ (web - base) . \quad (3.23)$$

This singularity is very weak. For example, suppose the singularity is in effect 10 mm from the rail end. Then the stress will not double due to the singularity until 0.1 mm from the end for the web-base region, and not until 0.01 mm from the end for the head-base region. These lengths to double are negligible compared

110

to an 18 mm (0.7 in) web thickness. Fillets with radii of the order of 20 to 25 mm ($\approx 3/4$ to 1 inch) at the head-web and web-base intersections smooth the thickness transitions and would practically eliminate the effects of stress singularities.

3.3 Discussion of model predictions

3.3.1 Stress transients near a cut rail end

Contour plots from the finite element model (Figs. 4-6) give a general picture of stress components σ_{zz}, σ_{yy}, and σ_{yz} near the rail end. Stresses have been plotted separately for the head, web, and base to avoid smoothing across the thickness transitions. Although there should be no visible singularities in stress at the rail ends near the thickness transitions, the plots of longitudinal and shear stress show small perturbations there. These probably result from approximating the actual stress fields using elements with linearly-varying stresses. As a confirmation of the finite element modelling, a uniform-thickness finite element model was applied to Horvay's problem, giving results within 15% for a parabolic stress distribution. Use of a fourth-order distribution did not affect the length of transients appreciably but increased the maximum vertical stress from 0.7 to 1.0 times σ_{zzmax}.

Length of stress transients

Table 1 summarizes the predictions from various models of the length L_{ss} to reach 95% of the mid-rail residual stress distribution, normalized by a rail height of 185 mm (7.3 in). For a free rail end, values of the length L_{ss} range from 0.69-1.22 times the rail height with the highest value coming from the beam-on-elastic-foundation model and the lowest value coming from the shear lag model. The finite element predictions for free and fixed rail ends are 1.10 and 1.12 rail heights, respectively, while the beam-on-elastic-foundation model predictions are at most 30% higher.

Maximum vertical stress

Table 1 also summarizes the analytical and finite element predictions of maximum vertical residual stress σ_{yy} at the rail end near mid-web, normalized by the maximum

111

value of mid-rail longitudinal residual stress $\sigma_{zzmax} = 138$ MPa (20 ksi). For a free rail end, values of maximum vertical residual stress range from 0.7 to 1.35 times the maximum σ_{zz}. The finite element predictions for free and fixed rail ends are 1.35 and 1.10, respectively, while the beam-on-elastic-foundation model predictions are at most 30% lower.

It can be concluded, then, that appropriately chosen beam-on-elastic-foundation models, requiring only algebraic calculations, can give estimates of stress transients at a cut rail end that are within 30% of the finite element results.

Shear stresses

The finite element contours of shear stress σ_{yz} (Fig. 6) show σ_{yz} to be zero at the rail end and at mid-rail, and to reach a maximum magnitude of 0.3 and -0.4 times the maximum σ_{zz} near the head-web and web-base intersections, respectively, about 0.3 rail heights (50 mm, or 2 inches) from the cut rail end. This can be compared with Horvay's solution (1957), which gives a maximum magnitude of shear stress σ_{yz} of 0.18 times the maximum value of applied stress, at 0.45 strip heights from the end.

3.3.2 Stress intensity on short end cracks

The worst location for a crack is at the cut rail end, near mid-web where the vertical residual stress is a maximum. The stress intensity K_I was estimated for a horizontal crack in the mid-web (uncracked) stress field resulting from the finite element analysis of a free rail end. Superposition of point load K_I solutions (from Hartranft and Sih (1973), in Murakami et al.(1987)) were used to represent the effect of the non-uniform distribution of vertical residual stress near the end. The resulting values of K_I versus crack length are shown in Fig. 7 by a solid line: the stress intensity reaches approximately 22 MPa$\sqrt{m}$ (20 ksi$\sqrt{in}$) for cracks 13 mm (0.5 in) long. A region bounded by light lines, representing the probable behavior, connects the stress intensity K_I for short cracks with K_I for long running cracks of 36-47 MPa$\sqrt{m}$ (33-43 ksi$\sqrt{in}$) from the energy release rate analysis in Wineman

and McClintock (1987).

These stress intensity values are comparable to the range of fracture toughnesses K_{Ic} of 27-55 MPa$\sqrt{m}$ (25-50 ksi$\sqrt{in}$) for carbon and alloy rails (see, for example, Orringer Morris and Steele 1984, Jones and Rice 1985).

3.3.3 Longitudinal displacements at the free rail end

For roller-straightened rail, when a short length is cut from mid-rail, for example to use in the Meier technique of residual stress measurement (Groom 1983), the flanges of the Meier length will be shorter and the web longer than the average length of the section. From the finite element model, this difference in displacement is as much as 0.1 mm (0.004 in). Failure to correct for these differences during initial cutting could result in an underestimate of the magnitude of longitudinal residual stress of as much as 48 MPa (7 ksi) on a 460 mm (18 in) Meier length. This is significant compared to typical residual stress maxima of 138 MPa (20 ksi) for roller-straightened rail. Thus, the length changes at various locations around the rail periphery should be measured and used in calculating residual stress, as is done in practice. A further, smaller effect is due to the variation of longitudinal stress across the head from surface to interior.

3.4 Conclusions

Rail with a self-equilibrating longitudinal residual stress field having maximum and minimum values of ±138 MPa (±20 ksi), representative of that found in roller-straightened rail, was modelled to determine the stress transients near a cut rail end and the location and severity of the worst possible end-crack.

1. Stress transients at a cut end of roller-straightened rail consist of a decrease to zero of longitudinal stress at the end and a vertical tensile residual stress in the web at the end. Finite element models for both a free end and an end with a fixed base gave the lengths to reach 95% of the mid-rail stress field to be 1.10 and 1.12 rail heights, respectively. The maximum vertical stresses at

the end were 1.35 and 1.10 times the maximum value of mid-rail longitudinal residual stress. Beam-on-elastic-foundation models give algebraic estimates of such stress transients agreeing within 30% of the finite element results.

2. An estimate of the stress intensity K_I on a short web crack at the rail end, in the (uncracked) vertical residual stress field there, gives K_I increasing with crack length and reaching 22 MPa$\sqrt{\text{m}}$ (20 ksi$\sqrt{\text{in}}$) for cracks 13 mm (0.5 in) long. Although K_I on short cracks may not be sufficient in itself to drive a web crack, in the presence of service loads the risk of fracture is greatly increased.

3. When a length of roller-straightened rail is taken from mid-rail the changes in longitudinal displacements can be large enough to affect subsequent residual stress measurements. For example, if the uneven length changes on cutting a 460 mm (18 in) Meier section are not accounted for, there may be an underestimate of the magnitude of measured longitudinal residual stress of as much as 48 MPa (7 ksi), significant compared to typical maxima of 138 MPa (20 ksi) for roller-straightened rail.

3.5 References

1. ABAQUS (1985) A general-purpose finite element code with emphasis on non-linear applications, version 4.5, *Hibbitt, Karlsson, and Sorensen Inc.*, Providence, RI.

2. Bogy, D.B. (1970) "On the problem of edge-bonded elastic quarter-planes loaded at the boundary", *Int. J. Solids Structures*, 6, 1287-1313.

3. Deroche, R.Y. et al., (1982) "Stress releasing and straightening of rails by stretching", Paper no. 82-HH-17, *Proc. Second International Heavy Haul Railway Conference*, Colorado Springs, CO.

4. Groom, J.J. (1983) "Determination of residual stresses in rails", Battelle Columbus Laboratories, Columbus, OH, FRA/ORD-83/05.

5. Hartranft, R.J., Sih, G.C. (1973) *Methods of Analysis and Solutions of Crack Problems*, G.C. Sih ed., Noordhoff, Holland.

6. Hetényi, M. (1962) "Beams on elastic foundation", in *Handbook of Engineering Mechanics*, W. Flügge ed., McGraw-Hill, sec 31.

7. Horvay, G. (1957) "Some aspects of Saint Venant's principle", *J. Mech. Phys. Solids*, 5, 77-94.

8. Joerms, M.W. (1987) "Calculation of residual stresses in railroad rails and wheels from sawcut displacement", *Residual Stress-in Design, Process and Material Selection*, W.B. Young ed., American Society of Metals, 205.

9. Jones, D.J., Rice, R.C. (1985) "Determination of K_{Ic} fracture toughness for alloy rail steel", final report to DOT Transportation Systems Center, Cambridge, MA.

10. Konyukhov, A.D., Reikhart, V.A., Kaportsev, V.N. (1973) "Comparison of two methods for assessing residual stresses in rails", *Industrial Laboratory (USSR)*, 39, 117-119.

11. Lempitskiy, V.V., Kazarnovskiy, D.S. (1973) "Improving the service life and reliability of railroad rails", *Russian Metallurgy*, 1, 111-117.

12. Masumoto, H., et al. (1982) "Production and properties of a rail of high serviceability", 61st Transportation Research Board Annual Meeting, Washington, D.C.

13. Murakami, Y., ed. (1987) *Stress Intensity Factors Handbook*, Pergamon, Oxford, **1**, 108.

14. ORE (1984) "Factors influencing the fracture resistance of rails in the unused condition", in: *Possibilities of Improving the Service Characteristics of Rails by Metallurgical Means, Report No. 1*, Office for Research and Experiments of the International Union of Railways (ORE/IUR), Utrecht.

15. Orringer, O., Morris, J.M., Jeong, D.Y. (1986) "Detail fracture growth in rails: test results", *Theor. Appl. Fracture Mech.*, **5**, 63-95.

16. Orringer, O., Morris, J.M., Steele, R.K. (1984) "Applied research on rail fatigue and fracture in the United States", *Theor. Appl. Fracture Mech.*, **1**, 23-49.

17. Wineman, S.J., McClintock, F.A. (1987) "Rail web fracture in the presence of residual stresses", *Theor. Appl. Fracture Mech.*, **8**, 87-99.

Table 1. Length L_{ss} to reach 95% of the mid-rail residual stresses, normalized by a rail height h_{rail} of 185 mm(7.3 in.), and maximum vertical residual stress σ_{yy} at the rail end, normalized by the maximum mid-rail longitudinal residual stress, σ_{zzmax}, of 138 MPa (20 ksi), from finite element and analytical predictions.

Model	L_{ss}/h_{rail}	$\sigma_{yy}/\sigma_{zzmax}$
Finite element		
Joerms (1987) (free end)	0.8–1.1	0.96
free end	1.10	1.35
base spiked to fixed ties	1.12	1.10
Analytical models		
Beam on elastic foundation		
free end	1.22	1.11
base spiked to fixed ties	1.45	0.79
Shear lag	0.69	–
Uniform strip solution (Horvay 1957)	1.8	0.7
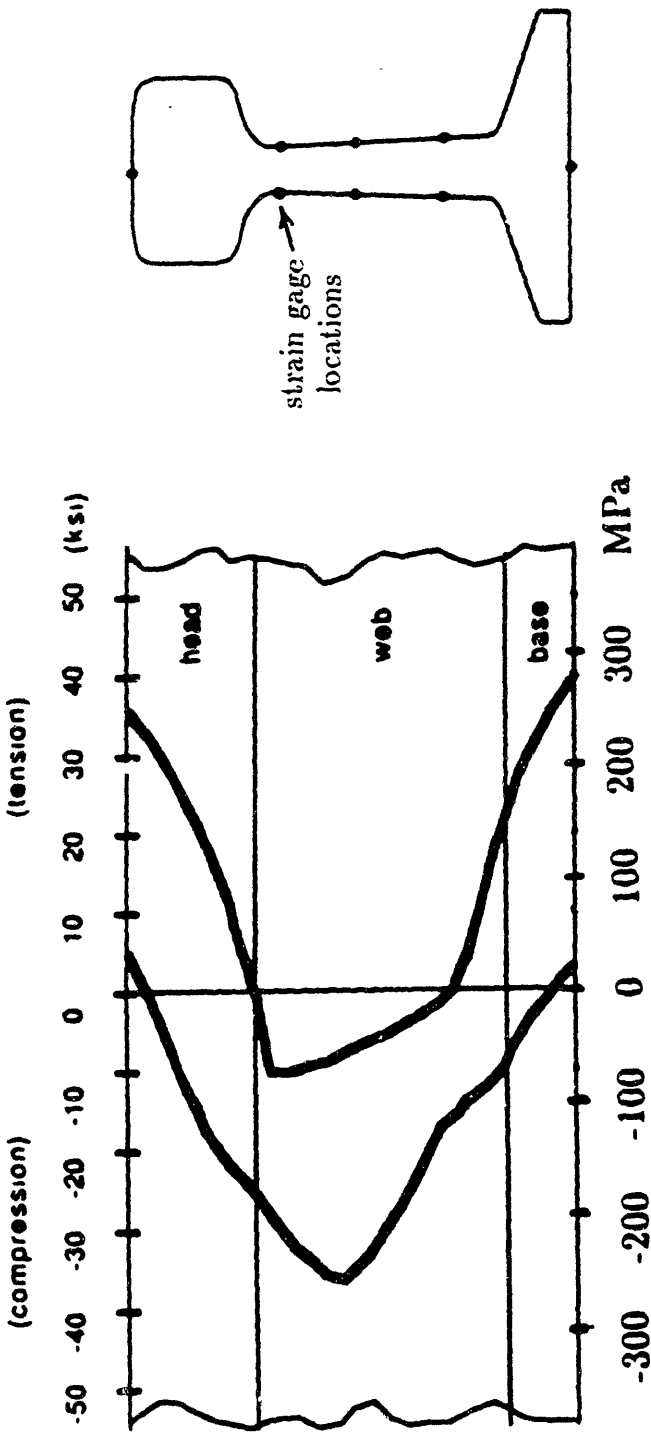
Fig. 1. Scatterband of longitudinal residual stress due to roller-straightening (sources: ORE 1984, Deroche 1982, Konyukhov, Reikhart, and Kaportsev 1973, Masumoto et al. 1982).

118
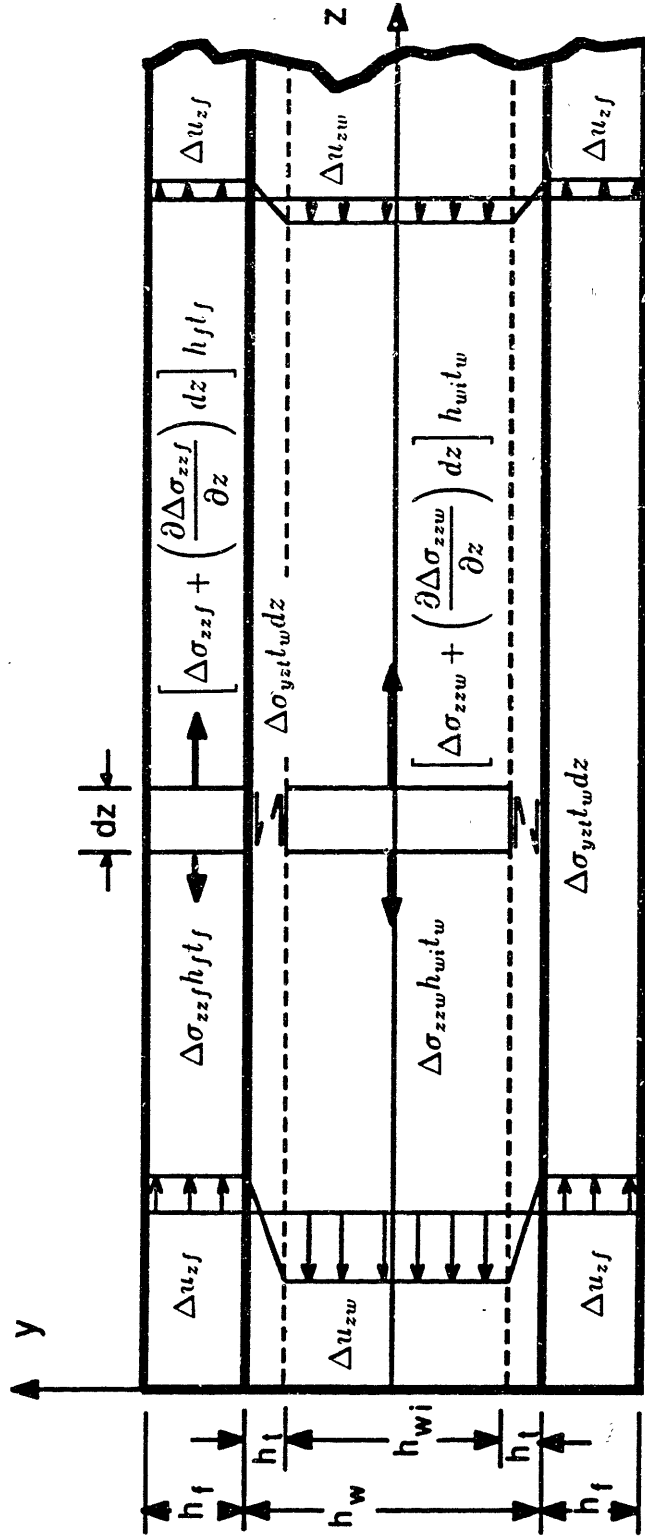
Fig. 2   Idealization of the rail for shear lag calculation.
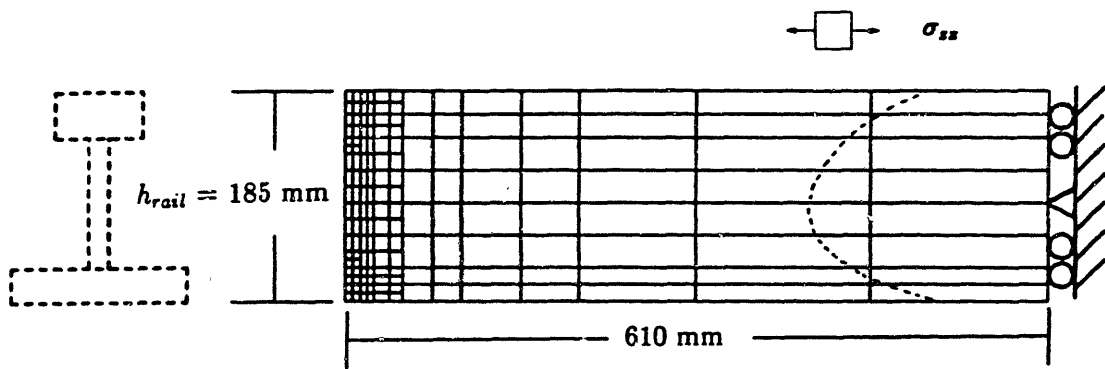
Fig. 3. Finite element model of the rail end.
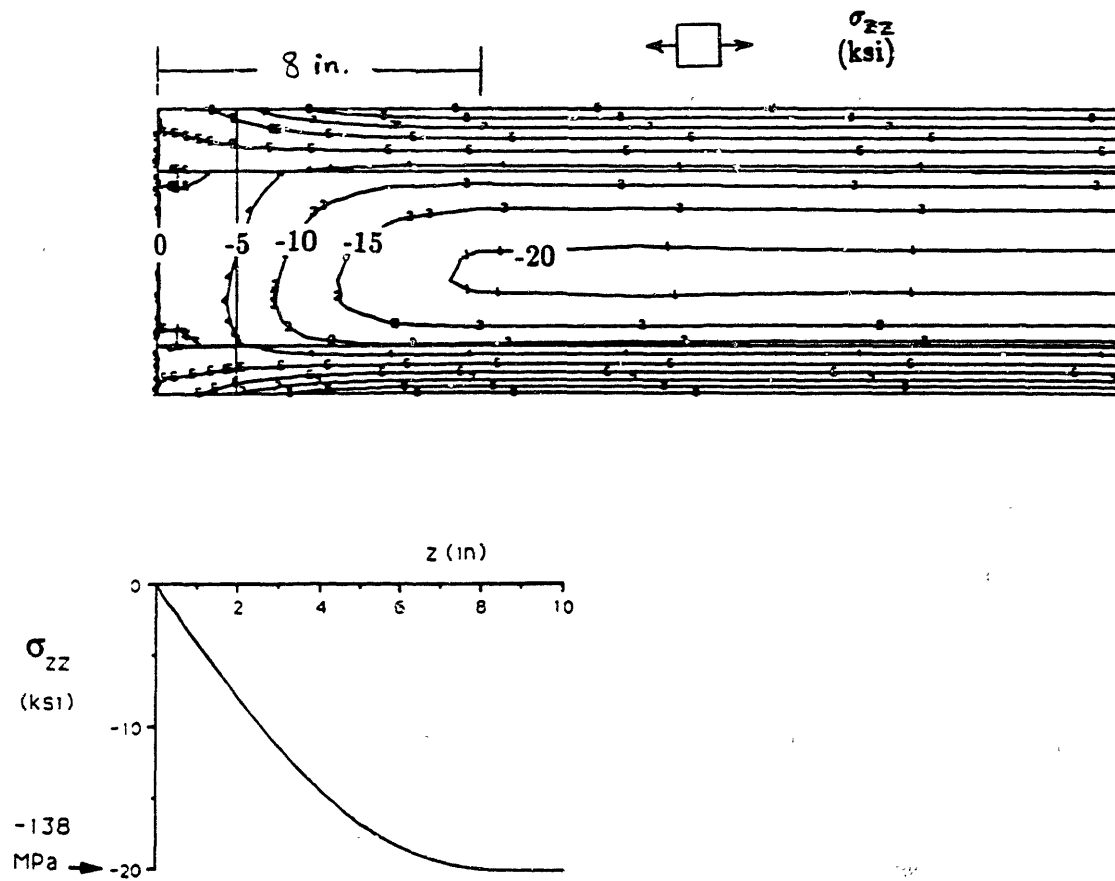
Fig. 4. Finite element contours of longitudinal residual stress near a cut rail end.
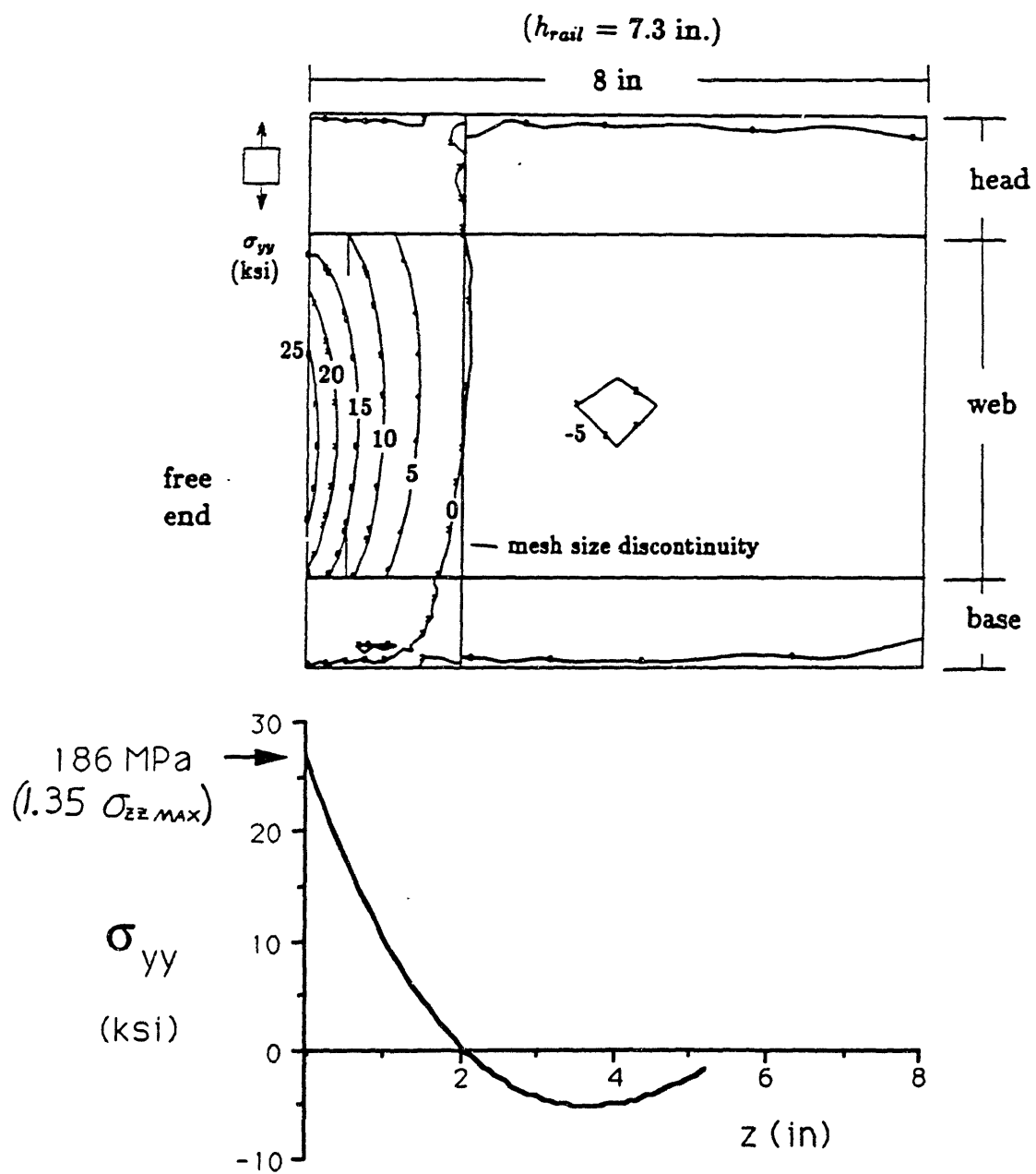
Fig. 5. Finite element contours of vertical residual stress near a cut rail end.

122
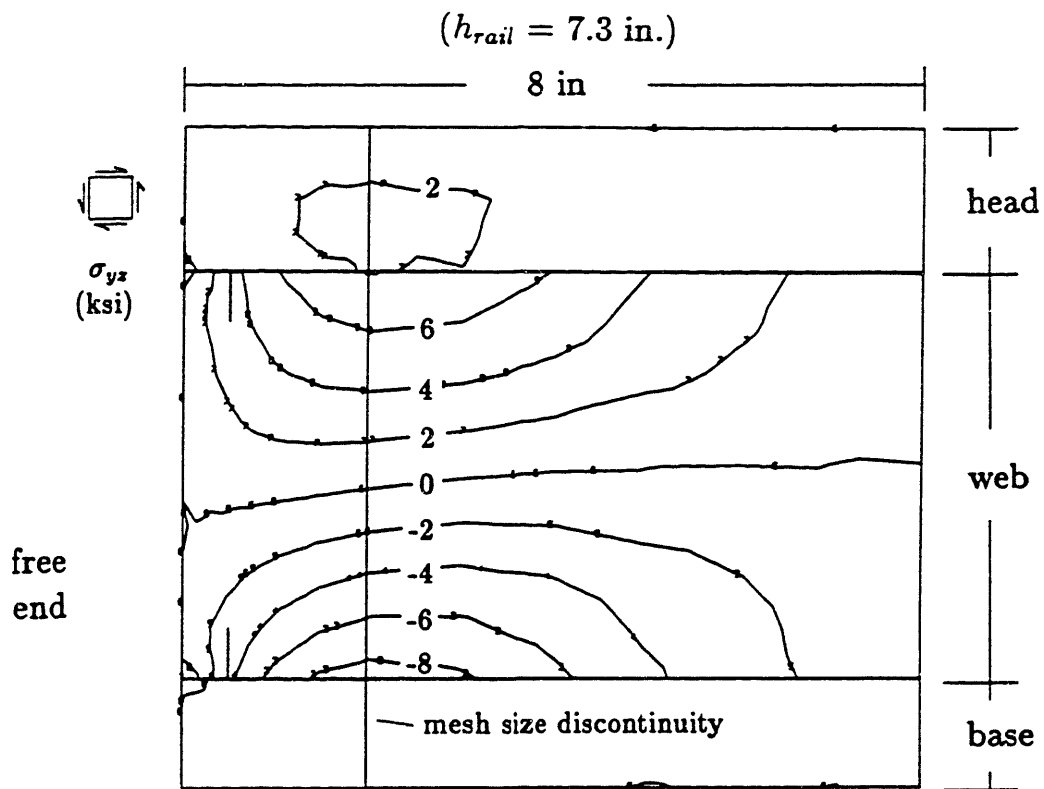
Fig. 6. Finite element contours of shear residual stress near a cut rail end.
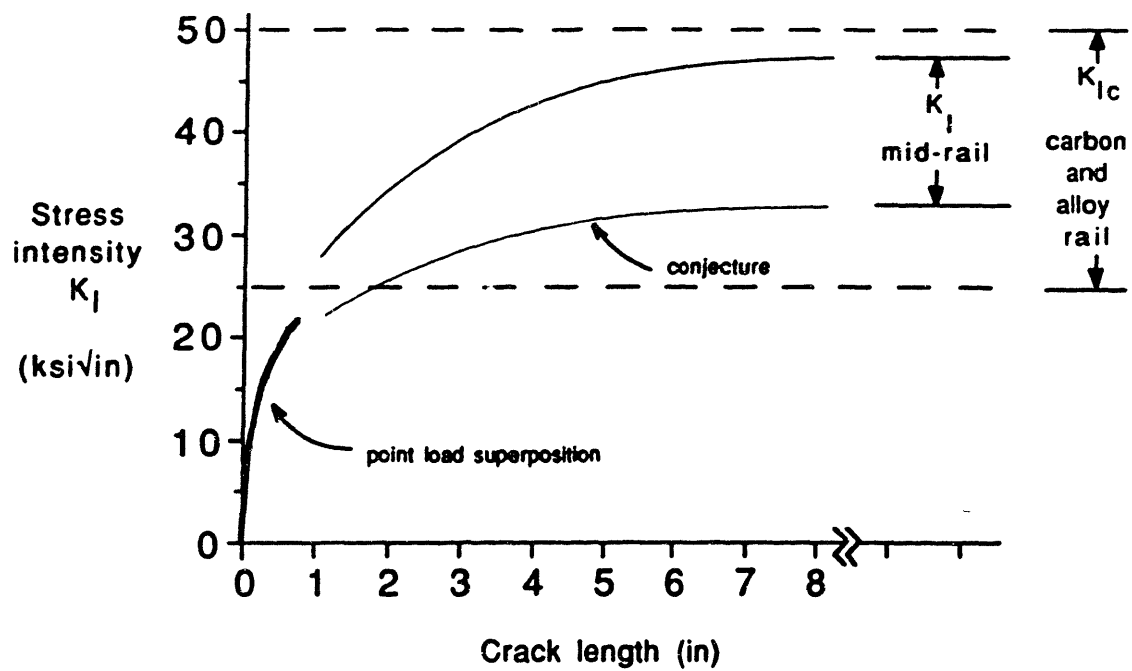
Fig. 7. Variation of stress intensity K_I with crack length for a horizontal crack in mid-web.

124

Chapter 4

A Saw-cutting test to quantify the severity of residual stresses

4.1 Introduction

Unstable web fracture due to residual stresses in roller-straightened rail can cause derailments. An estimate of the stress intensity K_I due to residual stresses and tending to grow a web crack can be made from a saw-cutting test (Fig. 1). In such a test, the rail web is saw-cut longitudinally and the change in curvature of the split ends due to residual stresses is measured. That the curvature change, rather than the opening displacement or shortening, is needed for a K_I estimate is based on the following argument. As discussed by Wineman and McClintock (1987), unstable fracture of a web crack due to residual stresses should depend on Mode I energy release rate, since Mode II would tend to produce a change in crack direction. Release of the longitudinal stresses present in roller-straightened rail would make a web crack tend towards mid-web, where there is zero K_{II} and maximum K_I. The total energy release rate from the change in curvature of the split rail ends is then concentrated into Mode I. If the resulting K_I is above the critical value K_{Ic} for the rail steel, the rail is capable of unstable web fracture driven by residual stresses. K_I must be less than K_{Ic} by some finite amount to avoid undue risk of fracture.

Some previous work has been done in saw-cutting the rail web to estimate residual stresses. Lempitskiy and Kazarnovskiy (1973) attempted to correlate saw-cut openings with measured residual stresses. Orringer and Tong (1985) mention work

done at the Association of American Railroads (AAR) in which the rail web was saw-cut and displacements of the cut openings measured. Indeed, it was these test results that Joerms (1987) used in his finite element work mentioned in Chapter 3, assuming uniform radii of curvature for the split ends to estimate the residual stresses in a rail end. However, none of these tests relates the curvature change of the split rail ends to the stress intensity K_I.

The saw-cutting test seems particularly attractive for the following reasons. First, it allows a simple estimate of the stress intensity K_I, requiring only a measurement of rail curvature and an algebraic calculation. Second, it is a static test, allowing isolation of residual stress effects from dynamic effects. Although crack growth may involve dynamic effects, such as stress wave propagation or inertia of the split ends, crack initiation due to wheel loads should not be dynamic, since the time to reach peak wheel load (R.R. John et al. 1984) is at least 30 times greater than the time for stress waves to travel one rail height. Therefore, a static fracture stability criterion should be sufficient for assessing rail safety in the presence of residual stresses.

In this work, the saw-cutting test procedure and the K_I calculation are described, and the uncertainties in the resulting K_I values are estimated. Then, the results of applying the stress intensity calculation procedure to deflection data from three rails split by the Association of American Railroads (AAR) are presented.

4.2 Procedure

Table 1 summarizes the procedure for estimating K_I from the curvature change of the saw-cut ends. The following is a discussion of this procedure.

The residual stresses are assumed to be fairly uniform along the cut rail; that is, the wavelength of any residual stress variation is greater than several rail heights. The presence of non-uniform residual stresses would be indicated, after cutting, by fluctuations in rail curvatures and resulting stress intensities along a short length of rail.

4.2.1 Saw-cutting and curvature change measurement

The rail web must be cut longitudinally into two split sections. The saw-cut must be long enough to provide a region for measuring curvatures away from stress transition regions at the start and end of the cut. These transition regions are estimated from Saint-Venant's principle to be at most 2 split-section heights (about 200 mm, or 8 inches) from a free split end or from the tip of the saw-cut.

Since the stress intensity K_I is a function of the residual stress *relieved* by saw-cutting or cracking, what is actually of interest is the *change* in curvature due to cutting. Therefore the curvature of the rail head and base should be measured both before and after cutting.

The radius of curvature at a point on the rail can be estimated in several ways. A plot of the rail profile could be made by running a dial gage referenced to a flat surface along the head or base of each split rail section. Local curvatures could then be estimated from, say, fitting a parabola to three evenly-spaced points along the rail profile. This was done for the AAR rail specimens discussed below. To find an expression for local curvature, denote the parabola in terms of deflection δ versus position along the rail x, where a is a constant to be found (Fig. 2):

$$\delta - \left[\delta_2 + \frac{\delta_3 - \delta_1}{x_3 - x_1}(x - x_2)\right] = a(x - x_2)^2 \ . \tag{4.1}$$

The constant a can be found from geometry in terms of the coordinates of the three points in Fig. 2:

$$\frac{1}{2}(\delta_3 + \delta_1) - \delta_2 = a(x_3 - x_2)^2 \ . \tag{4.2}$$

The local radius of curvature R, at the central point (x_2, δ_2), is the reciprocal of the second derivative of the curve (Eq. 4.1), where a is found from Eq. (4.2):

$$R = \frac{1}{\frac{d^2\delta}{dx^2}} = \frac{1}{2a} = \frac{(x_3 - x_2)^2}{\delta_3 + \delta_1 - 2\delta_2} \ . \tag{4.3}$$

The simplest means of curvature measurement, however, seems to be with a curvature measurement device consisting of a dial gage centrally mounted on a bar, with guides for alignment (Fig. 3). An averaged local curvature is found directly

127

from the difference in displacement between the dial gage and feet at each end of the bar. In terms of the dial gage deflection δ and the half-length L between the dial gage and feet at either end of the bar:

$$R = \frac{L^2}{2\delta} .$$

(4.4)

4.2.2 Calculation of stress intensity K_I

Moment released by cutting

The moment released during cutting or cracking can be related to the change in radius of curvature of the split ends by approximating the split ends as beams. The moment released, ΔM, for each split section is given in terms of Young's modulus E, the moment of inertia I of the split section (head plus part of web, or base plus rest of web), and the radius of curvature of the split section before and after cutting, R_{before} and R_{after}:

$$\Delta M = EI \left(\frac{1}{R_{after}} - \frac{1}{R_{before}} \right) .$$

(4.5)

Energy release rate

The strain energy release rate is the elastic strain energy released per unit crack area during fracture (see, for example, Broek (1982) pp. 115-119). In the rail, the elastic strain energy release contributing to K_I is assumed to come entirely from release of moments due to longitudinal residual stress on the split section. Saw-cutting the web causes a strain energy release similar to that in fracture with a small difference because material is removed or plastically deformed by the saw. Since the volume of this material is small compared with the total rail volume, this difference should be negligible.

The contribution $\mathcal{G}$ of each split section to the total energy release rate during fracture or saw-cutting can be written in terms of the moment released ΔM (Eq. 4.5), where t_{web} is the web thickness:

128

$$\mathcal{G} = \frac{1}{t_{web}} \frac{(\Delta M)^2}{2EI} = \frac{EI}{2t_{web}} \left(\frac{1}{R_{after}} - \frac{1}{R_{before}} \right)^2 . \tag{4.6}$$

The total energy release rate is the sum of that for each split section. In terms of the energy release rates for the head and base split sections, $\mathcal{G}_H$ and $\mathcal{G}_B$, the total energy release rate $\mathcal{G}_{total}$ is:

$$\mathcal{G}_{total} = \mathcal{G}_H + \mathcal{G}_B . \tag{4.7}$$

Stress intensity

The stress intensity K_I at a location along the rail is related to the total energy release rate (see, for example, Broek (1982) pp. 16-17). Rail web fracture should be plane strain fracture, since the estimated plastic zone size $r_p \approx (K_{Ic}/Y)^2/2\pi$ (where K_{Ic} is the fracture toughness and Y is the yield strength) is less than 1/20 of the web thickness. For plane strain fracture, then, where ν is Poisson's ratio:

$$K_I = \left[\mathcal{G}_{total} \frac{E}{(1 - \nu^2)} \right]^{1/2} . \tag{4.8}$$

This can be written in terms of the radii of curvature before and after cutting for the head and base split sections, denoted by subscripts H and B:

$$K_I = \frac{E}{[2t_{web}(1 - \nu^2)]^{1/2}} \left[I_H \left(\frac{1}{R_{H\,after}} - \frac{1}{R_{H\,before}} \right)^2 \right.$$
$$\left. + I_B \left(\frac{1}{R_{B\,after}} - \frac{1}{R_{B\,before}} \right)^2 \right]^{1/2} \tag{4.9}$$

This is the formula given in Table 1.

4.3 Uncertainty analysis

The uncertainty in a value of K_I estimated by the saw-cutting test (the possible value of the error at given odds) depends on the uncertainties in all of the variables used to obtain K_I. However, a plot of stress intensities calculated at several positions

along the rail will be affected in different ways by uncertainties in different variables. Uncertainty in a local radius of curvature (R) measurement affects only one point on a plot of K_I versus position along the rail. Uncertainties in other variables, such as rail dimensions and elastic constants, tend to affect all the points on the curve in the same manner, shifting the entire curve vertically. The effect on K_I of uncertainties in radius of curvature will be discussed first, followed by a mention of the effect of uncertainties in other variables.

4.3.1 Uncertainties in radius of curvature R.

Uncertainty in measured local radii of curvature, for example due to uncertainty in dial gage deflections and in spacings between points along the rail, can be quantified using a technique discussed by S.J. Kline and F.A. McClintock (1953) (see also Beckwith, Buck and Marangoni (1982)). If F is a function of n independent variables $(v_1, v_2, ... v_n)$, then the uncertainty u_F in F is related to the uncertainties u_{v_i} in the variables by:

$$u_F = \left[\left(\frac{\partial F}{\partial v_1} u_{v_1} \right)^2 + \left(\frac{\partial F}{\partial v_2} u_{v_2} \right)^2 + ... + \left(\frac{\partial F}{\partial v_n} u_{v_n} \right)^2 \right]^{1/2} . \tag{4.10}$$

In this case the function F is the stress intensity K_I and the uncertainty u_{K_I} in K_I is a function of the four measured radii of curvature: for the head split section before and after cutting, and for the base split section before and after cutting. In terms of the measured dial gage deflections (δ_i) and spacings between points along the rail ($x_3 - x_2 = \Delta x$) used in Eq. 3, K_I becomes:

$$K_I = \frac{E}{[t_{web}(1-\nu^2)]^{1/2}} \frac{1}{(\Delta x)^2} \{ I_H [(\delta_3 + \delta_1 - 2\delta_2)_{H\,after} - (\delta_3 + \delta_1 - 2\delta_2)_{H\,before}]^2$$
$$+ I_B [(\delta_3 + \delta_1 - 2\delta_2)_{B\,after} - (\delta_3 + \delta_1 - 2\delta_2)_{B\,before}]^2 \}^{1/2} . \tag{4.11}$$

For convenience, define

$$\beta = \delta_3 + \delta_1 - 2\delta_2 . \tag{4.12}$$

130

It turns out that, for uncertainties in Δx of $u_{\Delta x} = \pm 1.27$ mm (± 0.05 in), for the 51 mm (2 in) spacing (Δx) along the rail used in calculating from the AAR data, the contribution of Δx is negligible. Therefore, the fractional uncertainty in K_I, u_{K_I}/K_I, can be written as follows, assuming that uncertainties arise only from uncertainties in β, that u_β and β have similar values for the upper and lower split sections, and that the uncertainty u_δ is the same for all dial gage deflections:

$$\frac{u_{K_I}}{K_I} = \left[\left(\frac{u_\beta}{\beta} \right)^2 \right]^{1/2} = \frac{1}{\beta} \left[\left(\frac{\partial \beta}{\partial \delta_1} u_\delta \right)^2 + \left(\frac{\partial \beta}{\partial \delta_2} u_\delta \right)^2 + \left(\frac{\partial \beta}{\partial \delta_3} u_\delta \right)^2 \right]^{1/2} = \sqrt{6} \, \frac{u_\delta}{\beta} \; , (4.13)$$

where u_δ ($=\pm 0.00025$ in, or ± 0.00635 mm) is the estimated uncertainty in a faired plot of dial gage deflection versus position along the rail.

Note that for this analysis each curvature should be based on 3 independent dial gage deflection measurements. For the AAR data, curvatures were calculated from the deflection plots every 50 mm (2 in), although deflections were measured every 25 mm (1 in). There is then some correlation between curvatures, although we consider it of negligible importance. A detailed study of the sources of the uncertainties could be made by repeated measurements at various intervals along the uncut rail.

4.3.2 Uncertainties in other variables.

Uncertainties in the elastic constants E and ν are probably negligible. If the dimensions of each rail have been measured, the uncertainties here are also small and should have a negligible affect on K_I compared to uncertainty in curvature measurement. If the rail dimensions have not been measured, an uncertainty of, for example, ± 6 mm (± 0.25 in) in all rail dimensions results in an uncertainty of all K_I values for the rail of approximately $\pm 25\%$. An uncertainty of only ± 0.8 mm (± 0.030 in), such as is obtainable with a ruler, results in an uncertainty in K_I of approximately $\pm 3\%$, which is negligible compared to the uncertainty from measuring rail curvatures corresponding to K_{Ic} using a dial gage.

Another source of error comes from calculating the moments of inertia I by approximating the rail with rectangular regions. Although a more accurate calculation

131

can be done to account for fillets and the tapered web, the effect on K_I should not be large compared to uncertainties due to measuring the radius of curvature.

4.4   Results of applying procedure to AAR data

Plots of the deflection of three roller-straightened rails split by the Association of American Railroads (AAR) were used to estimate stress intensities along the rails. Figs. 4-6 are plots of calculated stress intensities along the rail for the three rail specimens, arbitrarily numbered Specimen 1 to 3. The rails were assumed straight before cutting ($R_{before} = 0$).

Error bars represent estimated uncertainty in the value of K_I, due to estimated uncertainties in measuring local radii of curvature of the split sections. Uncertainties u_{K_I}/K_I are typically $\pm21\%$ (20 to 1 odds). The uncertainty u_{K_I}/K_I depends on the value of β (Eq. 13), and for the AAR data β ranged from 0 to approximately 1.27 mm (0.005 in) (corresponding to radii of curvature $R = \infty$ to 750 inches (19 m)). Therefore, this range was divided into 5 regions and uncertainties u_{K_I}/K_I were calculated for each region separately.

The exact rail dimensions were not known, so typical dimensions were assumed: height of the rail head, web and base 43, 102, and 25 mm (1.7, 4.0, and 1.0 in), respectively; width of the rail head, web, and base 76, 18, and 152 mm (3.0, 0.7, and 6.0 in), respectively. Differences between these and the actual dimensions will change the vertical scale of the entire plot rather than affecting the error bars for individual measurements, as discussed above. Stress transition regions, shown on the plots by dotted lines, are estimated to be about 2 split section heights, or approximately 200 mm (8 in), from the free split end or from the tip of the saw-cut.

Calculated stress intensities in the middle portion of the specimens are:

Specimen 1 $K_I \approx$ 33-55 MPa$\sqrt{\text{m}}$ (30-50 ksi$\sqrt{\text{in}}$)

Specimen 2 $K_I \approx$ 66-88 MPa$\sqrt{\text{m}}$ (60-80 ksi$\sqrt{\text{in}}$)
(with one point at $\approx$ 22 MPa$\sqrt{\text{m}}$ = 20 ksi$\sqrt{\text{in}}$)

Specimen 3 $K_I \approx$ 33-55 MPa$\sqrt{\text{m}}$ (30-50 ksi$\sqrt{\text{in}}$)
(with one point at $\approx$ 93 MPa$\sqrt{\text{m}}$ = 85 ksi$\sqrt{\text{in}}$).

The low value for Specimen 2 occurs at a relatively flat spot on the deflection plot, and the high value for Specimen 3 occurs at a sharp bend of the deflection curve.

The fracture toughness K_{Ic} for these rails, or even the type of rail, was not known for the AAR specimens. However, the fracture toughness K_{Ic} for carbon and alloy rail ranges from about 27 to 55 MPa$\sqrt{m}$ (25 to 50 ksi$\sqrt{in}$), with typical values for carbon rail of 38 MPa$\sqrt{m}$ (35 ksi$\sqrt{in}$) (Orringer, Morris, and Steele 1984) and for chromium-vanadium (Cr-V) rail of approximately 31 MPa$\sqrt{m}$ (28 ksi$\sqrt{in}$) (Jones and Rice 1985). Therefore, there is danger of spontaneous cracking in these rails tested by the AAR.

These results are further reinforced by a K_I estimate from a photograph of a roller-straightened Cr-V rail which fractured in service. Visual estimates of the radii of curvature of the split sections from the photograph gave a stress intensity K_I of approximately 44 MPa$\sqrt{m}$ (40 ksi$\sqrt{in}$), well above K_{Ic} for chromium-vanadium rail.

4.5   Usefulness of this test and other methods of residual stress quantification

The saw-cutting test can give a quantitative estimate of the stress intensity K_I acting on a web crack at the saw-cut location. Therefore it is a more useful and direct test for tendency to web fracture than the drop-weight impact ("whomper") test or a saw-cutting test where the cut opening only is measured, both of which give at best only a qualitative indication of the residual stresses present in the rail. Also, the saw-cutting test is simple to perform, requiring a longitudinal saw cut, curvature measurements, and an algebraic calculation. The test is further simplified by using a device we have developed consisting of a dial gage mounted on a bar with aligning guides (Fig. 3). A calculator has been programmed to accept input data and calculate K_I.

Another promising method of residual stress measurement uses the DEBRO ultrasonic stress meter (1989). This device can measure the near-surface longitudinal residual stresses around the periphery of the rail and provides a quick, nondestructive method of residual stress measurement useful for production quality control.

However, it does not measure residual stresses within the head and base, which also contribute to K_I.

4.6 Conclusions

1. Calculation of stress intensity K_I from the saw-cutting test is relatively simple, requiring measurement of local radii of curvature of the saw-cut rail ends and an algebraic calculation to estimate K_I. The amount of uncertainty in stress intensity K_I using this technique can be brought to less than $\pm 20\%$.

2. Data from three roller-straightened rails split by the AAR were used to estimate stress intensity K_I due to residual stresses. The resulting stress intensities were comparable to the fracture toughness K_{Ic} for carbon and alloy rail, suggesting that there was indeed danger of spontaneous fracture in these rails.

3. Curvature measurement can be simplified by using a dial gage mounted on a bar with guides to align it on the rail head and base.

4.7 References

1. Beckwith, T.G., Buck, N.L., Marangoni, R.D. (1982) *Mechanical Measurements*, 3rd ed., Addison-Wesley, Sec. 9.6-9.7.

2. Broek, D. (1982) *Elementary Engineering Fracture Mechanics*, 3rd revised ed., Martinius Nijhoff, The Hague.

3. (DEBRO) (1989) Institute of Fundamental Technological Research of the Polish Academy of Sciences and ELTRONA GmbH, "DEBRO-30" ultrasonic stress measurements description and users' manual, 2102 Hamburg 93, Stenzelring 17, W. Germany.

4. John, R.R., et al. (1984) "Task force report–rail failure evaluation", DOT Transportation Systems Center, Cambridge, MA.

5. Joerms, M.W. (1987) "Calculation of residual stresses in railroad rails and wheels from sawcut displacement". *Residual Stress–in Design, Process and Material Selection*, W.B. Young ed., American Society of Metals, 205.

6. Jones, D.J., Rice, R.C. (1985) "Determination of K_{Ic} fracture toughness for alloy rail steel", final report to DOT Transportation Systems Center, Cambridge, MA.

7. Kline, S.J., McClintock, F.A. (1953) "Describing uncertainties in single-sample experiments", *Mechanical Engineering*, **75**, 3-8.

8. Lempitskiy, V.V., Kazarnovskiy, D.S. (1973) "Improving the service life and reliability of railroad rails", *Russian Metallurgy*, **1**, 111-117.

9. Orringer, O., Morris, J.M., Steele, R.K. (1984) "Applied research on rail fatigue and fracture in the United States", *Theoret. Appl. Fracture Mech.*, **1**, 23-49.

10. Orringer, O., Tong, P. (1985) "Investigation of catastrophic failure of a premium-alloy railroad rail", *Fracture Problems in the Transportation Industry*, Proc. ASCE Conference, Detroit, MI.

11. Wineman, S.J., McClintock, F.A. (1987) "Rail web fracture in the presence of residual stresses", *Theoret. Appl. Fracture Mech.*, **8**, 87-99.

Table 1. Summary of procedure for estimating stress intensity from saw-cutting test.

1. Measure local radius of curvature R before and after saw cutting, for upper and lower split sections, at same distances from rail end.

   Saw-cut length should be $\geq$ Measuring length (of at least 100 mm) + 2 split section heights at start and end of cut.

2. Calculate the stress intensity K_I:

$$K_I = \frac{E}{[2t_{web}(1-\nu^2)]^{1/2}} \left[I_H \left(\frac{1}{R_{H\,after}} - \frac{1}{R_{H\,before}} \right)^2 \right.$$

$$\left. + I_B \left(\frac{1}{R_{B\,after}} - \frac{1}{R_{B\,before}} \right)^2 \right]^{1/2}$$

where

   E = elastic modulus of rail steel

   ν = Poisson's ratio

   t_{web} = web thickness at saw-cut

   I_H, I_B = moments of inertia of head and base split sections

   $R_{Hbefore}$, R_{Hafter} = radii of curvature, head split section, before and after cutting

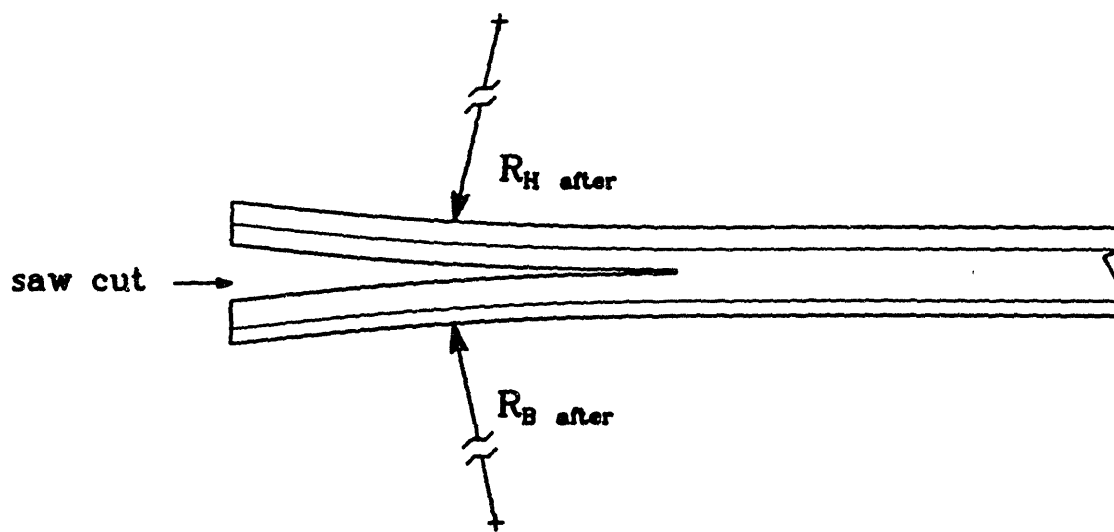 $R_{Bbefore}$, R_{Bafter} = radii of curvature, base split section, before and after cutting
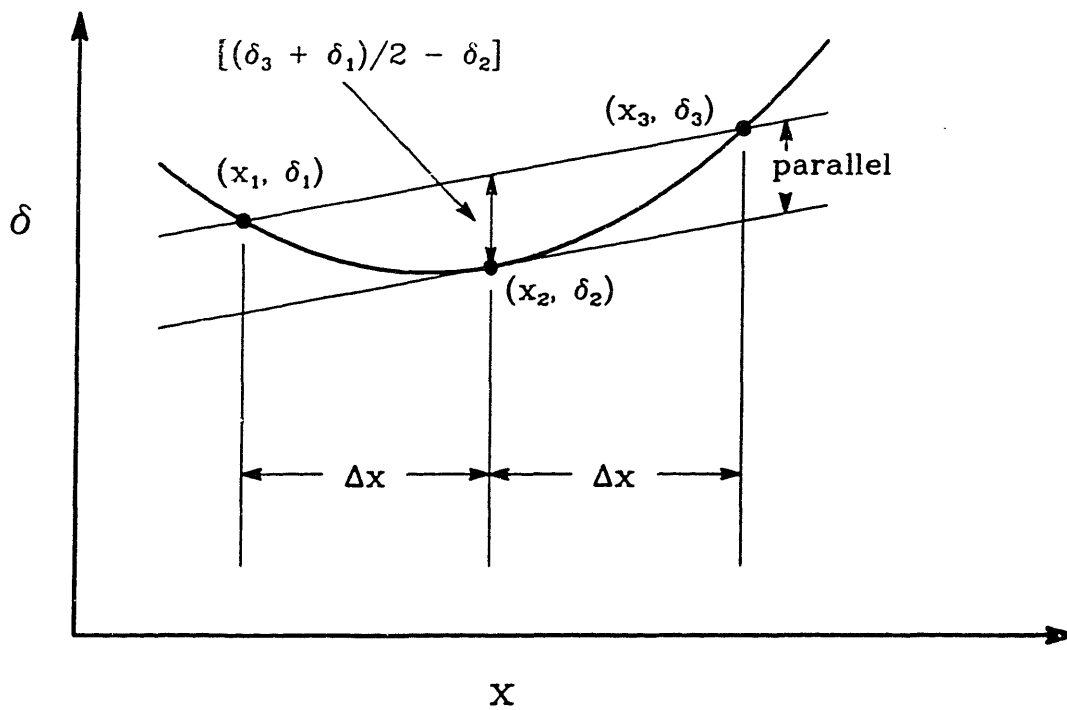
Fig. 1. The saw-cut rail.

Fig. 2. Fitting a parabola to three points on a curve of dial gage deflection (δ) versus position (x) along the rail.

(a)   top

(b)   side
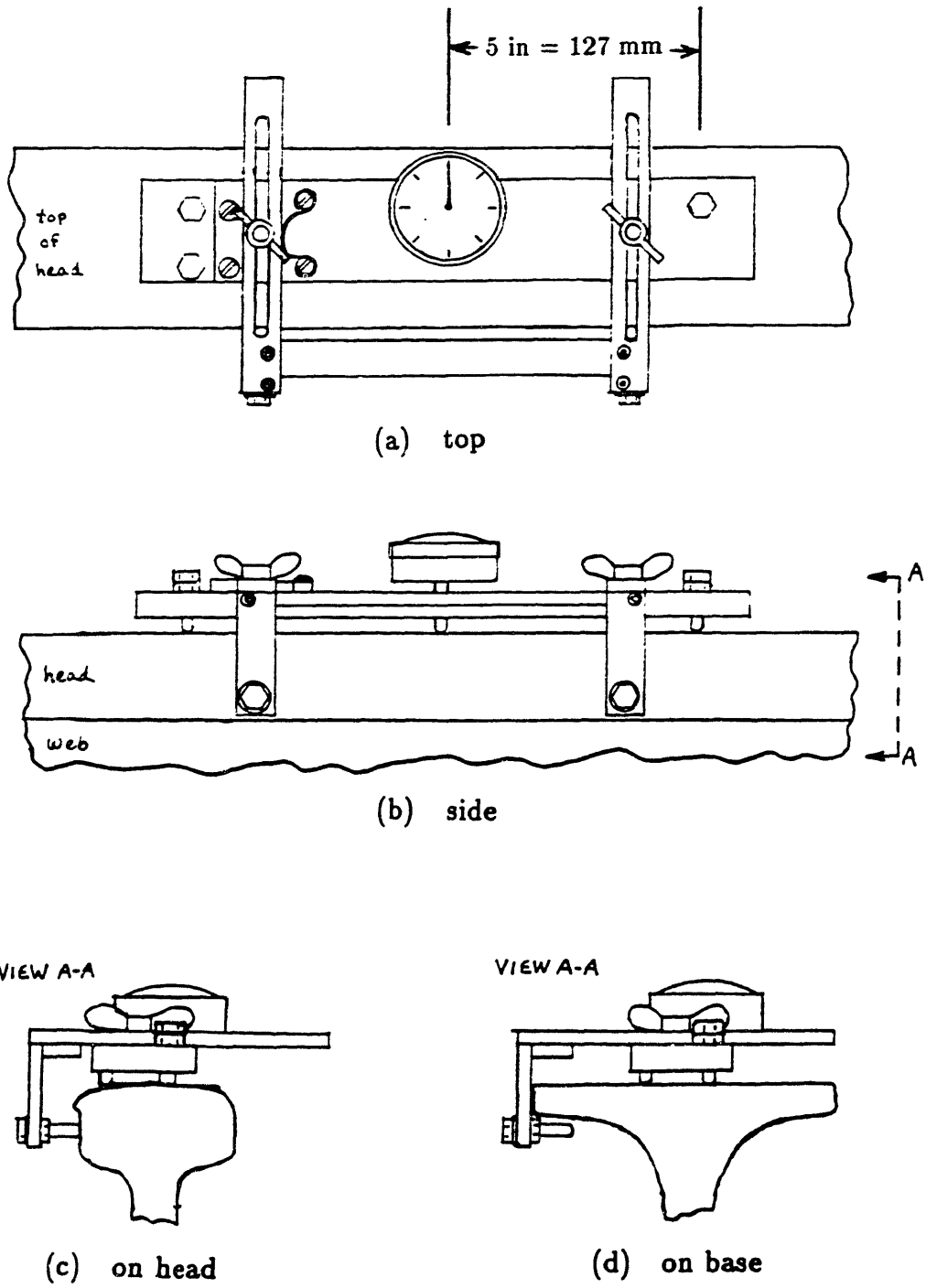
(c)   on head

(d)   on base

Fig. 3. Curvature measurement device for the saw-cutting test.

Fig. 4. Calculated stress intensity K_I versus position along the rail for Specimen 1. Error bars represent estimated (20:1) uncertainty in K_I due to measurements for local curvature.
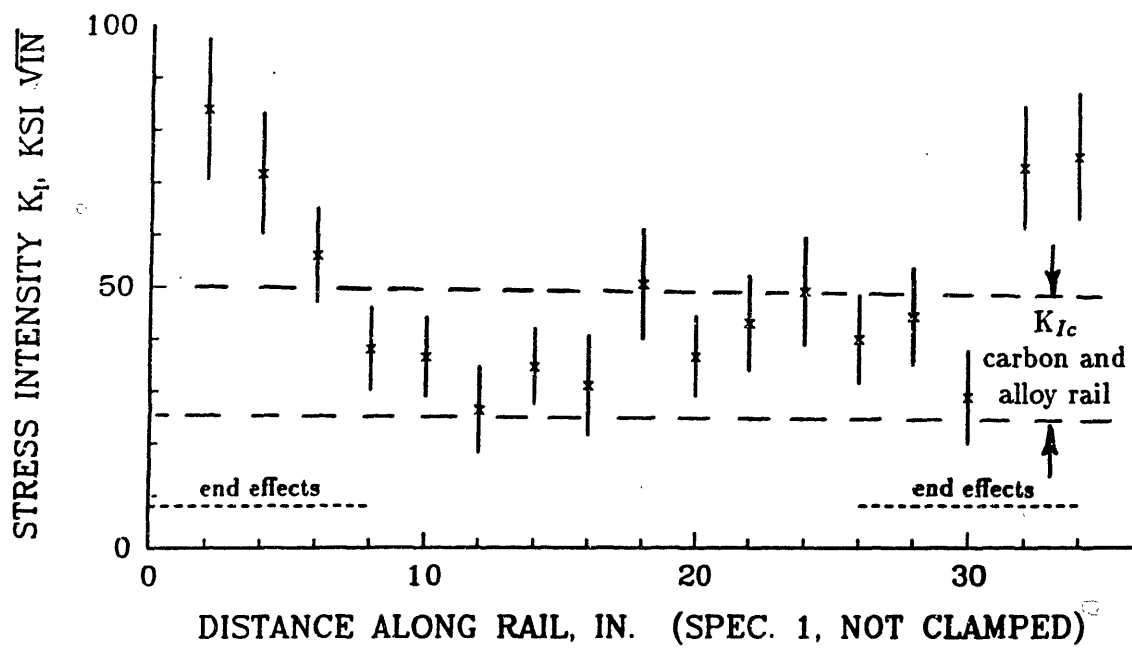
Fig. 5. Calculated stress intensity K_I versus position along the rail for Specimen 2. Error bars represent estimated (20:1) uncertainty in K_I due to measurements for local curvature.

Fig. 6. Calculated stress intensity K_I versus position along the rail for Specimen 3.
Error bars represent estimated (20:1) uncertainty in K_I due to measurements for
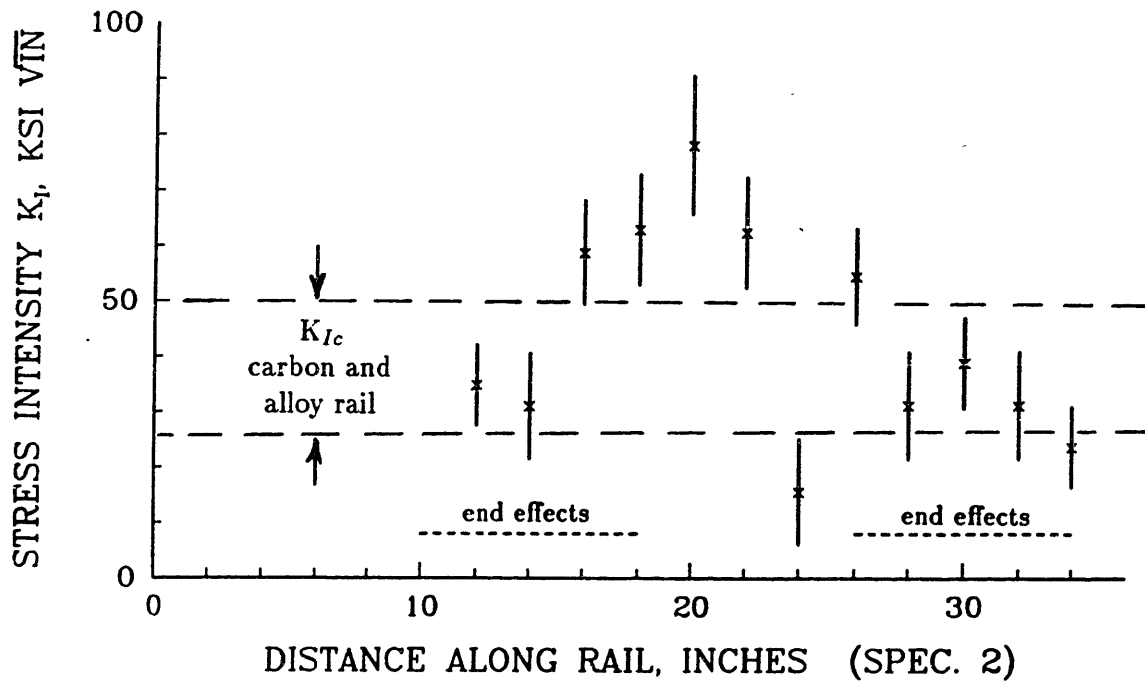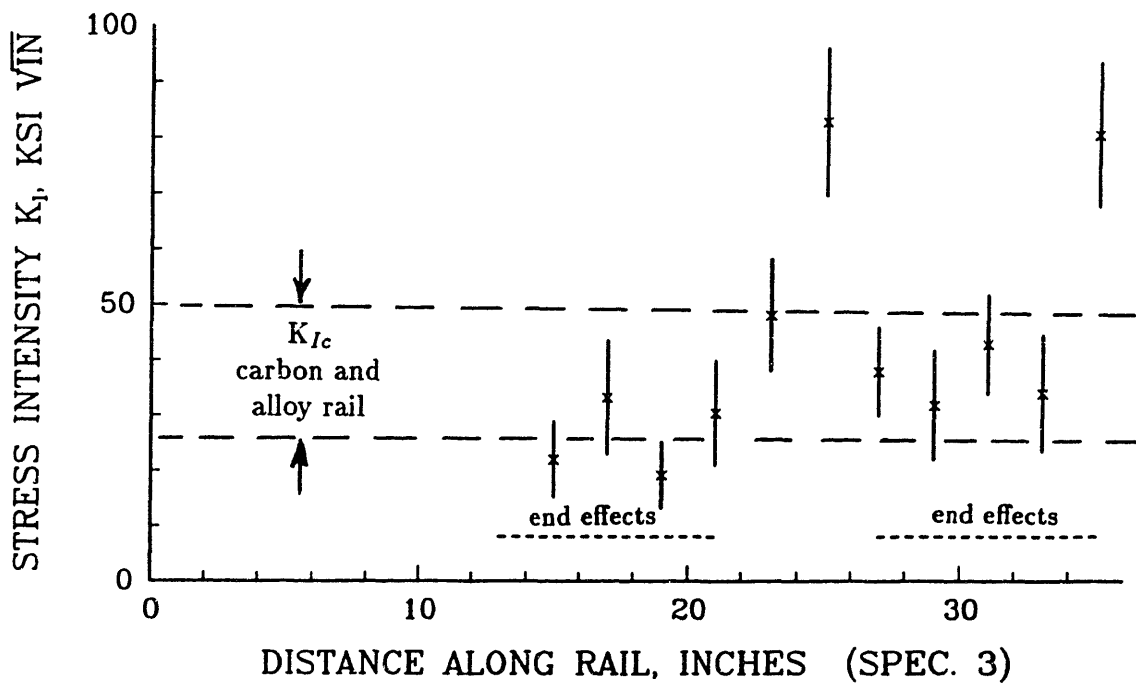local curvature.

Chapter 5

Conclusions and Recommendations

The goals of this study were to investigate the creation and modification of the unfavorable longitudinal residual stress due to roller-straightening, to determine the stress transients at a cut rail end, where the longitudinal stress must go to zero, and to develop a simple test to determine the tendency of residual stress to cause web fracture in a given rail. In Chapter 2 of this work, models for residual stress formation during roller-straightening were developed. Then, the effects of process parameters (applied roll load or displacement, roll diameter and spacing) were investigated in order to suggest ways to minimize unfavorable residual stresses.

1. The deformation of the rail in the straightener is really a three-dimensional problem. However, plane stress models of the straightener are adequate to model the resulting residual stresses.

2. A plane stress, "single-roll" model for the first two loaded rolls in the straightener gives qualitative agreement with strain gage data taken at three locations on the rail. Disparities between experimental and calculated residual stresses appear to result from idealization of boundary conditions and material behavior in the finite element model, and from the coarse mesh used.

3. The unfavorable, U-shaped longitudinal residual stress distribution found in roller-straightened rail arises from the last straightener rolls, where the bending

143

moment is relatively low and most of the plastic deformation occurs under the roll, due to the high contact stresses there.

4. Increasing the roll diameter by 20% has no effect on residual stresses, both in the initial, heavier loaded rolls, and in the final rolls producing the U-shaped stress distribution. This is not surprising since the amount of plastic deformation is too great for the elastic (Hertz) theory of contact to apply.

5. A straightener that maintained high bending moments throughout would avoid the U-shaped residual stress distribution, giving instead a Z-shape from bending deformation. This may mean that the spacing to the last roll must be very large, so that there can be a small force on the last roll and still a large moment at the next-to-last roll. Further investigation is needed to determine the combinations of roll force and bending moment to avoid the U-shaped residual stress distribution.

6. The best solution to the problem of unfavorable residual stresses from straightening must be based on the overall process of rail manufacture. It may be more economical to avoid the need to straighten, or to use an alternate method of straightening, than to redesign the roller-straightener.

In Chapter 3, rail with a self-equilibrating longitudinal residual stress field having maximum and minimum values of ±138 MPa (±20 ksi), representative of that found in roller-straightened rail, was modelled to determine the stress transients near a cut rail end and the location and severity of the worst possible end-crack.

1. Stress transients at a cut end of roller-straightened rail consist of a decrease to zero of longitudinal stress at the end and a vertical tensile residual stress in the web at the end. Finite element models for both a free end and an end with a fixed base gave the lengths to reach 95% of the mid-rail stress field to be 1.10 and 1.12 rail heights, respectively. The maximum vertical stresses at the end were 1.35 and 1.10 times the maximum value of mid-rail longitudinal

residual stress. Beam-on-elastic-foundation models give algebraic estimates of such stress transients agreeing within 30% of the finite element results.

An estimate of the stress intensity K_I on a short web crack at the rail end, in the (uncracked) vertical residual stress field there, gives K_I increasing with crack length and reaching 22 MPa$\sqrt{m}$ (20 ksi$\sqrt{in}$) for cracks 13 mm (0.5 in) long. Although K_I on short cracks may not be sufficient in itself to drive a web crack, in the presence of service loads the risk of fracture is greatly increased.

2. When a length of roller-straightened rail is taken from mid-rail the changes in longitudinal displacements can be large enough to affect subsequent residual stress measurements. For example, if the uneven length changes on cutting a 460 mm (18 in) Meier section are not accounted for, there may be an underestimate of the magnitude of measured longitudinal residual stress of as much as 48 MPa (7 ksi), significant compared to typical maxima of 138 MPa (20 ksi) for roller-straightened rail.

Chapter 4 describes a saw-cutting test for quantifying the severity of residual stress in a given rail.

1. Calculation of stress intensity K_I from the saw-cutting test is relatively simple, requiring measurement of local radii of curvature of the saw-cut rail ends and an algebraic calculation to estimate K_I. The amount of uncertainty in stress intensity K_I using this technique can be brought to less than ±20%.

2. Data from three roller-straightened rails split by the AAR were used to estimate stress intensity K_I due to residual stresses. The resulting stress intensities were comparable to the fracture toughness K_{Ic} for carbon and alloy rail, suggesting that there was indeed danger of spontaneous fracture in these rails.

3. Curvature measurement can be simplified by using a dial gage mounted on a bar with guides to align it on the rail head and base.